

**DEVELOPMENT OF NONLINEAR ROBUST  
CONTROL TECHNIQUES FOR UNMANNED  
AERIAL VEHICLES**

**A Thesis Submitted to  
the Graduate School of Engineering and Sciences of  
İzmir Institute of Technology  
in Partial Fulfillment of the Requirements for the Degree of**

**DOCTOR OF PHILOSOPHY**

**in Electrical and Electronics Engineering**

**by  
İlker TANYER**

**July 2015  
İZMİR**

We approve the thesis of **İlker TANYER**

**Examining Committee Members:**

---

**Prof. Dr. Cüneyt GÜZELİŞ**

Department of Electrical and Electronics Engineering  
İzmir University of Economics

---

**Prof. Dr. Serhan ÖZDEMİR**

Department of Mechanical Engineering  
İzmir Institute of Technology

---

**Prof. Dr. Aydođan SAVRAN**

Department of Electrical and Electronics Engineering  
Ege University

---

**Assoc. Prof. Dr. Enver TATLICIOđLU**

Department of Electrical and Electronics Engineering  
İzmir Institute of Technology

---

**Asst. Prof. Dr. Barbaros ÖZDEMİREL**

Department of Electrical and Electronics Engineering  
İzmir Institute of Technology

**10 July 2015**

---

**Assoc. Prof. Dr. Enver TATLICIOđLU**

Supervisor, Department of Electrical and Electronics Engineering  
İzmir Institute of Technology

---

**Prof. Dr. M. Salih DİNLEYİCİ**

Head of the Department of  
Electrical and Electronics Engineering

---

**Prof. Dr. Bilge KARAÇALI**

Dean of the Graduate School of  
Engineering and Sciences

## ACKNOWLEDGMENTS

First of all, I would like to thank my supervisor, Assoc. Prof. Dr. Enver TATLI-CIOĞLU for spending his time to help me in this project.

In addition, I would like to thank Prof. Dr. Cüneyt GÜZELİŞ, Asst. Prof. Dr. Barbaros ÖZDEMİREL, Prof. Dr. Serhan ÖZDEMİR, Prof. Dr. Aydoğan SAVRAN and Assoc. Prof. Dr. Erkan ZERGEROĞLU for giving me corrections and suggestions which helped me a lot in revising the thesis.

Also I would like to thank Alper BAYRAK and Meryem DENİZ for their help on experimental studies. The twin rotor system used in this work is manufactured by the funding received from IYTE University research grant with grant number 2010-IYTE-15, therefore I would like to thank IYTE University.

Finally I would like to thank my love Fatma Çangar Tanyer and my little son Cesur Tanyer for their help and support. Also I have to thank İlkay, Köksal-Devlet TANYER and Ayfer Çangar for their high-class motivation techniques. This project is also dedicated to my family as my other projects.

# ABSTRACT

## DEVELOPMENT OF NONLINEAR ROBUST CONTROL TECHNIQUES FOR UNMANNED AERIAL VEHICLES

In this thesis, model reference output tracking control of unmanned aircraft vehicles are aimed. The control problem is complicated due to the lack of accurate knowledge of nonlinear system dynamics and additive state-dependent nonlinear disturbance-like terms. Only the output of the vehicle is considered to be available for control design purposes. A novel robust controller is designed that ensured a global asymptotic stability result. In the design of the controller, proportional integral controller is fused with the integral of the signum of the tracking error to compensate uncertainties. Lyapunov type stability analysis are utilized to prove asymptotic convergence of the output tracking error. Extensions to optimal, adaptive and neural network controllers are also designed. Simulation and experiment results are presented to illustrate the performance of the robust controllers.

# ÖZET

## İNSANSIZ HAVA ARAÇLARI İÇİN DOĞRUSAL OLMAYAN GÜRBÜZ KONTROL TEKNİKLERİNİN GELİŞTİRİLMESİ

Bu tezde, insansız hava araçları için dayanak bir modelin çıktı izlemeli kontrolü hedeflenmiştir. Sistem dinamiklerindeki doğrusal olmayan belirsizlikler ve toplanır durum-bağımlı doğrusal olmayan bozan etken benzeri terimler kontrol problemini daha zor hale getirmektedir. Kontrol tasarımında sadece sistemin çıktısının kullanılabilir durumda olması dikkate alınmıştır. Çalışmamızda evrensel asimtotik kararlılığı sağlayacak yeni bir gürbüz denetçi tasarlanmıştır. Denetçi tasarımında bir oransal integral denetçi ile birlikte belirsizlikleri telafi etmek için izleme hatasının işaretinin integrali kullanılmıştır. Lyapunov tipi kararlılık analizleri kullanılarak çıktı izleme hatasının asimtotik yakınsaması ispatlanmıştır. Daha sonra gürbüz denetçinin optimal, uyarlanır ve sinir ağı tabanlı versiyonları geliştirilmiştir. Simulasyon ve deney sonuçları sunularak tasarlanan gürbüz denetçilerin performansları ortaya koyulmuştur.

# TABLE OF CONTENTS

LIST OF FIGURES .....	ix
LIST OF TABLES .....	xii
CHAPTER 1. INTRODUCTION .....	1
1.1. Unmanned Aerial Vehicles and Their Classifications .....	1
1.2. On Modeling of UAVs .....	2
1.3. On Control of UAVs.....	2
1.4. Literature Search .....	3
1.4.1. Robust Control Studies .....	4
1.4.2. Optimal Control Studies .....	4
1.4.3. Adaptive Control Studies .....	4
1.4.4. Neural Network Based Control Studies .....	5
1.5. Motivation .....	5
1.6. Contribution .....	6
1.7. Organization of Thesis .....	8
CHAPTER 2. AIRCRAFT MODEL .....	9
2.1. Examples of the Aircraft Model .....	9
2.1.1. Osprey Aircraft.....	9
2.1.2. Twin Rotor System.....	15
CHAPTER 3. ROBUST CONTROL OF UAV .....	19
3.1. Abstract .....	19
3.2. Control Design .....	19
3.3. Stability Analysis.....	23
3.4. Simulation Results .....	24
3.4.1. Osprey Aircraft.....	24
3.4.2. Twin Rotor System.....	32
3.5. Experiment Results.....	35
3.6. Conclusions.....	35

CHAPTER 4. ROBUST OPTIMAL CONTROL OF UAV .....	40
4.1. Abstract .....	40
4.2. Control Design .....	40
4.3. Stability and Optimality Analysis .....	43
4.4. Simulation Results .....	44
4.4.1. Osprey Aircraft .....	44
4.4.2. Twin Rotor System .....	50
4.5. Experiment Results .....	52
4.6. Conclusions .....	52
CHAPTER 5. ROBUST ADAPTIVE CONTROL OF UAV .....	56
5.1. Abstract .....	56
5.2. Control Design .....	56
5.3. Stability Analysis .....	57
5.4. Simulation Results .....	58
5.4.1. Osprey Aircraft .....	58
5.4.2. Twin Rotor System .....	66
5.5. Experiment Results .....	67
5.6. Conclusions .....	67
CHAPTER 6. ROBUST NEURAL NETWORK BASED CONTROL OF UAV .....	72
6.1. Abstract .....	72
6.2. Control Design .....	72
6.3. Stability Analysis .....	74
6.4. Simulation Results .....	75
6.4.1. Osprey Aircraft .....	75
6.4.2. Twin Rotor System .....	80
6.5. Experiment Results .....	82
6.6. Conclusions .....	85
CHAPTER 7. COMPARISON OF NUMERICAL RESULTS .....	86
7.1. Comparison of Simulation Results .....	86
7.2. Comparison of Experiment Results .....	90
CHAPTER 8. CONCLUSIONS .....	92
8.1. Future Work .....	95

REFERENCES ..... 97

APPENDICES

APPENDIX A. BOUNDEDNESS PROOF ..... 104  
APPENDIX B. LEMMA 1 AND ITS PROOF ..... 107  
APPENDIX C. LEMMA 2 AND ITS PROOF ..... 109  
APPENDIX D. ASYMPTOTIC STABILITY PROOF FOR CHAPTERS 3 AND 4 112  
APPENDIX E. ASYMPTOTIC STABILITY PROOF FOR CHAPTER 5 ..... 114  
APPENDIX F. ASYMPTOTIC STABILITY PROOF FOR CHAPTER 6 ..... 116



# LIST OF FIGURES

<u>Figure</u>	<u>Page</u>
Figure 2.1. Osprey aircraft testbed. ....	10
Figure 2.2. Pitch angle. ....	11
Figure 2.3. Bank angle. ....	12
Figure 2.4. Sideslip angle. ....	12
Figure 2.5. Aileron of a fixed wing aircraft. ....	13
Figure 2.6. Elevator of a fixed wing aircraft. ....	14
Figure 2.7. Rudder of a fixed wing aircraft. ....	14
Figure 2.8. Twin rotor system in control laboratory. ....	16
Figure 2.9. The block diagram of the twin rotor system. ....	16
Figure 2.10. The primary movements of the twin rotor system. ....	18
Figure 3.1. The reference forward velocity (dashed line) and the actual forward velocity (solid line). ....	26
Figure 3.2. The reference pitch rate (dashed line) and the actual pitch rate (solid line). ....	27
Figure 3.3. The reference roll rate (dashed line) and the actual roll rate (solid line). ....	27
Figure 3.4. The reference yaw rate (dashed line) and the actual yaw rate (solid line). ....	28
Figure 3.5. The output tracking error $e(t)$ . ....	28
Figure 3.6. The control input $u(t)$ . ....	29
Figure 3.7. Control input rates. ....	29
Figure 3.8. The reference and the actual states while high-disturbance is applied at $t = 3$ seconds. ....	30
Figure 3.9. The reference and the actual yaw rate while high-disturbance is applied at $t = 3$ seconds. ....	31
Figure 3.10. The reference pitch rate (dashed line) and the actual pitch rate (solid line). ....	33
Figure 3.11. The reference yaw rate (dashed line) and the actual yaw rate (solid line). ....	33
Figure 3.12. The output tracking error $e(t)$ . ....	34
Figure 3.13. The control input $u(t)$ . ....	34
Figure 3.14. Comparison of the signum function (solid line) and the hyperbolic tangent function (dashed line). ....	35

Figure 3.15. Tracking error for pitch rate. ....	36
Figure 3.16. Tracking error for yaw rate. ....	37
Figure 3.17. Control input for pitch rate. ....	38
Figure 3.18. Control input for yaw rate. ....	39
Figure 4.1. The reference velocity (dashed line) and the actual velocity (solid line). ....	45
Figure 4.2. The reference pitch rate (dashed line) and the actual pitch rate (solid line). ....	46
Figure 4.3. The reference roll rate (dashed line) and the actual roll rate (solid line). ....	46
Figure 4.4. The reference yaw rate (dashed line) and the actual yaw rate (solid line). ....	47
Figure 4.5. The output tracking error $e(t)$ . ....	47
Figure 4.6. The control input $u(t)$ . ....	48
Figure 4.7. The reference pitch rate (dashed line) and the actual pitch rate (solid line). ....	50
Figure 4.8. The reference yaw rate (dashed line) and the actual yaw rate (solid line). ....	51
Figure 4.9. The output tracking error $e(t)$ . ....	51
Figure 4.10. The control input $u(t)$ . ....	52
Figure 4.11. Pitch rate tracking error. ....	53
Figure 4.12. Yaw rate tracking error. ....	54
Figure 4.13. Control input for pitch rate. ....	55
Figure 4.14. Control input for yaw rate. ....	55
Figure 5.1. The reference velocity (dashed line) and the actual velocity (solid line). ....	62
Figure 5.2. The reference pitch rate (dashed line) and the actual pitch rate (solid line). ....	63
Figure 5.3. The reference roll rate (dashed line) and the actual roll rate (solid line). ....	64
Figure 5.4. The reference yaw rate (dashed line) and the actual yaw rate (solid line). ....	64
Figure 5.5. The output tracking error $e(t)$ . ....	65
Figure 5.6. The control input $u(t)$ . ....	65
Figure 5.7. The reference pitch rate (dashed line) and the actual pitch rate (solid line). ....	67
Figure 5.8. The reference yaw rate (dashed line) and the actual yaw rate (solid line). ....	68
Figure 5.9. The output tracking error $e(t)$ . ....	69
Figure 5.10. The control input $u(t)$ . ....	69

Figure 5.11. Pitch rate tracking error. ....	70
Figure 5.12. Yaw rate tracking error. ....	70
Figure 5.13. Control input for pitch rate. ....	71
Figure 5.14. Control input for yaw rate. ....	71
Figure 6.1. The reference velocity (dashed line) and the actual velocity (solid line). ....	76
Figure 6.2. The reference pitch rate (dashed line) and the actual pitch rate (solid line). ....	76
Figure 6.3. The reference roll rate (dashed line) and the actual roll rate (solid line). ....	77
Figure 6.4. The reference yaw rate (dashed line) and the actual yaw rate (solid line). ....	77
Figure 6.5. The output tracking error $e(t)$ . ....	78
Figure 6.6. The control input $u(t)$ . ....	78
Figure 6.7. The reference pitch rate (dashed line) and the actual pitch rate (solid line). ....	80
Figure 6.8. The reference yaw rate (dashed line) and the actual yaw rate (solid line). ....	81
Figure 6.9. The output tracking error $e(t)$ . ....	81
Figure 6.10. The control input $u(t)$ . ....	82
Figure 6.11. Pitch rate tracking error. ....	83
Figure 6.12. Yaw rate tracking error. ....	83
Figure 6.13. Control input for pitch rate. ....	84
Figure 6.14. Control input for yaw rate. ....	84
Figure 7.1. Tracking errors for the 5 runs of the robust controller simulation. ....	88
Figure 7.2. Tracking errors for the 5 runs of the robust optimal controller simulation. ....	89
Figure 7.3. Tracking errors for the 5 runs of the robust adaptive controller simulation. ....	89
Figure 7.4. Tracking errors for the 5 runs of the neural network based robust controller simulation. ....	90
Figure 7.5. Pitch rate tracking error results of twin rotor system. ....	91
Figure 7.6. Yaw rate tracking error results of twin rotor system. ....	91

## LIST OF TABLES

<u>Table</u>	<u>Page</u>
Table 3.1. Control input limits used in the simulations. ....	30
Table 3.2. Tabulated steady state error values for 5 simulation runs. ....	31
Table 3.3. Tabulated root mean square error values for 5 simulation runs. ....	31
Table 3.4. Limits of experimental system. ....	36
Table 4.1. Tabulated steady state error values for 5 simulation runs. ....	48
Table 4.2. Tabulated root mean square error values for 5 simulation runs. ....	49
Table 4.3. Tabulated performance index $J$ for different values of weighting matrix $R$ . ....	49
Table 4.4. Comparison of robust controller and robust optimal controller. ....	49
Table 4.5. Tabulated performance index $J$ for different values of weighting matrix $R$ . ....	52
Table 5.1. Tabulated steady state error values for 5 simulation runs. ....	62
Table 5.2. Tabulated root mean square error values for 5 simulation runs. ....	63
Table 5.3. Comparison of robust controller and robust adaptive controller. ....	63
Table 6.1. Tabulated steady state error values for 5 simulation runs. ....	79
Table 6.2. Tabulated root mean square error values for 5 simulation runs. ....	79
Table 6.3. Comparison of robust controller and neural network based robust con- troller. ....	79
Table 7.1. Comparison of proposed robust controllers. ....	86
Table 7.2. Tabulated values for the 5 runs for the developed controllers on the Osprey aircraft model while the initial conditions are varied as in (7.1). .	88
Table 7.3. Comparison of the proposed robust controllers. ....	90

# CHAPTER 1

## INTRODUCTION

### 1.1. Unmanned Aerial Vehicles and Their Classifications

Unmanned aerial vehicle (UAV) is an aerial vehicle that does not carry a human pilot or crew Department of Defense (2010). They can fly autonomously using pre-programmed flight plans or be piloted remotely.

UAVs are generally used in military operations such as exploration, intelligence and freight. They are also used in non-military services including fire fighting, surveillance of pipelines, coast guard and meteorological studies. They can keep a lethal or non-lethal payload. In future scenarios, collaborating UAVs will be expected to perform sophisticated maneuvers (such as air combat scenarios) How et al. (2012).

Nowadays, UAVs are categorized into four types according to performance characteristics such as range and/or altitude Austin (2010).

- High altitude long endurance (HALE) is a long-range UAV and it operates over 15000 meters altitude and 24+ hours endurance.
- Medium altitude long endurance (MALE) is a long-range UAV and it operates over 5000 – 15000 meters altitude and 24 hours endurance.
- Tactical UAV (TUAV) is a medium-range UAV and its range is between 100 and 300 kilometers.
- Mini UAV (MUAV) is a close-range UAV and its range is up to about 30 kilometers.

The main advantage of UAVs is their successful performance on dirty, dangerous and covert roles in military and civil missions. They are also preferred because of the economic reasons where their operating costs are much lower than manned aircrafts. In last decade, UAV studies increased significantly because of the evolution of computer technologies, lighter materials, new production technologies of small components, advances on navigation and communications technologies and advanced sensor systems. For these reasons, only the UAV inventory of USA increased more than 40 times from 2002 to 2010 Gertler (2012).

UAV studies are also very important for Turkey and other developing countries. Market on manned aircrafts is currently dominated by developed countries and developing countries obviously missed that race. However, UAV technologies became popular in the last decade and it can be a new competitive market for developing countries including Turkey Kahvecioglu and Oktal (2014).

## **1.2. On Modeling of UAVs**

Modeling a UAV is a complicated research problem and a reliable and complete model is unavailable mostly because of some hard to model aerodynamic effects. Generally, uncertainties are classified as structured and unstructured uncertainties. Structured uncertainties are generally known as parametric uncertainties where they are commonly written as multiplication of uncertain parameters with known and available terms. Unstructured uncertainties are related with the unmodeled dynamics, time-varying parameters or disturbances Levine (1996), Blanchini (2009).

There can always be some unmodeled and negligible effects during the flight such as an unmodeled delay in aircraft response or unmodeled limits of the aircraft states. One of these effects is that the parameters of the model can vary with the flight conditions. This problem is generally related to time varying parameters such as the weight of the aircraft which obviously decreases slowly during the flight because of the reduction of fuel. Unpredictable external effects such as a gust or gravity can alter the trajectory of a UAV. As a result of these, in most cases the model of a UAV is commonly considered as fully or partially uncertain.

Appropriate compensation strategies should be developed to deal with both structured and unstructured uncertainties. Due to their partially known structure, dealing with parametric uncertainties are usually less complicated than dealing with unstructured ones.

## **1.3. On Control of UAVs**

The flight control system of a UAV is required to ensure the flight stability and trajectory tracking with high accuracy while rejecting external disturbances, model uncertainties and other undesirable effects. Therefore, controller design of a UAV is critical and an inaccurate design, lack of robustness to parameter variations or a sensor failure could result in reduction in performance or crash of the aircraft.

Control development of a UAV is a difficult engineering problem. UAVs are non-linear systems because of external disturbances like inertial effects, gusts and gravity. Also parameter variations and model uncertainty complicate the control of a UAV. Compensating these undesired effects and controlling these devices are among the popular subjects within the control engineering community.

In many UAV control studies, model of the aircraft is assumed to be known Zhang et al. (2011), Enns and Keviczky (2006), Chen et al. (2006). These works are usually not realizable because accurate or partial model knowledge is generally unavailable in real world scenarios. Since model and disturbance uncertainties are inevitable for aircraft models, control designs that require minimum knowledge of system dynamics must be used in the control development for UAVs.

#### **1.4. Literature Search**

As discussed in the previous section, the nonlinear robust control design techniques are considered as the most feasible method to control UAVs. In the literature, feedback linearization is a nonlinear control technique. The main idea of feedback linearization is algebraically transforming the nonlinear system's dynamics to a linear system, then linear control techniques can be used to achieve control objective Slotine et al. (1991). Dynamic inversion (DI) technique is a special type of feedback linearization. DI applications are generally used for controlling nonlinear aircraft systems Stevens and Lewis (2003), Enns et al. (1994). The main idea of this technique is based on inverting the nonlinear dynamics and using them as a feedback. In Oppenheimer and Doman (2005) and Adams and Banda (1993), DI was used for stabilizing and tracking problems for unmanned aircraft systems. In Zhang et al. (2011), Enns and Keviczky (2006) and Cai et al. (2008), DI based flight control systems were developed for autonomous small-scale unmanned helicopters. DI was also utilized in quadrotor control studies Das et al. (2009) and Al-Hiddabi (2009).

In control studies, DI technique is generally utilized when system dynamics is known. However, in many cases, and specifically for flight systems, exact dynamics is not available. When the system dynamics is subject to uncertainties (be it structured or unstructured), DI based algorithms can have difficulty in compensating for these uncertainties due to the increase in inversion error. Another reason for the increase of inversion error is the uncertainties in the input matrix. To avoid the increase in inversion error, uncertainties must be compensated by fusing the DI technique with robust and/or adaptive

techniques.

### **1.4.1. Robust Control Studies**

Some past research was devoted to fusing DI technique with robust controllers. In Liu et al. (2006), a robust DI method based on sliding mode control was proposed for tracking control of an unpowered flying vehicle. Yamasaki et al. proposed a robust DI controller for tracking control of an unmanned aerial vehicle (UAV) Yamasaki et al. (2007). In John and Mija (2014), a robust control algorithm is developed for twin rotor system to improve the tracking performance. In Wang and Stengel (2005), a stochastic robust nonlinear control approach fused with DI technique was applied to a highly nonlinear complicated aircraft model. In Xie et al. (2011), a nonlinear dynamic inversion controller is combined with a PI controller to linearize the dynamics of UAVs. An asymptotic tracking controller is designed in MacKunis et al. (2010) which combines DI technique in conjunction with the robust integral of the signum of the error (RISE) technique for output tracking of an aircraft in the presence of parametric uncertainty and uncertain additive disturbances.

### **1.4.2. Optimal Control Studies**

In last years, optimal control studies are also designed for UAVs. In Nodland et al. (2013), an optimal controller design is introduced for trajectory tracking of a helicopter UAV model with known dynamics. Optimal control of a twin rotor system is presented in Phillips and Sahin (2014). In Satici et al. (2013), robust optimal control of a quadrotor UAV model is performed in presence of parametric uncertainty and measurement noise. In Kim et al. (2000), optimal control of robotic manipulators is considered in the presence of large modeling uncertainties and external disturbances. Asymptotic optimal control of an uncertain system is studied in Dupree et al. (2011) and Dupree (2009) where RISE control structure is utilized to learn the uncertain dynamics asymptotically.



### 1.4.3. Adaptive Control Studies

Some other past research fused adaptive control techniques with DI to compensate for linearly parameterizable uncertainties. For example, in Doman and Ngo (2002), DI technique based null-space injection controller, and in Tandale and Valasek (2005), an adaptive DI based switching control methodology was proposed to compensate for structured uncertainties. In Liu et al. (2004), DI was used in conjunction with a nonlinear model reference adaptive controller (MRAC) based on neural networks. An adaptive second-order sliding mode controller is designed for stabilizing and trajectory tracking of a twin rotor system Mondal and Mahanta (2012). In Chen et al. (2006), an adaptive dynamic inversion (ADI) based feedback linearization control was proposed for a flexible spacecraft. To compensate for modeling errors and external disturbances, Wang and Stengel designed an ADI controller for a miniature UAV Wang et al. (2011). In Calise and Rysdyk (1998), Calise and Rysdek proposed an ADI controller which was a combination of adaptive feedforward neural networks with feedback linearization. In Lavretsky and Hovakimyan (2005), a direct MRAC augmented with a DI controller is designed. ADI based controllers, while compensating for structured uncertainties, mostly failed to address unstructured uncertainties.

### 1.4.4. Neural Network Based Control Studies

To compensate for both structured and unstructured uncertainties, neural networks were utilized in conjunction with ADI based controllers Leitner et al. (1997), Shin (2005), Johnson and Calise (2000), Schumacher and Johnson (1999) and Rysdyk et al. (1999). However, in these works, while boundedness of the tracking error was ensured, asymptotic tracking was lost. Recently, Shin *et al.* developed a position tracking control system for a rotorcraft-based unmanned aerial vehicle (RUAV) by using RISE feedback and neural network feedforward terms Shin et al. (2010), Shin et al. (2012). Different from typical neural network based robust controllers, this method guaranteed semi-global asymptotic tracking. In Savran et al. (2006), a neural network based adaptive controller is designed for a high performance aircraft.

## 1.5. Motivation

In MacKunis (2009), MacKunis *et al.* fused the robust controller in Xian et al. (2004), Patre et al. (2008) with DI technique to achieve asymptotic output tracking for aircraft systems with an uncertain input matrix and subject to additive unknown nonlinear disturbances. However, the estimation of the input matrix and the signum of the time derivative of the output was utilized (*i.e.*, acceleration information was required) in the design of the controller. Acceleration measurements may be used in aircraft systems for system identification or control design. While acceleration measurements are available for some aircraft systems, utilizing these measurements in control design may not be preferred from control theory perspective. Additionally, although accelerometers may be seen as good and practical solutions in system identification and control applications, there are several reasons for not using them in some applications. Firstly, aside from onerousness in implementation, one needs to deal with sensor-related issues such as calibration and possible sensor failures. One way to avoid calibration requirements and sensor failures is, *if possible*, not to use them. For some cases, using them may be considered as redundant due to their costs. While the costs of sensors are decreasing rapidly, using them still adds to the cost of the overall system. Furthermore, aside from these, it should also be noted that using an additional sensor complicates the sensing system. The second deficit is that the utilization of the estimation of uncertain system matrices in the control input, it was not clear how the estimation procedure was designed in MacKunis (2009). This constitutes high risks for UAVs because estimation errors or a failure in estimation process can result in an inaccurate trajectory or a crash.

## 1.6. Contribution

In this thesis, model reference robust tracking control of an uncertain aircraft model subject to uncertainties is discussed. Specifically, the state and the input matrices are considered to be uncertain, and the dynamics is subject to an additive state-dependent nonlinear disturbance-like terms, and robustness to possible sensor noise is not considered within this thesis. Furthermore, to remove the need for acceleration measurements, we consider that only the output of the aircraft being available for control development. In the design of the controllers, the robust integral of the sign of the error component in Xian et al. (2004), Patre et al. (2008) is utilized. Since the input matrix of the aircraft system is considered to be uncertain, a matrix decomposition is utilized in the develop-

ment of the error system which does not require estimation of the uncertain input matrix. The control designs are based on Lyapunov based design and analysis techniques, and global asymptotic stability of the tracking error is ensured. Numerical simulation and experiment results are then presented to demonstrate the validity of the proposed robust controller.

The main contributions of this thesis are:

1. The unstructured uncertainties in the model are compensated based on the restriction that only the output of the aircraft is utilized in the robust control design, the need for acceleration measurements and the estimation of input matrix is removed.
2. The proposed robust controller is advanced to optimal, adaptive and neural network based robust controllers.
3. A matrix decomposition is proposed to compensate the uncertainty in the input gain matrix. This decomposition was previously utilized for some control problems, however its utilization for the problem considered in this thesis is novel.
4. A novel four-step Lyapunov based stability analysis is proposed to guarantee stability of the robust controllers designed in this thesis.
5. Different from most of the similar works, experimental verification is presented.

The results in this thesis are presented in the following publications:

1. Tanyer, I., E. Tatlicioglu, and E. Zergeroglu (2013). A Robust Dynamic Inversion Technique for Asymptotic Tracking Control of an Aircraft. In Asian Control Conference (ASCC), 2013.
2. Tanyer, I., E. Tatlicioglu, and E. Zergeroglu (2014). A robust adaptive tracking controller for an aircraft with uncertain dynamical terms. In International Federation of Automatic Control Congress, 2014.
3. Tanyer, I., E. Tatlicioglu, and E. Zergeroglu (2013). İha'lar için gürbüz takip denetçisi. In Signal Processing and Communications Applications Conference (SIU), 2013, IEEE.
4. Tanyer, I., E. Tatlicioglu, and E. Zergeroglu (2014). İha'lar için optimal gürbüz takip denetçisi. In National Conference of Turkish National Comitee of Automatic Control, 2014.

## 1.7. Organization of Thesis

In Chapter 2, mathematical background of the general aircraft model considered in this thesis and examples of the model are given. The dynamics of an Osprey aircraft and a twin rotor system are explained.

In Chapter 3, a new robust controller is presented for the general aircraft model given in Chapter 2. Control objective is to develop a stable control law that ensures that the output of the aircraft model tracks the output of a reference model. Lyapunov stability analysis are utilized to prove the global asymptotic stability of the tracking error. Numerical simulations and experimental studies with twin rotor system are performed to demonstrate the efficacy of the proposed controller.

In Chapter 4, the robust controller in Chapter 3 is advanced to a robust optimal controller. Control objective in Chapter 3 is satisfied, also a quadratic performance index is minimized by the help of an optimal term in the control input. Lyapunov stability analysis are utilized to prove the asymptotic stability of the tracking error and also optimality. Numerical simulations and experimental studies performed on the twin rotor system are given that demonstrate the efficacy of the proposed optimal controller.

In Chapter 5, the robust controller in Chapter 3 is advanced to a robust adaptive controller. An adaptive term is utilized with the robust controller to compensate for uncertain linearly parameterizable model parameters. Global asymptotic stability of the tracking error is shown via Lyapunov methods. Numerical simulations and experiments on the twin rotor system demonstrate the efficacy of the proposed adaptive controller.

In Chapter 6, the robust controller in Chapter 3 is advanced to a neural network based robust controller. A neural network term is utilized in the controller to compensate for some of the model uncertainties. Global asymptotic stability of the closed-loop system is shown. Numerical simulations and experiments on twin rotor system demonstrate the performance of the proposed neural network based robust controller.

In Chapter 7, comparisons of the simulation and experiment results is several aspects are given for the proposed controllers in Chapter 3 to 6.

In Chapter 8, the whole work in this thesis is summarized, the novelties are highlighted and the comparison of the numerical results which were given in Chapter 7 is interpreted. At the end of this chapter, open research problems associated with the works in this thesis are given as possible future works.

## CHAPTER 2

### AIRCRAFT MODEL

In this thesis, aircrafts with models of the following form are considered Stevens and Lewis (2003)

$$\begin{aligned}\dot{x} &= Ax + f + Bu \\ y &= Cx\end{aligned}\tag{2.1}$$

where  $x(t) \in \mathbb{R}^n$  denotes the state vector,  $A \in \mathbb{R}^{n \times n}$  is the constant state matrix,  $f(x, t) \in \mathbb{R}^n$  is a state-dependent nonlinear disturbance-like term (including gravity, inertial coupling and nonlinear gust modeling effects),  $B \in \mathbb{R}^{n \times m}$  is the constant input matrix,  $u(t) \in \mathbb{R}^m$  is the control input,  $C \in \mathbb{R}^{m \times n}$  is the output matrix, and  $y(t) \in \mathbb{R}^m$  is the output. The number of states is considered to be greater than the number of outputs (*i.e.*,  $n > m$ ). In the subsequent control development,  $C$  is considered to be known, while  $A$ ,  $B$  and  $f(x, t)$  are considered to be uncertain, thus, will not be utilized in the control design. The disturbance-like term  $f(x, t)$  is considered to be equal to the sum of state-dependent uncertainties, denoted by  $f_1(x) \in \mathbb{R}^n$ , and time-dependent uncertainties, denoted by  $f_2(t) \in \mathbb{R}^n$ . The time-dependent uncertainty vector  $f_2(t)$  is continuously differentiable and bounded up to its first order time derivative, and the state-dependent uncertainty vector  $f_1(x)$  depends on the state vector  $x(t)$  via trigonometric and/or bounded arguments only and thus it is assumed that  $f_1(x)$  and  $\partial f_1(x)/\partial x$  are bounded for all  $x(t)$  (see MacKunis (2009) for the precedence of this type of assumption). When the disturbance-like term  $f$  satisfies the above and provided that  $(A, B)$  is a controllable pair, then model in (2.1) is controllable Arapostathis et al. (2001).

#### 2.1. Examples of the Aircraft Model

In this section, two examples of the general aircraft model in (2.1) are given. First, the model of Osprey fixed wing aerial vehicle, which was utilized in the numerical simulations, is given. Next, the model of a twin rotor system, which was utilized in both numerical simulations and experimental studies, is given.

### 2.1.1. Osprey Aircraft

The model of Osprey fixed wing aerial vehicle in MacKunis et al. (2010), MacKunis (2009), which is a commercially available, low-cost experimental flight testbed, was used in the numerical simulations. A photograph of the Osprey aircraft testbed is given in Figure 2.1. Provided the standard assumption that the longitudinal and lateral subsystems of the aircraft are decoupled, the state space model for the Osprey aircraft testbed can be represented as in (2.1). The system matrices  $A \in \mathbb{R}^{8 \times 8}$ ,  $B \in \mathbb{R}^{8 \times 4}$  and  $C \in \mathbb{R}^{4 \times 8}$  are given as<sup>1</sup>

$$A = \begin{bmatrix} A_{lon} & 0_{4 \times 4} \\ 0_{4 \times 4} & A_{lat} \end{bmatrix} \quad B = \begin{bmatrix} B_{lon} & 0_{4 \times 2} \\ 0_{4 \times 2} & B_{lat} \end{bmatrix} \quad C = \begin{bmatrix} C_{lon} & 0_{2 \times 4} \\ 0_{2 \times 4} & C_{lat} \end{bmatrix} \quad (2.2)$$

where  $A_{lon}, A_{lat} \in \mathbb{R}^{4 \times 4}$ ,  $B_{lon}, B_{lat} \in \mathbb{R}^{4 \times 2}$ ,  $C_{lon}, C_{lat} \in \mathbb{R}^{2 \times 4}$  are system matrices for the longitudinal and lateral subsystems. The state vector  $x(t) = [x_{lon}^T, x_{lat}^T]^T \in \mathbb{R}^8$  where  $x_{lon}(t), x_{lat}(t) \in \mathbb{R}^4$  denote the longitudinal and lateral state vectors and are defined as

$$x_{lon} = \begin{bmatrix} v \\ \alpha \\ q \\ \theta \end{bmatrix} \quad x_{lat} = \begin{bmatrix} \gamma \\ p \\ \mu \\ \phi \end{bmatrix} \quad (2.3)$$

where the state variables  $v(t)$ ,  $\alpha(t)$ ,  $q(t)$ ,  $\theta(t)$ ,  $\gamma(t)$ ,  $p(t)$ ,  $\mu(t)$  and  $\phi(t)$  are velocity, angle of attack, pitch rate, pitch angle, side slip angle, roll rate, yaw rate and bank angle, respectively.



Figure 2.1. Osprey aircraft testbed.

The primary movements of the aircrafts are pitch, roll and yaw Stevens and Lewis (2003). Demonstrations of these movements are given in Figures 2.2-2.4. Pitching is the

---

<sup>1</sup>Throughout the thesis,  $I_n$  and  $0_{m \times r}$  will be used to represent an  $n \times n$  standard identity matrix and an  $m \times r$  zero matrix, respectively.

movement of the nose of the aircraft up and down along an axis running from wing to wing. Pitch angle  $\theta$  and angle of attack  $\alpha$  are demonstrated in Figure 2.2. Among the states in (2.3), pitch rate is the derivative of the pitch angle

$$q(t) = \dot{\theta}(t). \quad (2.4)$$

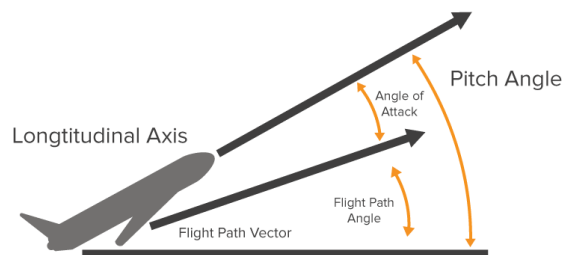


Figure 2.2. Pitch angle.

Rolling is the rotation movement along an axis running from nose of the aircraft to tail. The roll angle is also known as bank angle on a fixed wing aircraft. A demonstration of the roll movement is given in Figure 2.3. The roll rate in (2.3) is the derivative of the bank angle

$$p(t) = \dot{\phi}(t). \quad (2.5)$$

Yaw movement is the turning left or right of nose of the aircraft. Yaw angle is the angle between north and the projection of the aircraft longitudinal axis onto the horizontal plane. A demonstration of the sideslip angle is given in Figure 2.4.

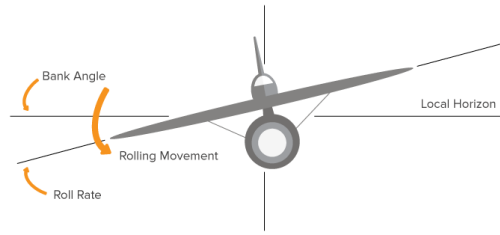


Figure 2.3. Bank angle.

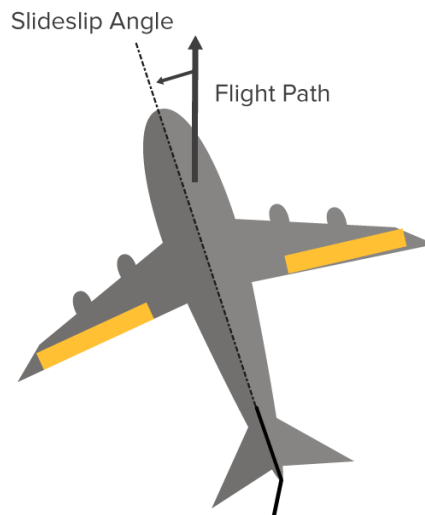


Figure 2.4. Sideslip angle.



In the numerical simulations, tracking control of velocity, pitch rate, roll rate and yaw rate are considered. These four states are controlled by four control inputs. Control inputs are thrust for the forward velocity, aileron for the roll movement, elevator for the pitch movement and rudder for the yaw movement. In Figures 2.5-2.7, primary control surfaces of the aircraft systems are given. The control input  $u(t) \triangleq [u_{lon}^T, u_{lat}^T]^T \in \mathbb{R}^4$  where  $u_{lon}(t), u_{lat}(t) \in \mathbb{R}^2$  denote longitudinal and lateral control inputs and are given as

$$u_{lon} = \begin{bmatrix} u_e \\ u_t \end{bmatrix} \quad u_{lat} = \begin{bmatrix} u_a \\ u_r \end{bmatrix} \quad (2.6)$$

where the control inputs  $u_e(t), u_t(t), u_a(t)$  and  $u_r(t)$  are elevator deflection angle, control thrust, aileron deflection angle and rudder deflection angle, respectively.

Thrust is a mechanical force generated by the engines to move the aircraft through the air. It is a result of a propulsion system which is usually generated through the reaction of accelerating a mass of gas. Examples of the thrust sources are propeller, rotating fan, jet engine or a rocket engine.

Ailerons control the roll movement along the longitudinal axis. They are mounted on the trailing edge of each wing and move in opposite directions. A demonstration of an aileron is given in Figure 2.5.

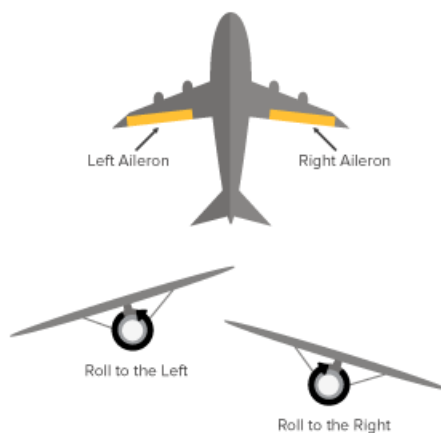


Figure 2.5. Aileron of a fixed wing aircraft.

Elevators control pitch movement along the lateral axis. They are mounted at the rear end of the aircraft as a part of the tail. A demonstration of an elevator is given in Figure 2.6.

The rudder controls yaw movement of the airplane. Like the other primary control surfaces, the rudder is a movable surface located to a fixed surface. Generally it is

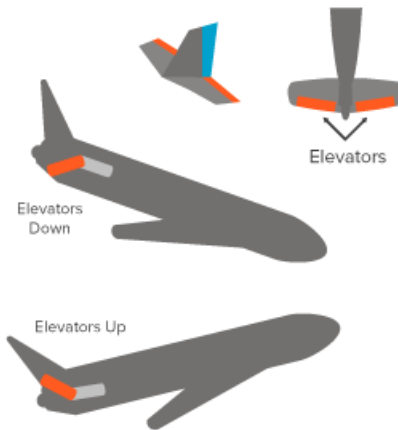


Figure 2.6. Elevator of a fixed wing aircraft.

mounted at the rear end of the aircraft as elevators. A demonstration of a rudder is given in Figure 2.7.

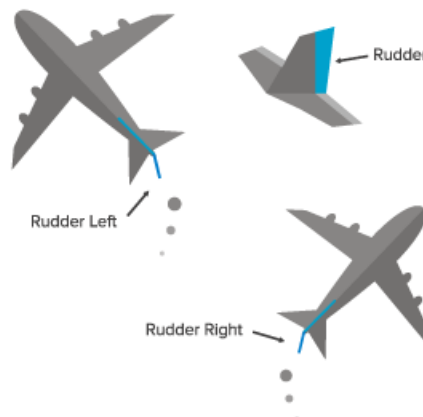


Figure 2.7. Rudder of a fixed wing aircraft.

Following system matrices of the Osprey aircraft, are based on experimentally determined data at a cruising velocity of 25 [m/s] and at an altitude of 60 [m]

$$A_{lon} = \begin{bmatrix} -0.15 & 11.08 & 0.08 & 0 \\ -0.03 & -7.17 & 0.83 & 0 \\ 0 & -37.35 & -9.96 & 0 \\ 0 & 0 & 1 & 0 \end{bmatrix} \quad A_{lat} = \begin{bmatrix} -0.69 & -0.03 & -0.99 & 0 \\ -3.13 & -12.92 & 1.1 & 0 \\ 17.03 & -0.10 & -0.97 & 0 \\ 0 & 1 & -0.03 & 0 \end{bmatrix}$$

$$\begin{aligned}
B_{lon} &= \begin{bmatrix} 3 \times 10^{-3} & 0.06 \\ 10^{-5} & 10^{-4} \\ 0.98 & 0 \\ 0 & 0 \end{bmatrix} & B_{lat} &= \begin{bmatrix} 0 & 0 \\ 1.5 & -0.02 \\ -0.09 & 0.17 \\ 0 & 0 \end{bmatrix} \\
C_{lon} &= \begin{bmatrix} 0 & 0 & 1 & 0 \\ 1 & 0 & 0 & 0 \end{bmatrix} & C_{lat} &= \begin{bmatrix} 0 & 1 & 0 & 0 \\ 0 & 0 & 1 & 0 \end{bmatrix}.
\end{aligned} \tag{2.7}$$

Dynamical system of the Osprey aircraft above is said to be stable and controllable from the state and input matrices. The state-dependent nonlinear disturbance-like term  $f(x, t) \triangleq [f_{lon}(x, t)^T, f_{lat}(x, t)^T]^T$  with  $f_{lon}(x, t), f_{lat}(x, t) \in \mathbb{R}^4$  being defined as

$$f_{lon} \triangleq \begin{bmatrix} -9.81 \sin \theta \\ 0 \\ 0 \\ 0 \end{bmatrix} + g(x), \quad f_{lat} \triangleq \begin{bmatrix} 0.39 \sin \phi \\ 0 \\ 0 \\ 0 \end{bmatrix} \tag{2.8}$$

where  $g(x) \in \mathbb{R}^4$  is defined as

$$g \triangleq \frac{1}{V_0} \frac{U_{ds}}{2} [1 - \cos(\frac{\pi d_g}{H})] \begin{bmatrix} -11.1 \\ 7.2 \\ 37.4 \\ 0 \end{bmatrix} \tag{2.9}$$

where  $H$  denotes the distance along the airplane's flight path for the gust to reach its peak velocity,  $V_0$  is the forward velocity of the aircraft when it enters the gust,  $d_g = \int_{t_1}^{t_2} V(t) dt$  represents the distance penetrated into the gust and  $U_{ds}$  is the design gust velocity as specified in Part (2002). Parameter values were chosen as  $U_{ds} = 10.12[m/s]$ ,  $H = 15.24[m]$  and  $V_0 = 25[m/s]$  MacKunis (2009).

### 2.1.2. Twin Rotor System

The twin rotor system is a low cost experimental system which looks like a simplified helicopter model. Twin rotor systems consist of two rotors, namely the main rotor and the tail rotor. Each rotor is driven by a DC motor. The twin rotor system used in this work is manufactured in the Control Laboratory by the funding received from IYTE University research grant with grant number 2010-IYTE-15. A photograph of the twin rotor system is given in Figure 2.8.

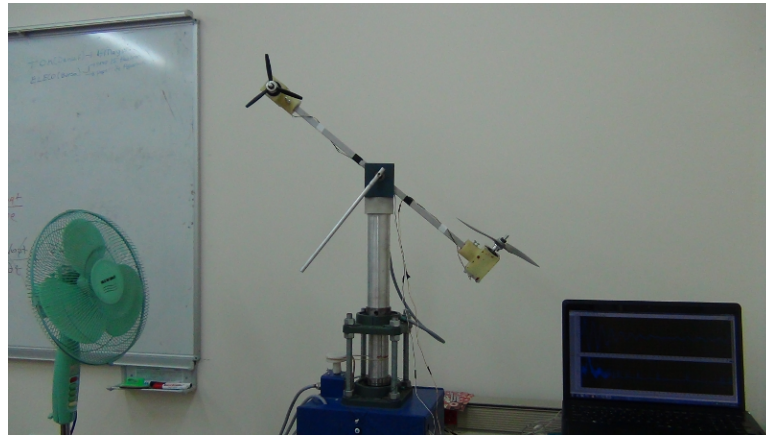


Figure 2.8. Twin rotor system in control laboratory.

The block diagram of the twin rotor system is given in Figure 2.9 Dogan (2014), Bayrak et al. (2015). Encoder readers obtain the data coming from the optical encoders and they compute the angular positions. Position and velocity transmitter circuits send the angular position and angular velocity data to the main circuit via universal asynchronous receiver/transmitter. Main circuit collects the angular positions and the angular velocities, and sends them to the computer via RS232 connection. The computer evaluates the control inputs (by using LabVIEW) which are the required voltage values for the two DC motors, and sends the control input data to the motor controller circuits. Then the motor controller circuit drives the motors.

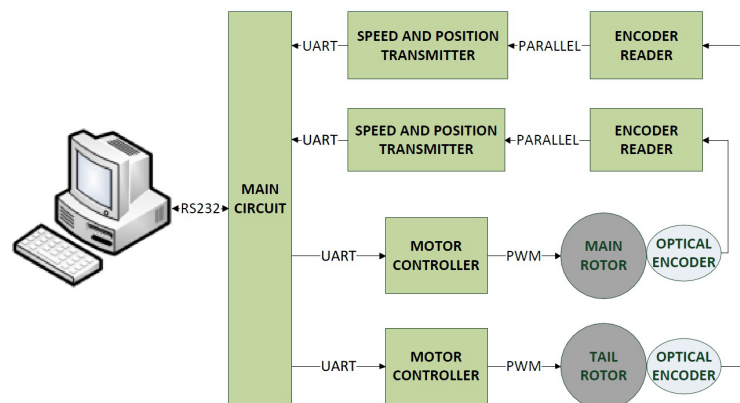


Figure 2.9. The block diagram of the twin rotor system.

Provided the standard assumption that longitudinal and lateral subsystems of the twin rotor system are decoupled, its state space model can be also represented as in (2.1) with the system matrices  $A \in \mathbb{R}^{4 \times 4}$ ,  $B \in \mathbb{R}^{4 \times 2}$  and  $C \in \mathbb{R}^{2 \times 4}$  are given as

$$A = \begin{bmatrix} A_{lon} & 0_{2 \times 2} \\ 0_{2 \times 2} & A_{lat} \end{bmatrix} \quad B = \begin{bmatrix} B_{lon} & 0_{2 \times 1} \\ 0_{2 \times 1} & B_{lat} \end{bmatrix} \quad C = \begin{bmatrix} C_{lon} & 0_{1 \times 2} \\ 0_{1 \times 2} & C_{lat} \end{bmatrix} \quad (2.10)$$

where  $A_{lon}, A_{lat} \in \mathbb{R}^{2 \times 2}$ ,  $B_{lon}, B_{lat} \in \mathbb{R}^{2 \times 1}$ ,  $C_{lon}, C_{lat} \in \mathbb{R}^{1 \times 2}$  are system matrices for longitudinal and lateral subsystems. The state vector  $x(t) = [x_{lon}^T, x_{lat}^T]^T \in \mathbb{R}^4$  where  $x_{lon}(t), x_{lat}(t) \in \mathbb{R}^2$  denote the longitudinal and lateral state vectors and are defined as

$$x_{lon} = \begin{bmatrix} \theta_p \\ \omega_p \end{bmatrix} \quad x_{lat} = \begin{bmatrix} \theta_y \\ \omega_y \end{bmatrix} \quad (2.11)$$

where the state variables  $\theta_p, \omega_p, \theta_y$  and  $\omega_y$  are pitch angle, pitch rate, yaw angle and yaw rate, respectively. Primary movements of the twin rotor system is demonstrated in Figure 2.10. Among the states in (2.11), pitch rate is the derivative of the pitch angle

$$\omega_p(t) = \dot{\theta}_p(t) \quad (2.12)$$

while the yaw rate is the derivative of the yaw angle

$$\omega_y(t) = \dot{\theta}_y(t). \quad (2.13)$$

In the experiments, tracking control of pitch rate and yaw rate of the twin rotor system are considered. These states are controlled by two control inputs which are the supply voltages of the DC motors.

Following system matrices of the twin rotor system, are based on experimentally determined data

$$A_{lon} = \begin{bmatrix} 0 & 1 \\ -10.08 & -0.92 \end{bmatrix} \quad A_{lat} = \begin{bmatrix} 0 & 1 \\ -12.72 & -37.27 \end{bmatrix}$$

$$B_{lon} = \begin{bmatrix} -55.47 \\ 25.49 \end{bmatrix} \quad B_{lat} = \begin{bmatrix} -1.03 \\ 1.70 \end{bmatrix}$$

$$C_{lon} = \begin{bmatrix} 0 & 1 \end{bmatrix} \quad C_{lat} = \begin{bmatrix} 0 & 1 \end{bmatrix}. \quad (2.14)$$

Dynamical system of the twin rotor system above is said to be stable and controllable from the state and input matrices.

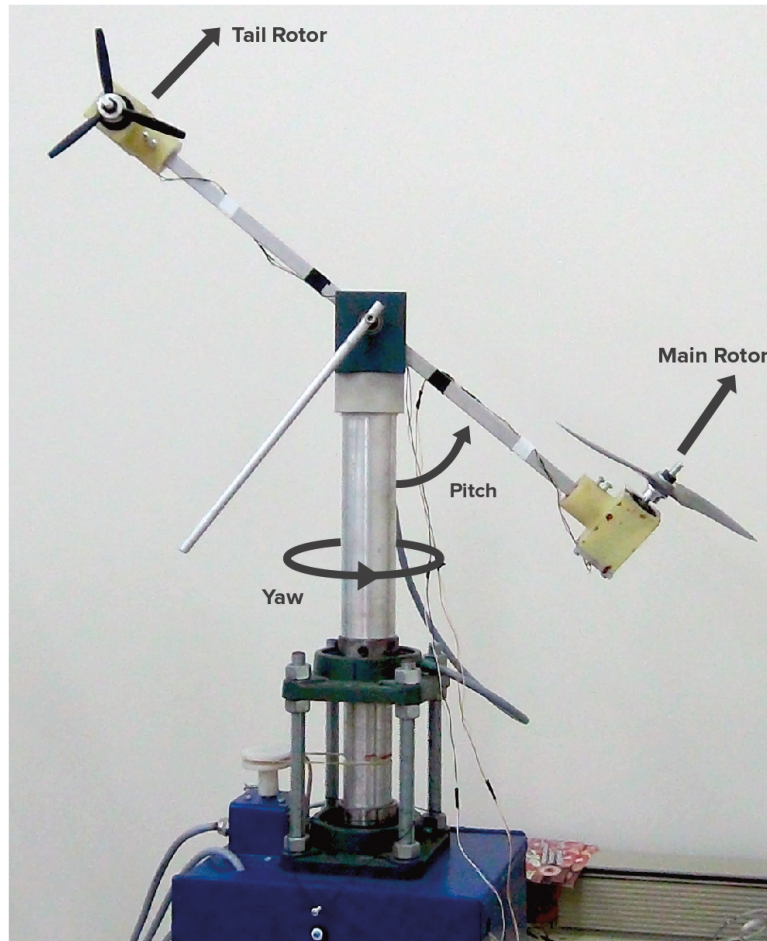


Figure 2.10. The primary movements of the twin rotor system.

## CHAPTER 3

### ROBUST CONTROL OF UAV

#### 3.1. Abstract

In this chapter, design and analysis of a robust control algorithm is presented. Firstly, the output tracking error is introduced then an auxiliary error term is defined which is motivated by to avoid second order time derivatives in the stability analysis. When the system dynamics are substituted into the auxiliary error term, the control input is multiplied with an uncertain gain matrix. This constitutes a problem in the control design which is solved by a matrix decomposition. Next, the dynamics of the auxiliary error term is obtained where the uncertain terms grouped as the ones that can be bounded by constants and the ones that can be bounded by error terms. The control design is then presented where integral of the signum of the error terms are fused with a proportional integral controller. Then the stability of the closed-loop error system is investigated via Lyapunov type analysis. The control problem mandates the analysis to be performed in four steps. Specifically, first the boundedness of the closed-loop system is proven. The results of this one then utilized to provide an upper bound on the integral of the absolute value of time derivatives of the entries of the output tracking error. This upper bound is then utilized in the design of a novel Lyapunov like integral function which is fused with the Lyapunov function chosen to ensure boundedness. Finally, global asymptotic stability is proven. The performance of the proposed robust controller is then evaluated by numerical simulations on an Osprey aircraft and a twin rotor system and by experiments on a twin rotor system.

#### 3.2. Control Design

The control design objective is to develop a robust control law that ensures that the output  $y(t)$  of the aircraft model in (2.1) tracks the output of a reference model that will be given subsequently, and additionally, all closed-loop signals are required to remain bounded.

The subsequent development is derived based on the restriction that only the out-

put  $y(t)$  is available for control design purposes.

The reference model is represented as

$$\begin{aligned}\dot{x}_m &= A_m x_m + B_m u_m \\ y_m &= C x_m\end{aligned}\tag{3.1}$$

where  $x_m(t) \in \mathbb{R}^n$  is the reference state vector,  $A_m \in \mathbb{R}^{n \times n}$  is the reference state matrix,  $B_m \in \mathbb{R}^{n \times m}$  is the reference input matrix,  $u_m(t) \in \mathbb{R}^m$  is the reference input,  $y_m(t) \in \mathbb{R}^m$  is the reference output, and  $C$  is the same output matrix in (2.1). The reference state matrix  $A_m$  is chosen to be Hurwitz, and the reference input  $u_m(t)$  and its time derivative are designed as bounded functions. Linear analysis tools can then be utilized along with these to prove that  $x_m(t)$ ,  $\dot{x}_m(t)$ ,  $\ddot{x}_m(t)$  and thus,  $y_m(t)$ ,  $\dot{y}_m(t)$ ,  $\ddot{y}_m(t)$  are bounded functions.

To quantify the tracking control objective, an output tracking error, denoted by  $e(t) \in \mathbb{R}^m$ , is defined as

$$\begin{aligned}e &\triangleq y - y_m \\ &= C(x - x_m)\end{aligned}\tag{3.2}$$

where (2.1) and (3.1) were utilized to obtain the second line. From the structure of the tracking error in (3.2), it is clear that when the tracking control objective is met, output tracking is ensured in the following sense

$$y(t) \rightarrow y_m(t).\tag{3.3}$$

In the subsequent development, the error system will be designed based on an auxiliary tracking error, denoted by  $r(t) \in \mathbb{R}^m$ , which is defined as

$$r \triangleq \dot{e} + \Lambda e\tag{3.4}$$

where  $\Lambda \in \mathbb{R}^{m \times m}$  is a constant, positive definite, diagonal control gain matrix. The main benefit of utilizing  $r(t)$  in the control development is to discard the second derivatives of the states from the Lyapunov stability analysis. It is noted that since only the output of the aircraft  $y(t)$  is available then  $\dot{e}(t)$  and thus  $r(t)$  are not available, and cannot be utilized in the control design.

After substituting (2.1), (3.1) and (3.2) into (3.4), following expression can be obtained

$$r = CAx + \Omega u + Cf - CA_m x_m - CB_m u_m + \Lambda e\tag{3.5}$$

where  $\Omega \triangleq CB \in \mathbb{R}^{m \times m}$  is an auxiliary constant matrix. Since  $B$  is uncertain, then  $\Omega$  is uncertain as well. Furthermore, neither symmetry nor positive definiteness of  $\Omega$  are



known. Given these restrictions, the SDU decomposition in Kokotović et al. (2003) and Tao (2003) is applied to  $\Omega$  as

$$\Omega = SDU \quad (3.6)$$

where  $S \in \mathbb{R}^{m \times m}$  is a constant, symmetric, positive definite matrix,  $D \in \mathbb{R}^{m \times m}$  is a constant, diagonal matrix with entries  $\pm 1$  and  $U \in \mathbb{R}^{m \times m}$  is a constant, unity upper triangular matrix.

The SDU decomposition of  $\Omega$  for our simulation model, for the model of the twin rotor system and also for different aircraft models in the literature resulted in the diagonal matrix  $D$  being equal to an identity matrix. However, for the completeness of the presentation, the subsequent controller will be designed to be applicable to any aircraft model without imposing any restrictions on  $D$ .

The time derivative of (3.5) is obtained as

$$\dot{r} = CA\dot{x} + SDU\dot{u} + C\dot{f} - CA_m\dot{x}_m - CB_m\dot{u}_m + \Lambda\dot{e} \quad (3.7)$$

where the SDU decomposition in (3.6) was utilized. After premultiplying (3.7) with  $M \triangleq S^{-1} \in \mathbb{R}^{m \times m}$ , following expression can be obtained

$$M\dot{r} = M[CA\dot{x} + C\dot{f} - CA_m\dot{x}_m - CB_m\dot{u}_m + \Lambda\dot{e}] + DU\dot{u}. \quad (3.8)$$

It is noted that, since  $S$  is symmetric and positive definite, then so is  $M$ . An auxiliary vector, denoted by  $N(x, \dot{x}, t) \in \mathbb{R}^m$  is defined as

$$N \triangleq M[CA\dot{x} + C\dot{f} - CA_m\dot{x}_m - CB_m\dot{u}_m + \Lambda\dot{e}] + e \quad (3.9)$$

which can be utilized to rewrite the expression in (3.8) as

$$M\dot{r} = N - e + DU\dot{u}. \quad (3.10)$$

The auxiliary vector  $N$  in (3.9) can be partitioned as

$$N = N_d + \tilde{N} \quad (3.11)$$

where  $N_d(t) \in \mathbb{R}^m$  contains functions that can be bounded by constants in the sense that

$$|N_{d,i}| \leq \zeta_{N_i} \quad \forall i = 1, \dots, m \quad (3.12)$$

where  $N_{d,i}(t) \in \mathbb{R}$  is the  $i$ th entry of  $N_d$ ,  $\zeta_{N_i} \in \mathbb{R}$  are positive bounding constants and  $\tilde{N}(x, \dot{x}, e, \dot{e}) \in \mathbb{R}^m$  contains functions that can be bounded by error terms as

$$|\tilde{N}_i| \leq \rho_i \|z\| \quad \forall i = 1, \dots, m \quad (3.13)$$

where  $\tilde{N}_i(t) \in \mathbb{R}$  is the  $i$ th entry of  $\tilde{N}$ ,  $\rho_i \in \mathbb{R}$  are positive bounding constants and  $z(t) \in \mathbb{R}^{2m}$  is the combined error defined as

$$z \triangleq \begin{bmatrix} e \\ r \end{bmatrix}. \quad (3.14)$$

In view of (3.12) and (3.13), the entries of the auxiliary vector  $N$  can be bounded as

$$|N_i| \leq \rho_i \|z\| + \zeta_{N_i} \quad \forall i = 1, \dots, m. \quad (3.15)$$

Based on the subsequent stability analysis, the control input is designed as

$$u = -DK[e(t) - e(0) + \Lambda \int_0^t e(\tau) d\tau] - D\Pi \quad (3.16)$$

where  $\Pi(t) \in \mathbb{R}^m$  is an auxiliary filter term updated according to

$$\dot{\Pi}(t) = \beta \text{Sgn}(e(t)) \text{ with } \Pi(0) = 0_{m \times 1} \quad (3.17)$$

where  $\beta \in \mathbb{R}^{m \times m}$  is a constant, positive definite, diagonal control gain matrix,  $\text{Sgn}(\cdot)$  denotes the vector signum function, and  $K \in \mathbb{R}^{m \times m}$  is a constant, positive definite, diagonal control gain matrix designed as

$$K = I_m + k_g I_m + \text{diag}\{k_{d,1}, k_{d,2}, \dots, k_{d,m-1}, 0\} \quad (3.18)$$

with  $k_g, k_{d,1}, \dots, k_{d,m-1} \in \mathbb{R}$  being positive gains.

The controller in (3.16) and (3.17) is a proportional integral controller fused with integral of the signum of the error for uncertainty compensation. Different from the sliding mode controllers, the controller in (3.16) and (3.17) is not discontinuous.

The time derivative of the control input in (3.16) is obtained as

$$\dot{u} = -DKr - D\beta \text{Sgn}(e) \quad (3.19)$$

where (3.4) and (3.17) were utilized. After substituting (3.19) into (3.10), following closed-loop error system is obtained

$$M\dot{r} = N - e - DUD\beta \text{Sgn}(e) - D(U - I_m)DKr - Kr. \quad (3.20)$$

Since  $U$  is unity upper triangular then  $U - I_m$  is strictly upper triangular, thus  $D(U - I_m)DKr$  term can be written as

$$D(U - I_m)DKr = \begin{bmatrix} \Phi \\ 0 \end{bmatrix} \quad (3.21)$$

where the entries of  $\Phi(r) \in \mathbb{R}^{(m-1) \times 1}$  are defined as

$$\Phi_i = d_i \sum_{j=i+1}^m d_j k_j U_{i,j} r_j \text{ for } i = 1, \dots, (m-1). \quad (3.22)$$

Since  $d_i = \pm 1 \forall i = 1, \dots, m$ , following upper bound can be obtained for the entries of  $\Phi$

$$|\Phi_i| \leq \zeta_{\Phi_i} \|z\| \quad (3.23)$$

where  $\zeta_{\Phi_i}$  are positive bounding constants. It is important to highlight that  $\zeta_{\Phi_i}$  depends on the control gains  $k_{i+1}, \dots, k_m$ .

### 3.3. Stability Analysis

**Theorem 3.3.1** *The robust controller given in (3.16) and (3.17) ensures global asymptotic tracking in the sense that*

$$\|e(t)\| \rightarrow 0 \text{ as } t \rightarrow \infty \quad (3.24)$$

*provided that the entries of the control gain matrices  $K$  and  $\beta$  are selected by using the following procedure:*

1. For  $i = m$ ,  $\beta_m$  is selected according to

$$\beta_m \geq \zeta_{\Theta_m} \left(1 + \frac{\gamma_2}{\Lambda_m}\right) \quad (3.25)$$

*and from  $i = m - 1$  to  $i = 1$ ,  $\beta_i$  are selected according to*

$$\beta_i \geq \left( \zeta_{\Theta_i} + \sum_{j=i+1}^m \zeta_{\Psi_j} \beta_j \right) \left(1 + \frac{\gamma_2}{\Lambda_i}\right) \quad (3.26)$$

*where  $\zeta_{\Theta_i}, \zeta_{\Psi_i}, \gamma_2 \in \mathbb{R}$  are positive bounding constants and the subscript  $i = 1, \dots, m$  denotes the  $i$ -th element of the vector or the diagonal matrix.*

2. Control gain  $k_g$  is chosen big enough to decrease the constant  $\sum_{i=1}^m \frac{\rho_{\Delta,i}^2}{4k_g}$  where  $\rho_{\Delta,i}$  are positive bounding constants.
3. Control gains  $k_{d,i}$ ,  $i = 1, \dots, (m-1)$  are chosen big enough to decrease the constant  $\sum_{i=1}^{m-1} \frac{\zeta_{\Phi_i}^2}{4k_{d,i}}$ .

**Proof** The proof of the theorem consists of four subproofs. Firstly, in Appendix A, boundedness of all the signals under the closed-loop operation will be presented. In

Appendix A,  $\Theta_i = N_{d,i}$  and  $\Delta_i = \tilde{N}_i$  are utilized in (A.3). Secondly, in Appendix B, a supporting lemma and its proof is presented. The proof of this lemma provides us to form an upper bound on the terms  $\int_0^t |\dot{e}_i(\sigma)| d\sigma$ , which will then be utilized in the next part of the proof. In Appendix C, the non-negativeness of an auxiliary integral term will be demonstrated with  $\Theta_i = N_{d,i}$ . Finally, in Appendix D, the asymptotic convergence of the output tracking error is proven.

The stability analysis mandates the control gains to be chosen to satisfy the procedure detailed in Theorem 3.3.1. However, this is a tedious procedure. To address this issue, the authors utilized the self-tuning algorithm developed in Bidikli et al. (2013) and Bidikli et al. (2014) which was designed for similar type of robust controllers.

### 3.4. Simulation Results

In this section, two numerical simulations performed on the models of Osprey aircraft and twin rotor system are presented.

#### 3.4.1. Osprey Aircraft

Following system matrices were utilized for the reference model

$$\begin{aligned}
 A_{lonm} &= \begin{bmatrix} 0.6 & -1.1 & 0 & 0 \\ 2 & -2.2 & 0 & 0 \\ 0 & 0 & -4 & -600 \\ 0 & 0 & 0.1 & -10 \end{bmatrix} & A_{latm} &= \begin{bmatrix} -4 & -600 & 0 & 0 \\ 0.1 & -10 & 0 & 0 \\ 0 & 0 & 0.6 & -1.1 \\ 0 & 0 & 2 & -2.2 \end{bmatrix} \\
 B_{lonm} &= \begin{bmatrix} 0 & 0.5 \\ 0 & 0 \\ 10 & 0 \\ 0 & 0 \end{bmatrix} & B_{latm} &= \begin{bmatrix} 0 & 0 \\ 10 & 0 \\ 0 & 0.5 \\ 0 & 0 \end{bmatrix}. & (3.27)
 \end{aligned}$$

Reference model is said to be stable and controllable from the state and input matrices above. Entries of the reference input  $u_m(t) \in \mathbb{R}^4$  are elevator deflection angle, control thrust, aileron deflection angle and rudder deflection angle, respectively, and was designed

as

$$u_m = \begin{bmatrix} 0.2[u_s(t-2) - u_s(t-4)] \\ 3 \\ 0.2[u_s(t-4) - u_s(t-6)] \\ 0.2 \sin(t)[u_s(t-6) - u_s(t-10)] \end{bmatrix} \quad (3.28)$$

where  $u_s$  is the unit step function and initial condition of the system was chosen as

$$x(0) = \begin{bmatrix} 1 \\ 0 \\ 0.2 \\ 0 \\ 0 \\ 0.2 \\ 0.2 \\ 0 \end{bmatrix}. \quad (3.29)$$

The self-tuning algorithm in Bidikli et al. (2013) and Bidikli et al. (2014) was used as an add-on and after the algorithm converged, numerical simulations were re-run for the final values of the control gains. Specifically, control gains  $\beta$  and  $K$  were obtained from the self-tuning algorithm as

$$\beta = \begin{bmatrix} 72.4 & 0 & 0 & 0 \\ 0 & 81 & 0 & 0 \\ 0 & 0 & 79.6 & 0 \\ 0 & 0 & 0 & 80.8 \end{bmatrix} \quad K = \begin{bmatrix} 300 & 0 & 0 & 0 \\ 0 & 300.03 & 0 & 0 \\ 0 & 0 & 300 & 0 \\ 0 & 0 & 0 & 300.1 \end{bmatrix} \quad (3.30)$$

and  $\Lambda$  was chosen as follows

$$\Lambda = \begin{bmatrix} 2 & 0 & 0 & 0 \\ 0 & 2 & 0 & 0 \\ 0 & 0 & 2 & 0 \\ 0 & 0 & 0 & 2 \end{bmatrix}. \quad (3.31)$$

In the simulations, the output vector consisted of pitch rate and forward velocity for the longitudinal subsystem, and roll rate and yaw rate for the lateral subsystem. Sampling time was chosen as 0.001 seconds.

The tracking performance, tracking error and the control inputs are presented in Figures 3.1-3.4, 3.5 and 3.6, respectively. From Figures 3.1-3.4 and 3.5, it is clear that the tracking objective was satisfied. Control surface limits are given in Table 3.1 MacKunis

(2009). These limits were determined via the detailed specifications sheet given with the Futaba S3010 standard ball bearing servo. From Figure 3.6, 3.7 and Table 3.1, it is clear that the control inputs are in acceptable limits. In Figure 3.8 and 3.9, result of a specific study is given. A high disturbance is applied to the system at the third second of the simulation run and the proposed robust controller compensated this kind of disturbance.

In Tables 3.2 and 3.3, average maximum steady state error and average root mean square error are presented. Five Monte Carlo simulations are performed for different initial state values. Maximum steady state error is defined as the mean of the last 5 seconds of the error values. The error values in Tables 3.2 and 3.3 show that the proposed controller ensured asymptotic tracking for different initial values of the states.

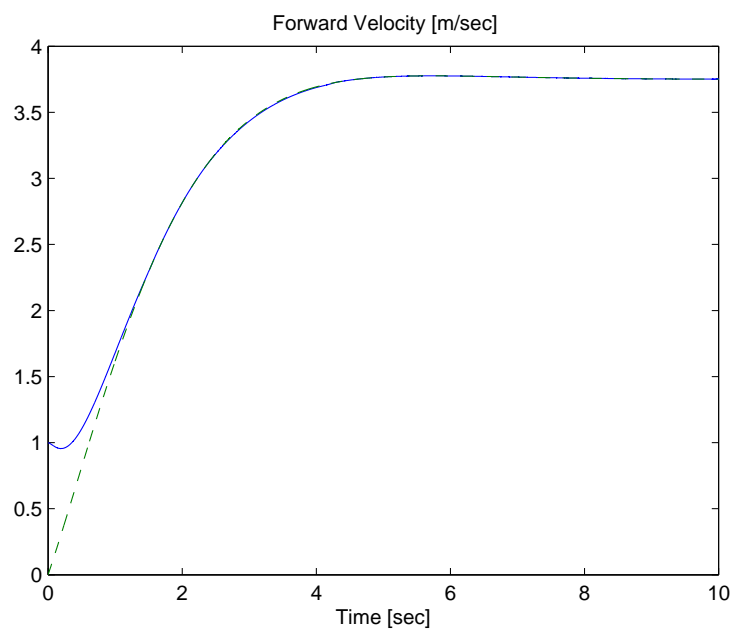


Figure 3.1. The reference forward velocity (dashed line) and the actual forward velocity (solid line).

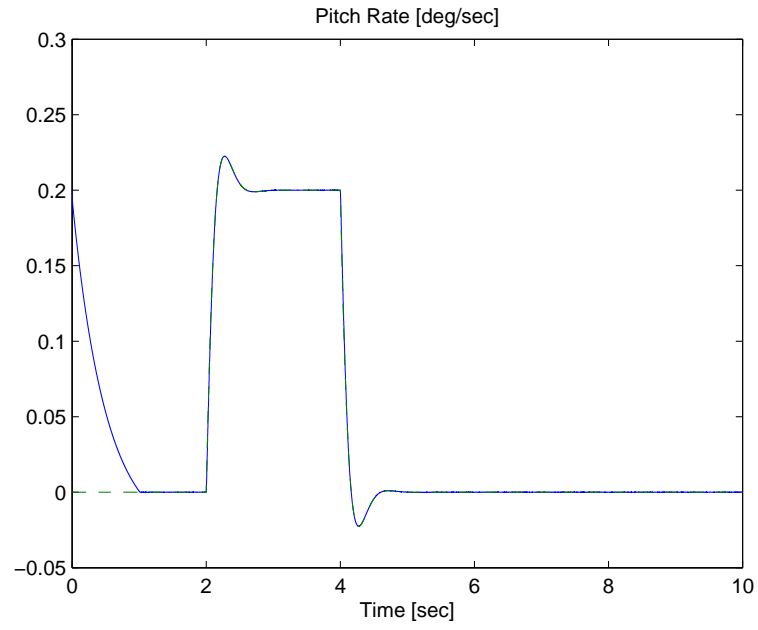


Figure 3.2. The reference pitch rate (dashed line) and the actual pitch rate (solid line).

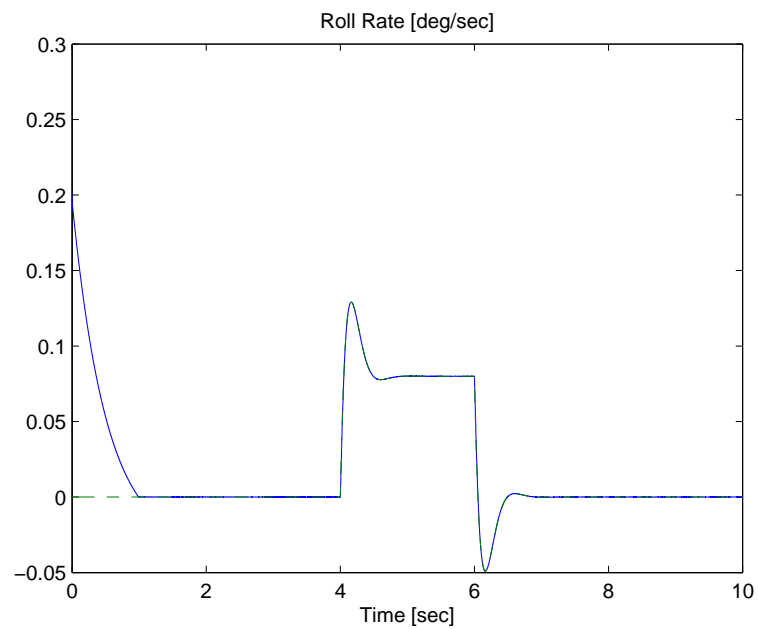


Figure 3.3. The reference roll rate (dashed line) and the actual roll rate (solid line).

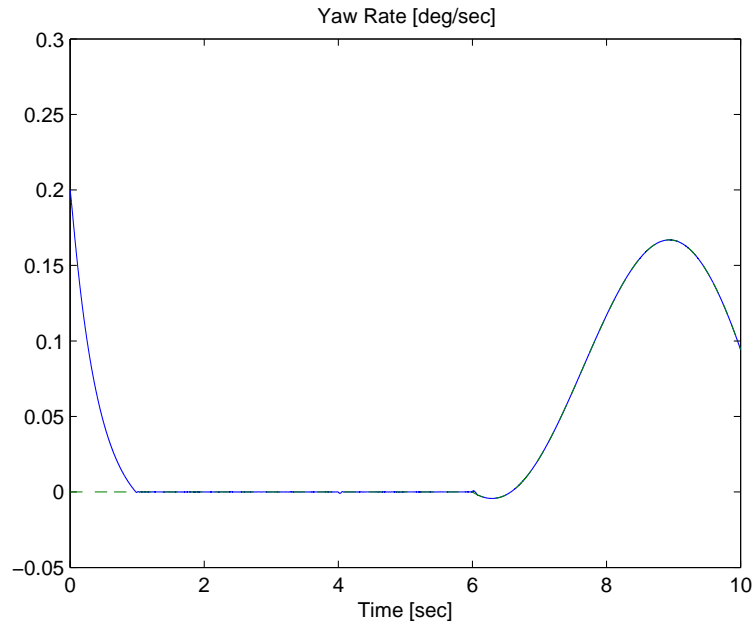


Figure 3.4. The reference yaw rate (dashed line) and the actual yaw rate (solid line).

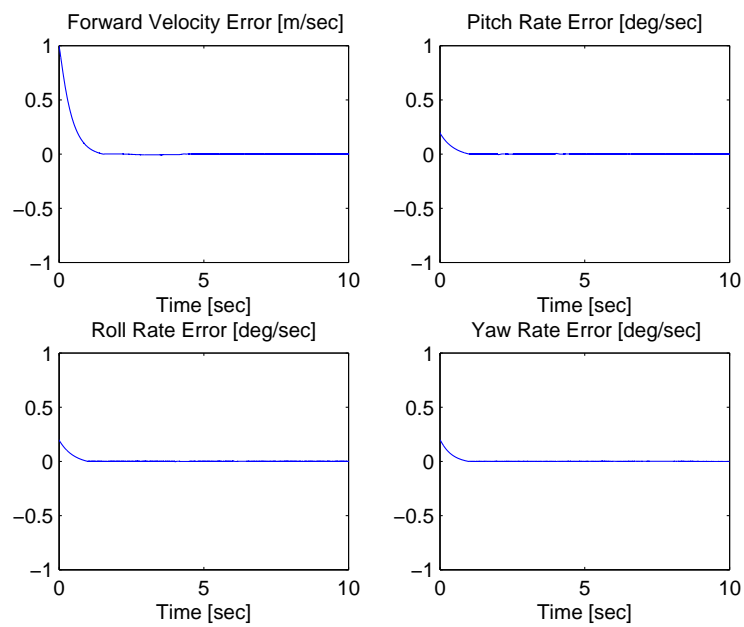


Figure 3.5. The output tracking error  $e(t)$ .



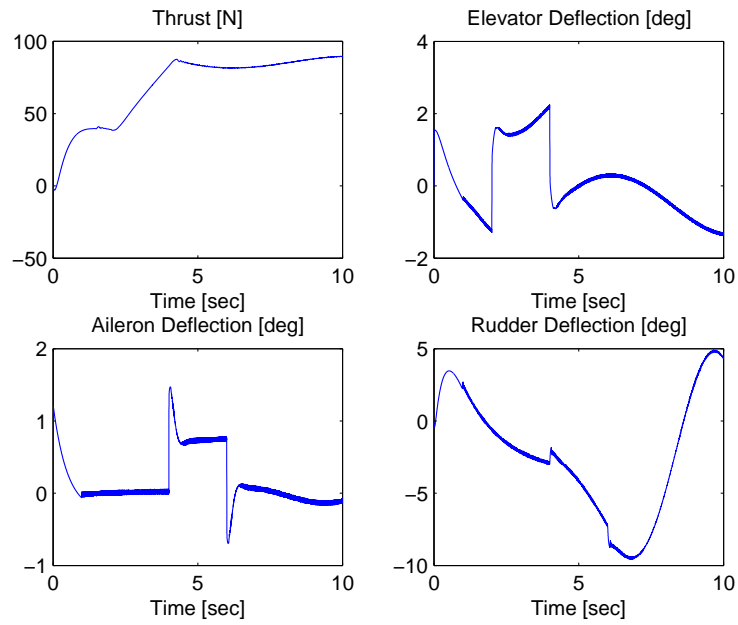


Figure 3.6. The control input  $u(t)$ .

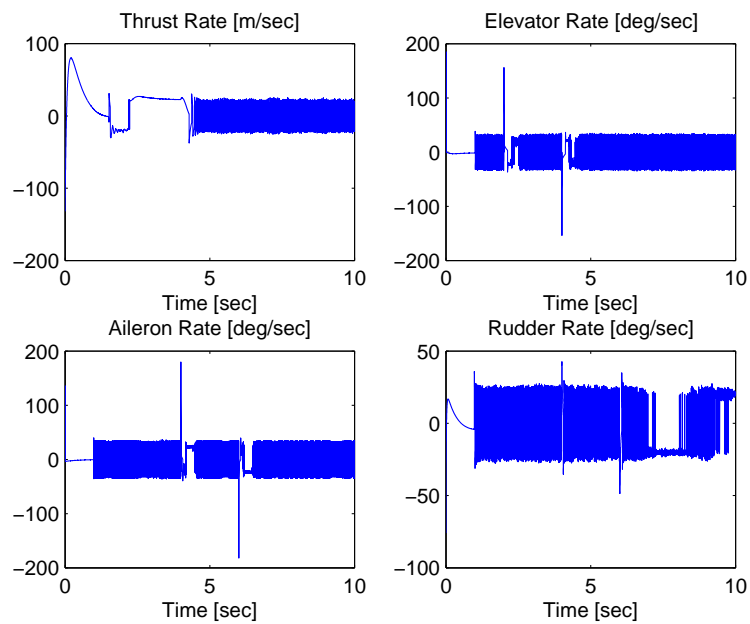


Figure 3.7. Control input rates.

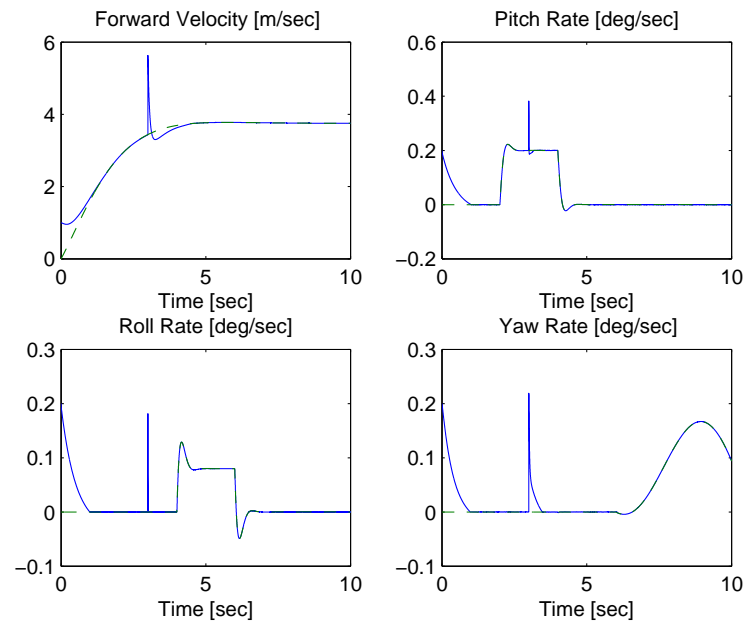


Figure 3.8. The reference and the actual states while high-disturbance is applied at  $t = 3$  seconds.

Table 3.1. Control input limits used in the simulations.

Control Thrust Saturation Limit	$\pm 200$ N
Control Thrust Rate Limit	$\pm 200$ N/sec
Elevator Saturation Limit	$\pm 30$ deg
Elevator Rate Limit	$\pm 300$ deg/sec
Aileron Saturation Limit	$\pm 30$ deg
Aileron Rate Limit	$\pm 300$ deg/sec
Rudder Saturation Limit	$\pm 30$ deg
Rudder Rate Limit	$\pm 300$ deg/sec

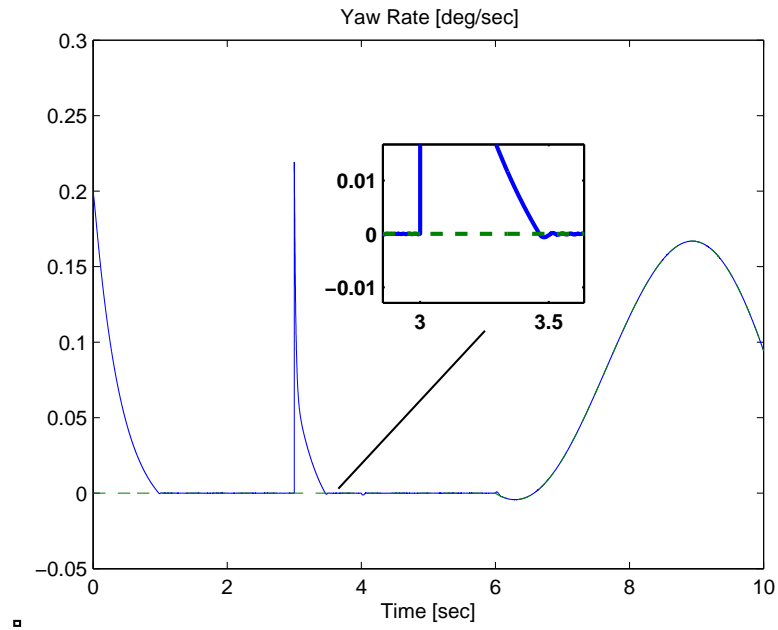


Figure 3.9. The reference and the actual yaw rate while high-disturbance is applied at  $t = 3$  seconds.

Table 3.2. Tabulated steady state error values for 5 simulation runs.

State	Average Maximum Steady State Error
Forward Velocity	$3.2 \times 10^{-4}$
Pitch Rate	$1 \times 10^{-4}$
Roll Rate	$3.8 \times 10^{-3}$
Yaw Rate	$1.5 \times 10^{-3}$

Table 3.3. Tabulated root mean square error values for 5 simulation runs.

State	Average Root Mean Square Error
Forward Velocity	0.81
Pitch Rate	0.09
Roll Rate	0.09
Yaw Rate	0.08

### 3.4.2. Twin Rotor System

Following system matrices were utilized for the reference model

$$\begin{aligned} A_{lonm} &= \begin{bmatrix} 0 & 1 \\ 0 & -1 \end{bmatrix} & A_{latm} &= \begin{bmatrix} 0 & 1 \\ 0 & -1 \end{bmatrix} \\ B_{lonm} &= \begin{bmatrix} 0 \\ 1 \end{bmatrix} & B_{latm} &= \begin{bmatrix} 0 \\ 1 \end{bmatrix}. \end{aligned} \quad (3.32)$$

Reference model is said to be stable and controllable from the state and input matrices. The reference input  $u_m(t)$  was designed as

$$u_m = \begin{bmatrix} \sin(t) \\ \sin(t) \end{bmatrix} \quad (3.33)$$

and initial condition of the system was chosen as

$$x(0) = \begin{bmatrix} 0 \\ 1 \\ 0 \\ 1 \end{bmatrix}. \quad (3.34)$$

In the simulations, the output vector consisted of pitch rate and yaw rate. Control gains were chosen as  $\beta = 5I_2$ ,  $K = 15I_2$  and  $\Lambda = 2I_2$ . Sampling time was chosen as 0.001 seconds.

The tracking performance, tracking error and the control inputs are presented in Figures 3.10, 3.11, 3.12 and 3.13, respectively. From Figures 3.10, 3.11 and 3.12, it is clear that the tracking objective was satisfied.

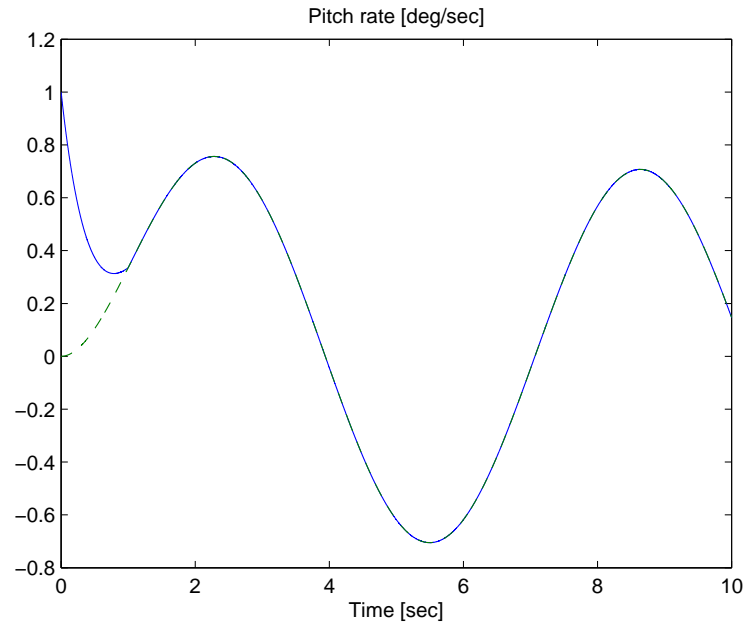


Figure 3.10. The reference pitch rate (dashed line) and the actual pitch rate (solid line).

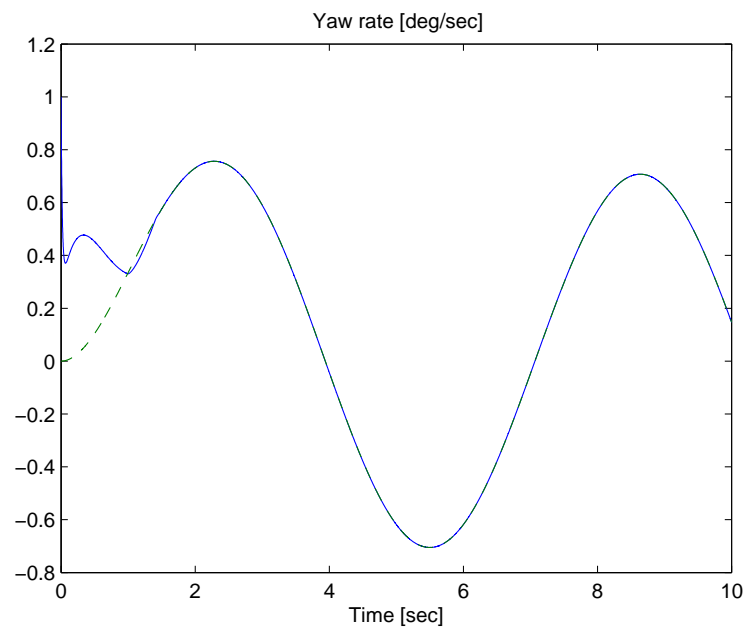


Figure 3.11. The reference yaw rate (dashed line) and the actual yaw rate (solid line).

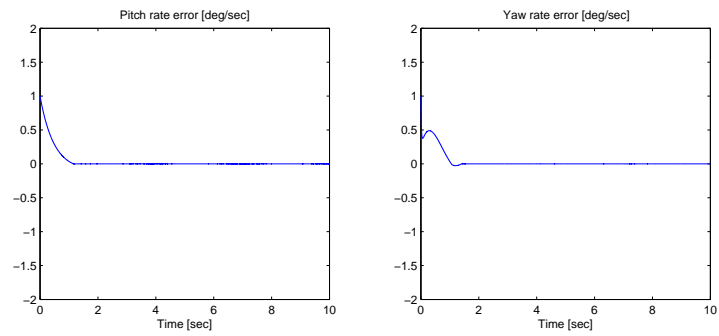


Figure 3.12. The output tracking error  $e(t)$ .

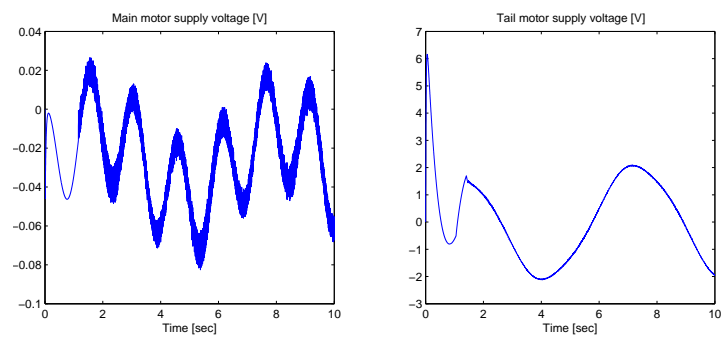


Figure 3.13. The control input  $u(t)$ .

### 3.5. Experiment Results

In this section, proposed robust controller is experimentally validated on the twin rotor system. Details of the model were given in Section 2.1.2.

A continuous approximation of the signum function namely hyperbolic tangent function was used in the control input. Specifically,  $\text{Tanh}(5e)$  was utilized in (3.17) in lieu of  $\text{Sgn}(e)$ . A comparison of the signum function and the hyperbolic tangent function is given in Figure 3.14.

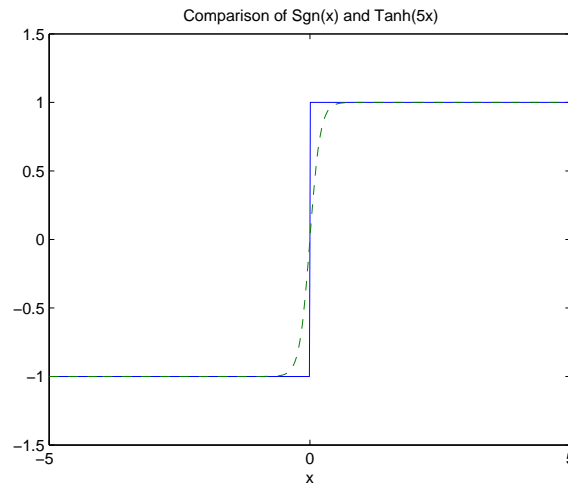


Figure 3.14. Comparison of the signum function (solid line) and the hyperbolic tangent function (dashed line).

In the experiment, both pitch rate and yaw rate of the twin rotor system are controlled. Reference pitch rate and yaw rate were chosen as  $2 \sin(0.4\pi t)$  deg/sec and  $2 \sin(0.4\pi t)$  deg/sec, respectively. Control gains were chosen as  $\beta = 3I_2$ ,  $K = 6I_2$  and  $\Lambda = 4I_2$ . Limits of the twin rotor system are given in Table 3.4 Dogan (2014). The tracking errors and the control inputs are presented in Figures 3.15-3.16 and 3.17-3.18, respectively. From Figures 3.15 and 3.16, it is clear that the tracking objective was satisfied.

### 3.6. Conclusions

A robust controller was designed for the general aircraft model given in the Chapter 2. In the design of the controller, robust integral of the sign of the error control ap-

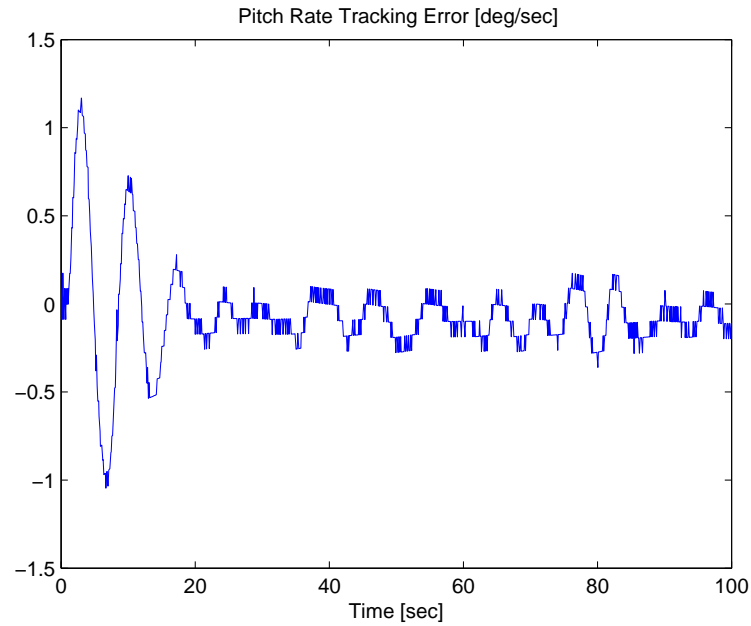


Figure 3.15. Tracking error for pitch rate.

Table 3.4. Limits of experimental system.

Main Motor Supply Voltage Limit	24 V
Tail Motor Supply Voltage Limit	24 V
Pitch Rate Limit	$\pm 97.4$ deg/sec
Yaw Rate Limit	$\pm 57.3$ deg/sec

proach was used to compensate for uncertainties in the dynamic model. Lyapunov type stability analysis techniques were utilized to ensure global asymptotic tracking of the output of a reference model. Numerical simulations were conducted that demonstrate the efficacy of the proposed robust controller where robustness to external disturbances and variation of the initial states were also shown. The performance of the proposed controller was experimentally evaluated on a twin rotor system.

The closest works in the literature to the proposed robust controller are MacKunis (2009) and MacKunis et al. (2010). Thus a comparison between the proposed controller and the controller in MacKunis (2009) and MacKunis et al. (2010) is presented. Following robust controller was designed in MacKunis (2009) and MacKunis et al. (2010) for output



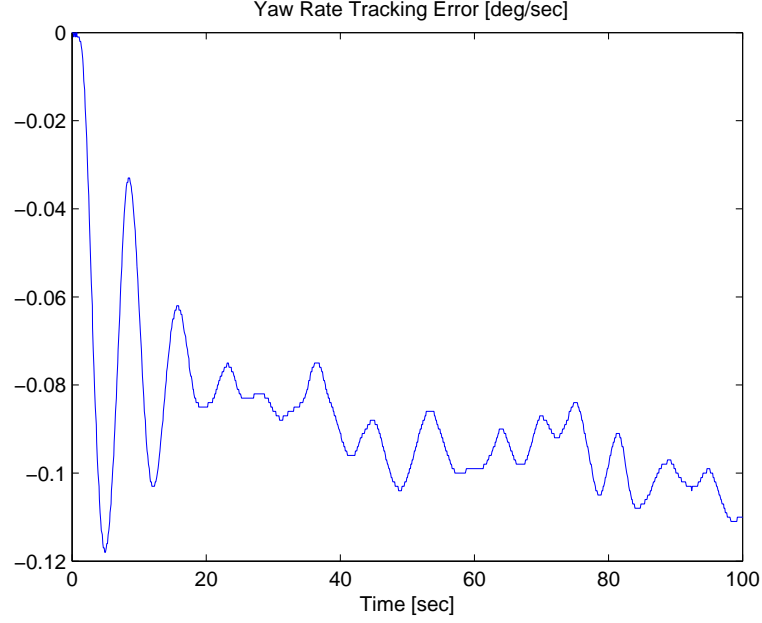


Figure 3.16. Tracking error for yaw rate.

tracking of the same aircraft model considered in this thesis

$$\begin{aligned}
 u = & - \int_0^t \alpha u(\tau) d\tau - \hat{\Omega}^{-1} \left[ - (k_s + I_{m \times m}) e(t) + (k_s + I_{m \times m}) e(0) \right. \\
 & \left. - \int_0^t [Y_A(\tau) \hat{\theta}_A(\tau) + \alpha((k_s + I_{m \times m}) e(\tau))] d\tau - \int_0^t \beta \text{Sgn}(e(\tau)) d\tau \right] \quad (3.35)
 \end{aligned}$$

where  $\alpha, \beta, k_s \in \mathbb{R}^{m \times m}$  are control gain matrices and  $Y_A \hat{\theta}_A$  is an adaptive term which depends on the reference model trajectories  $x_m(t), \dot{x}_m(t)$  and the measurements of  $e(t)$ ,  $\hat{\Omega} \in \mathbb{R}^{m \times m}$  is a constant matrix and defined as  $\hat{\Omega} = C \hat{B}$  where  $\hat{B}$  is the estimate of the input matrix  $B$ . Potential deficit of this controller is the utilization of integral of the control input in evaluating the control input. Control inputs may increase and exceed the practical limits given in Table 3.1 because of the integral of the control input in (3.35). Another disadvantage is the utilization of the estimate of the input matrix. Control objectives may not be achieved because of the estimation errors, also this kind of estimation needs extra processing and power consumption. In this chapter, following robust controller<sup>1</sup> is designed to overcome the shortcomings of the controller in (3.35)

$$u = -DK[e(t) - e(0) + \Lambda \int_0^t e(\tau) d\tau] - D \int_0^t \beta \text{Sgn}(e(\tau)) d\tau.$$

<sup>1</sup>The proposed robust controller in (3.16) and (3.17) is combined for a better comparison with (3.35).

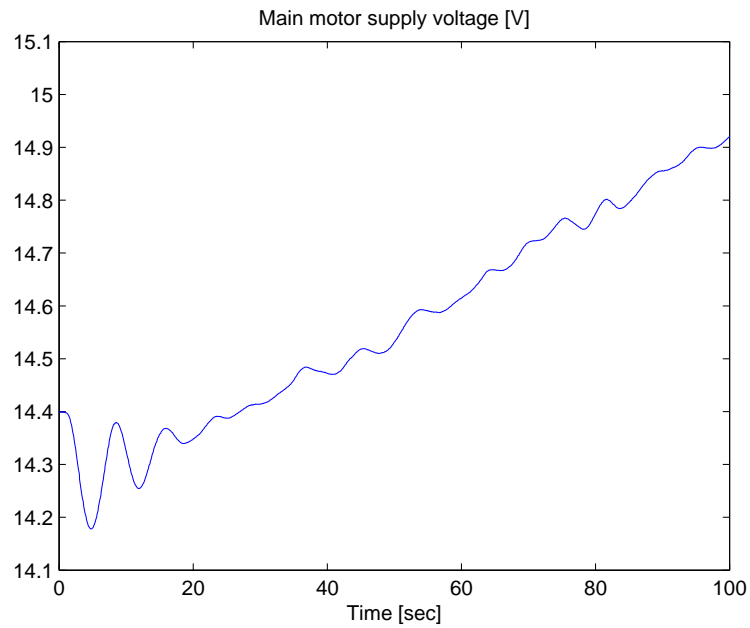


Figure 3.17. Control input for pitch rate.

By the help of this contribution, the aircraft system will be protected against estimation errors and sudden rises of the control inputs. Also the control architecture becomes simpler.

An additional controller is also designed for the cases when acceleration measurements are available for the control design. The details of this design is available in Tanyer et al. (2013).

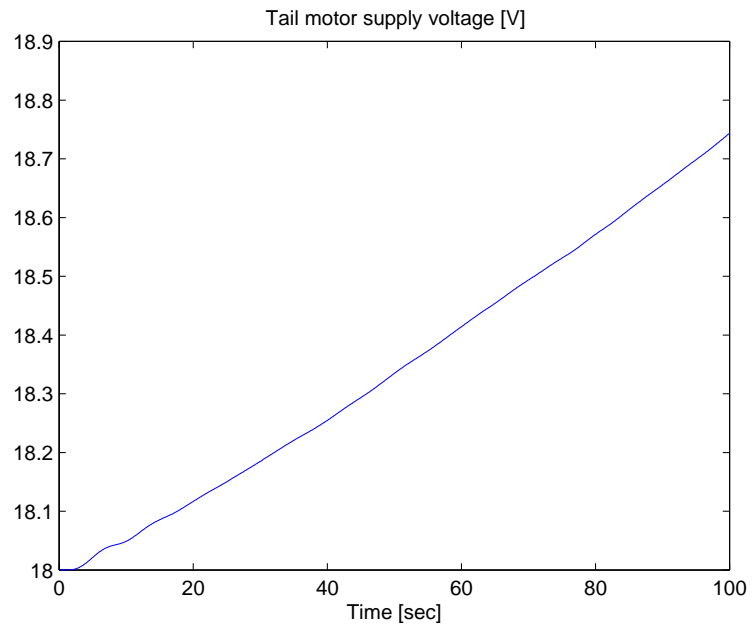


Figure 3.18. Control input for yaw rate.

## CHAPTER 4

### ROBUST OPTIMAL CONTROL OF UAV

#### 4.1. Abstract

In this chapter, design and accompanying analysis of an optimal controller is presented. The design is constrained by the lack of accurate dynamic model knowledge, thus a robust approach is aimed. While the derivations are similar to that of the robust, the design related to optimal part are novel according to our best knowledge. Specifically, after the open-loop dynamics of output tracking error are obtained, the uncertain terms are considered to be available, which is followed by the design of the optimal part of the controller. Next, an observer-like term is introduced to estimate the uncertainties which were considered as available and known. After following a similar stability analysis to that of the robust controller's both global asymptotic stability and the asymptotic convergence of the proposed controller to optimal one that was designed under the assumption of accurate knowledge of system dynamics. This seems like the only way to deal with model uncertainty while achieving an optimal result. Numerical simulation results performed on the models of Osprey aircraft and twin rotor system and the experiment results on the twin rotor system are then presented to verify the performance of the proposed controller.

#### 4.2. Control Design

The derivations are same as derivations of the robust controller in Chapter 3 till (3.6) and thus continues afterwards.

Using (2.1) and (3.1), the time derivative of the output tracking error  $e(t)$  in (3.2) can be written as

$$\dot{e} = CAx + \Omega u + Cf - CA_m x_m - CB_m u_m \quad (4.1)$$

where  $\Omega$  is the same auxiliary constant matrix as in (3.5). Premultiplying (4.1) with  $M$  yields

$$M\dot{e} = W + Du \quad (4.2)$$

where  $W(t) \in \mathbb{R}^m$  is an auxiliary vector defined as

$$W \triangleq MCAx + D(U - I)u + MCf - MCA_m x_m - MCB_m u_m. \quad (4.3)$$

It should be noticed that since the system dynamics are uncertain, then  $W(t)$  includes uncertain terms. The uncertainties in  $W(t)$  must be compensated to achieve asymptotic tracking.

In this case, a state space form will be developed for the tracking error dynamics. Then, an optimal controller will be designed that minimizes a quadratic performance index under the assumption that the auxiliary vector in (4.3) is known. After the design of the optimal controller that requires knowledge of the auxiliary vector in (4.3), a robust controller will be designed where an auxiliary term will be utilized to estimate  $W(t)$  and asymptotic optimality will be demonstrated. According to our best knowledge, this is the only way to obtain an optimal result when the system dynamics are uncertain Lewis et al. (2012), Dupree et al. (2011).

Provided the temporary assumption that the auxiliary vector  $W(t)$  in (4.3) is known, the control input can be designed as

$$u = -D(W - u^*) \quad (4.4)$$

where  $u^*(t) \in \mathbb{R}^m$  is the subsequently designed optimal part of the controller. By substituting (4.4) into (4.2), the time derivative of the tracking error can be written as

$$\dot{e} = M^{-1}u^* \quad (4.5)$$

which can be represented in state space form as

$$\dot{e} = \bar{A}e + \bar{B}u^* \quad (4.6)$$

where  $\bar{A} = 0_{m \times m}$  and  $\bar{B} = M^{-1}$ .

In this case, a quadratic performance index  $J(u) \in \mathbb{R}$  is defined as follows

$$J(u) = \int_{t_0}^{\infty} L(e, u)dt \quad (4.7)$$

where  $L(e, u) \in \mathbb{R}$  is defined as

$$L(e, u) = \frac{1}{2}e^T(t)Qe(t) + \frac{1}{2}u^{*T}(t)Ru^*(t). \quad (4.8)$$

where  $Q, R \in \mathbb{R}^{m \times m}$  are constant, positive definite, symmetric weighting matrices. Given the performance index  $J(u)$ , the control objective is to find the auxiliary control input  $u(t)$  that minimizes (4.7) subject to the differential constraint imposed by (4.6). The optimal control that achieves this objective is denoted by  $u^*(t)$ .

A necessary and sufficient condition for  $u^*(t)$  to minimize (4.7) subject to (4.6) is that there exists a positive definite value function  $V_{opt}(e, t)$  satisfying the Hamilton-Jacobi-Bellman (H-J-B) equation Lewis et al. (2012)

$$\min_u [e^T(t)Qe(t) + u^T(t)Ru(t) + \frac{\partial V_{opt}}{\partial e} \dot{e} + \frac{\partial V_{opt}}{\partial t}] = 0 \quad (4.9)$$

where the value function  $V_{opt}(e) \in \mathbb{R}$  is chosen as

$$V_{opt} = e^T \bar{K} e \quad (4.10)$$

where  $\bar{K} \in \mathbb{R}^{m \times m}$  is a constant, positive definite matrix. Partial derivative of the value function with respect to time and with respect to tracking error can be obtained as

$$\frac{\partial V_{opt}}{\partial t} = 0, \quad \frac{\partial V_{opt}}{\partial e} = 2e^T \bar{K}. \quad (4.11)$$

Substituting (4.11) into (4.9) yields

$$\min_u [e^T(t)Qe(t) + u^T(t)Ru(t) + 2e^T \bar{K} \bar{A}e + 2e^T \bar{K} \bar{B}u] = 0. \quad (4.12)$$

To minimize (4.12), partial derivative of (4.12) with respect to the control input  $u$  is evaluated

$$\frac{\partial}{\partial u} [e^T(t)Qe(t) + u^T(t)Ru(t) + 2e^T \bar{K} \bar{A}e + 2e^T \bar{K} \bar{B}u] = 0. \quad (4.13)$$

The solution for the control input  $u$  results

$$u = -R^{-1} \bar{B}^T \bar{K} e. \quad (4.14)$$

Evaluation of  $\bar{K}$  in (4.10) can be achieved from the following Riccati equation

$$\bar{K} \bar{A} + \bar{A}^T \bar{K}^T - \bar{K} \bar{B} R^{-1} \bar{B}^T \bar{K} + Q = 0. \quad (4.15)$$

Riccati equation in (4.15) is obtained by substituting the control input solution in (4.14) into (4.12). The value function  $V_{opt}$  is designed for the state space form in (4.6) by choosing  $\bar{K} = M$  as

$$V_{opt}(e) = e^T M e. \quad (4.16)$$

In this case, optimal controller  $u^*$  that minimizes (4.7) can be found as

$$\begin{aligned} u^* &= -R^{-1} M^{-T} M e \\ &= -R^{-1} e. \end{aligned} \quad (4.17)$$

By using  $\bar{A}$  and  $\bar{B}$  in (4.6), from the Riccati equation in (4.15), it can be easily found that  $Q = R^{-1}$ . This concludes the design of the optimal part of the controller.

Recall from (4.4) and (4.17) that the control input was designed as  $u = -D(W + R^{-1}e)$  where the auxiliary vector  $W(t)$  in (4.3) is considered to be known. In the subsequent robust controller development, we will design a control input that will converge to (4.4). In our design, the error system will be designed based on an auxiliary tracking error, denoted by  $r(t) \in \mathbb{R}^m$ , which was previously defined in (3.4) as  $r = \dot{e} + \Lambda e$ . From (3.10), following expression can be obtained

$$Mr = N - e + D\dot{u} + D(U - I)\dot{u} \quad (4.18)$$

where  $N$  was previously defined in (3.9). In this case, motivated by the subsequent stability analysis, the control input  $u(t)$  is designed as

$$u = -D\hat{W} - DR^{-1}e \quad (4.19)$$

where  $\hat{W}(t) \in \mathbb{R}^m$  is designed as

$$\hat{W} = K[e(t) - e(0) + \Lambda \int_0^t e(\tau)d\tau] + \beta \int_0^t \text{Sgn}(e(\tau))d\tau \quad (4.20)$$

where  $D$ ,  $K$ ,  $\Lambda$  are same as in (3.16). The auxiliary  $\hat{W}(t)$  term in the control input in (4.19) is designed to estimate  $W(t)$  in (4.4). When this estimation is achieved in the sense that

$$\hat{W}(t) \rightarrow W(t) \quad (4.21)$$

then the control input in (4.19) converges to the optimal controller in (4.4). The time derivative of the auxiliary control input in (4.19) is obtained as follows

$$\dot{u} = -DKr - D\beta\text{Sgn}(e) - DR^{-1}\dot{e} \quad (4.22)$$

where (3.4) and the time derivative of (4.20) were utilized. By using (4.22) and (4.18), following closed-loop error system can be obtained

$$Mr = N - e - DUD\beta\text{Sgn}(e) - D(U - I_m)DKr - Kr - DUDR^{-1}(r - \Lambda e). \quad (4.23)$$

### 4.3. Stability and Optimality Analysis

**Theorem 4.3.1** *The robust optimal controller given in (4.19) with the uncertainty estimation in (4.20) ensures asymptotic tracking and minimizes the performance index in (4.7) provided that the control gain matrices  $K$  and  $\beta$  are selected by using the following procedure:*

1. For  $i = m$ ,  $\beta_m$  is selected according to (3.25) and from  $i = m - 1$  to  $i = 1$ ,  $\beta_i$  are selected according to (3.26).
2. Control gain  $k_g$  is chosen big enough to decrease the constant  $\sum_{i=1}^m \frac{\rho_{\Delta,i}^2}{4k_g}$  where  $\rho_{\Delta,i}$  are positive bounding constants.
3. Choose  $k_{d,i}$ ,  $i = 1, \dots, (m - 1)$  to decrease the constant  $\sum_{i=1}^{m-1} \frac{\zeta_{\Phi_i}^2}{4k_{d,i}}$ .

**Proof** Similar to the proof of Theorem 3.3.1, the proof consists of four subproofs. Firstly, boundedness of all the signals under the closed-loop operation will be presented by utilizing  $\Theta_i = N_{d,i}$  and  $\Delta_i = \tilde{N}_i - [DU DR^{-1}(r - \Lambda e)]_i$  in (A.3) of Appendix A. Secondly, in Appendix B, a supporting lemma and its proof is presented. The non-negativeness of an auxiliary integral term will be demonstrated with  $\Theta_i = N_{d,i}$  in Appendix C. Finally, in Appendix D, the asymptotic convergence of the output tracking error is proven.

Now, the optimality analysis for the proposed robust optimal controller in (4.19) is presented. By using equations (3.4) and (4.2), the following equation can be obtained

$$Mr = W + Du + M\Lambda e. \quad (4.24)$$

Substituting the controller in (4.19) into (4.24) we obtain

$$Mr = W - \hat{W} - R^{-1}e + M\Lambda e. \quad (4.25)$$

From the convergence proof in Appendix D,  $e(t)$  and  $r(t)$  go asymptotically to zero, then, in (4.25),  $Mr$ ,  $R^{-1}e$ ,  $M\Lambda e$  will go to zero, as a result,  $\hat{W}$  will asymptotically converge to  $W$ . Thus the control input in (4.19) will asymptotically converge to the optimal controller in (4.4). This concludes the optimality analysis of the proposed robust controller.

## 4.4. Simulation Results

Two sets of numerical simulations performed on the Osprey aircraft and twin rotor system are presented in this section.

### 4.4.1. Osprey Aircraft

The system matrices in (3.27) and the reference input in (3.28) were utilized for the reference model. Control gains  $\beta$ ,  $K$  and  $\Lambda$  were chosen same as in (3.30) and (3.31)



for a better comparison of the results. Weighting matrices  $Q$  and  $R$  were chosen as identity matrix.

The tracking performance, tracking error and the control inputs are presented in Figures 4.1-4.4, 4.5 and 4.6, respectively. From Figures 4.1-4.4 and 4.5, it is clear that the tracking objective was satisfied. From Figure 4.6 and Table 3.1, it is clear that the control inputs are in acceptable limits.

In Tables 4.1 and 4.2, average maximum steady state error and average root mean square error are presented. Five Monte Carlo simulations are performed for different initial state values. The error values in Tables 4.1 and 4.2 shows that the proposed controller ensures asymptotic tracking for different initial values of the states.

In Table 4.3, the values of quadratic performance index  $J$  for different values of weight matrix  $R$  are given.

In Table 4.4, a comparison of robust optimal controller in this chapter and robust controller in Chapter 3 is given for different values of weight matrices.

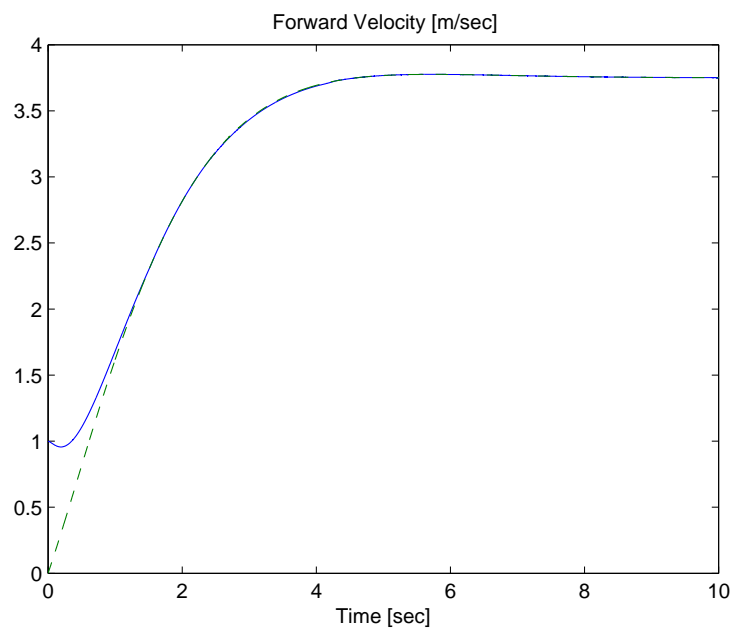


Figure 4.1. The reference velocity (dashed line) and the actual velocity (solid line).

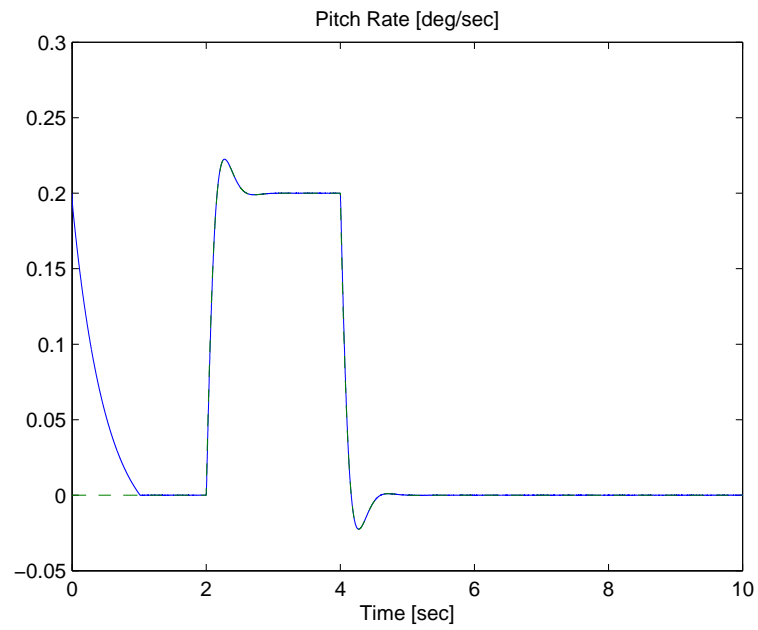


Figure 4.2. The reference pitch rate (dashed line) and the actual pitch rate (solid line).

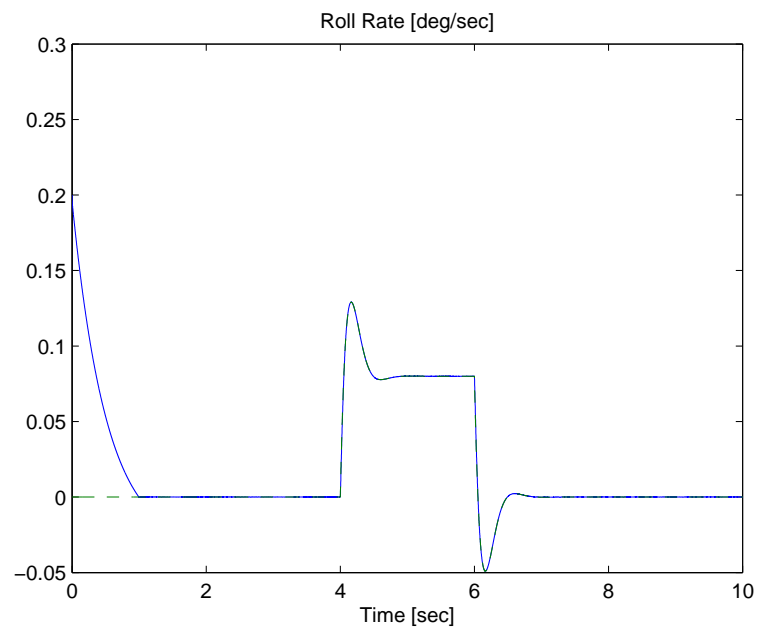


Figure 4.3. The reference roll rate (dashed line) and the actual roll rate (solid line).

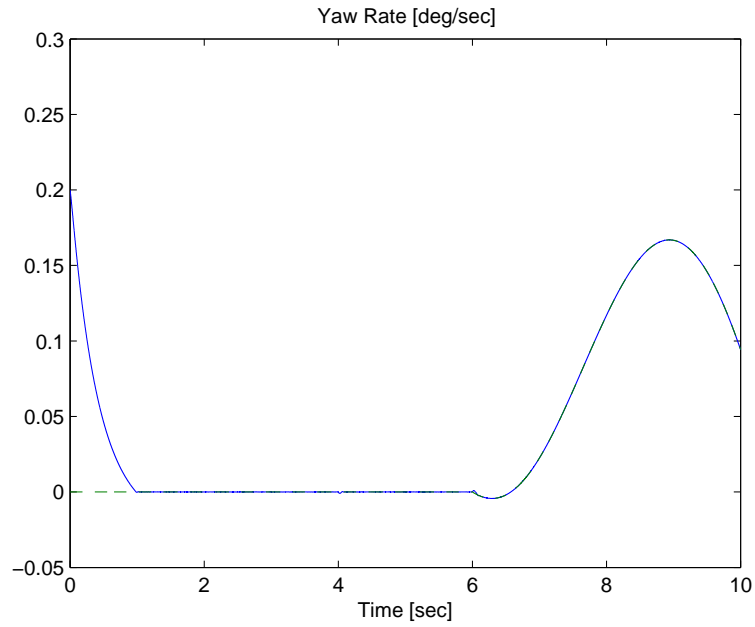


Figure 4.4. The reference yaw rate (dashed line) and the actual yaw rate (solid line).

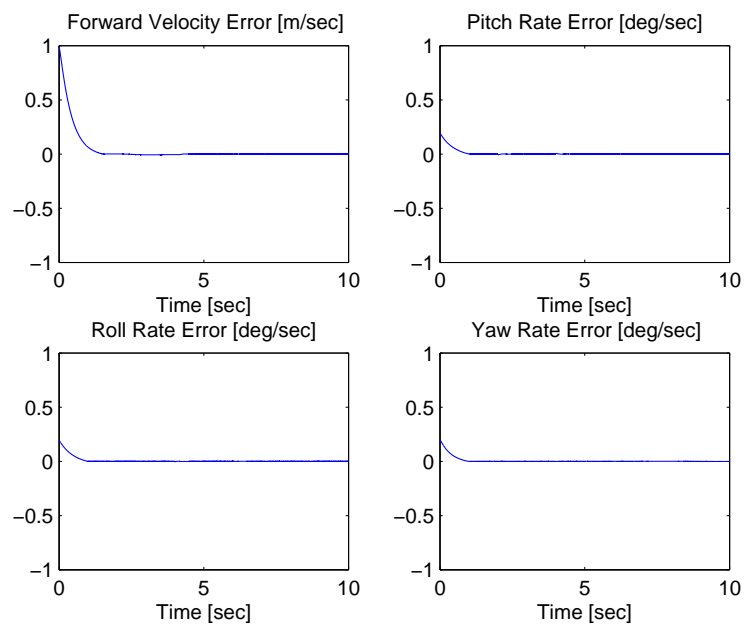


Figure 4.5. The output tracking error  $e(t)$ .

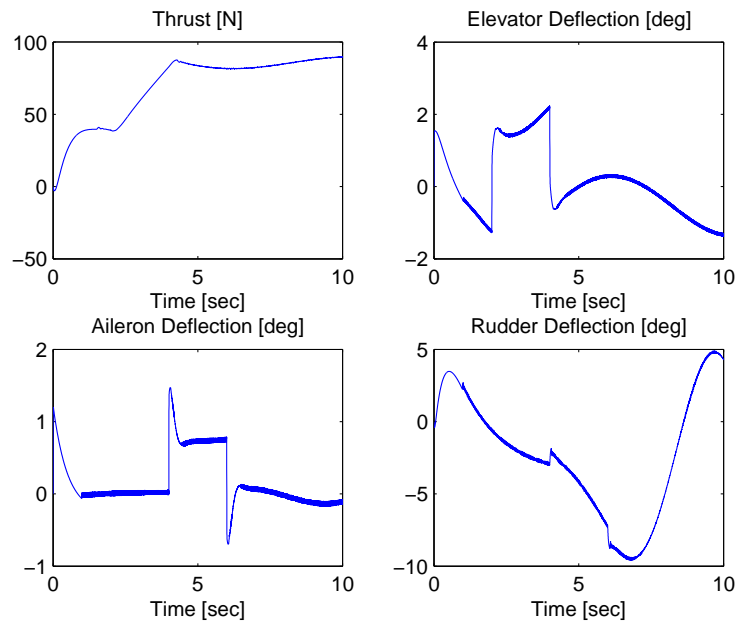


Figure 4.6. The control input  $u(t)$ .

Table 4.1. Tabulated steady state error values for 5 simulation runs.

State	Average Maximum Steady State Error
Forward Velocity	$3.2 \times 10^{-4}$
Pitch Rate	$1 \times 10^{-4}$
Roll Rate	$3.7 \times 10^{-3}$
Yaw Rate	$1.5 \times 10^{-3}$

Table 4.2. Tabulated root mean square error values for 5 simulation runs.

State	Average Root Mean Square Error
Forward Velocity	0.80
Pitch Rate	0.089
Roll Rate	0.089
Yaw Rate	0.086

Table 4.3. Tabulated performance index  $J$  for different values of weighting matrix  $R$ .

$Q$	$R$	Performance Index $J$
$0.01I_4$	$100I_4$	$2.5074 \times 10^9$
$0.1I_4$	$10I_4$	$2.5077 \times 10^8$
$I_4$	$I_4$	$2.5411 \times 10^7$
$10I_4$	$0.1I_4$	$5.8484 \times 10^6$
$100I_4$	$0.01I_4$	$3.3594 \times 10^7$

Table 4.4. Comparison of robust controller and robust optimal controller.

Type of controller	$Q$	$R$	Mean Squared Error
Robust	0	0	$7.1 \times 10^{-3}$
Robust Optimal	$10I_4$	$0.1I_4$	$7 \times 10^{-3}$
Robust Optimal	$100I_4$	$0.01I_4$	$6.5 \times 10^{-3}$
Robust Optimal	$1000I_4$	$0.001I_4$	$4.6 \times 10^{-3}$

## 4.4.2. Twin Rotor System

The system matrices in (3.32) and the reference input in (3.33) were utilized for the reference model. Control gains and initial conditions were chosen same as in Section 3.4.2. Weighting matrices were chosen as  $Q = 10I_2$  and  $R = 0.1I_2$  to penalize the output tracking error.

In the simulation, the output vector consisted of pitch rate and yaw rate. The tracking performance, tracking error and the control inputs are presented in Figures 4.7, 4.8, 4.9 and 4.10, respectively. From Figures 4.7, 4.8 and 4.9, it is clear that the tracking objective was satisfied. From Figure 4.10, it is clear that the control inputs are bounded.

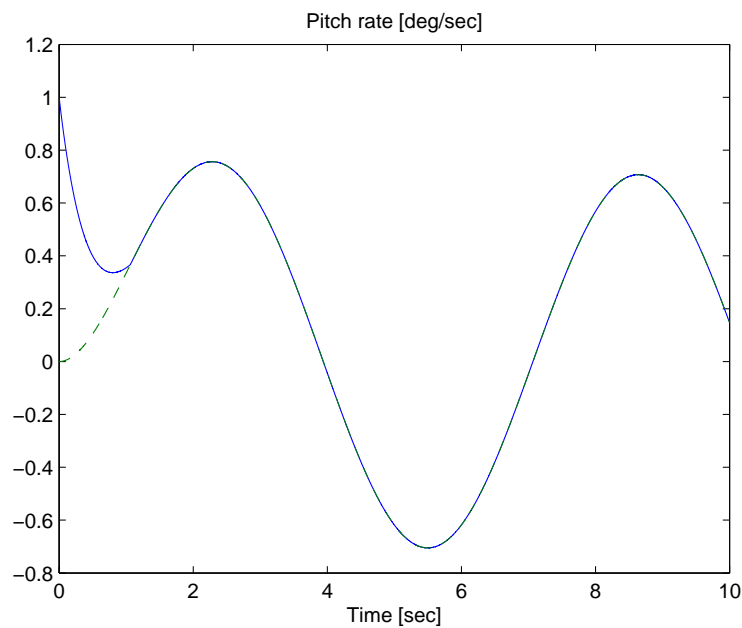


Figure 4.7. The reference pitch rate (dashed line) and the actual pitch rate (solid line).

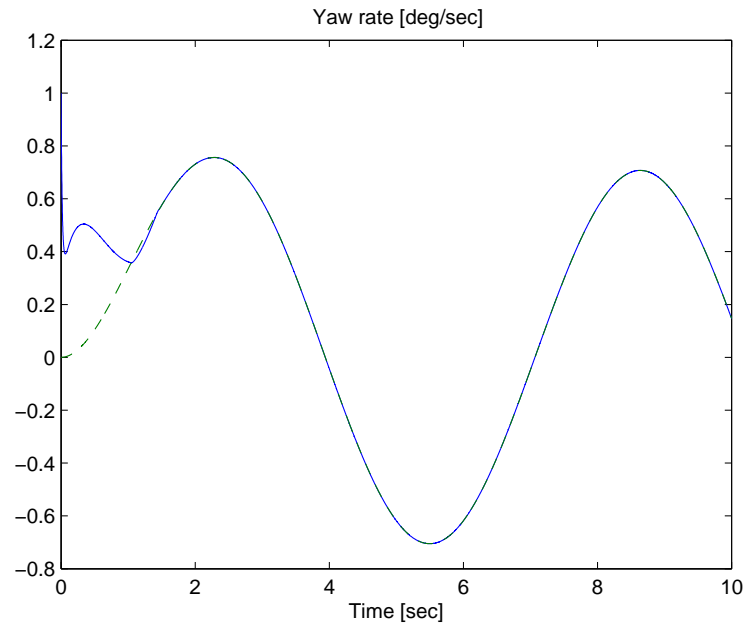


Figure 4.8. The reference yaw rate (dashed line) and the actual yaw rate (solid line).

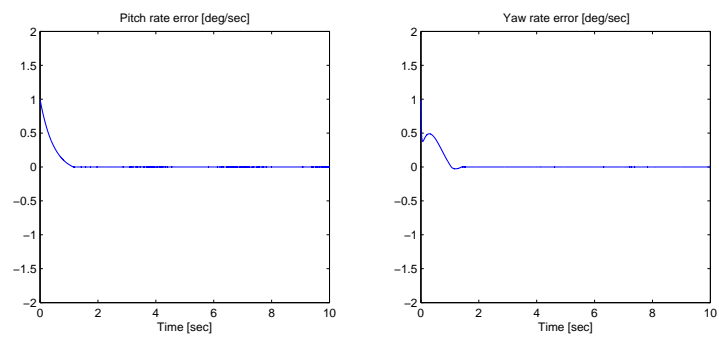


Figure 4.9. The output tracking error  $e(t)$ .

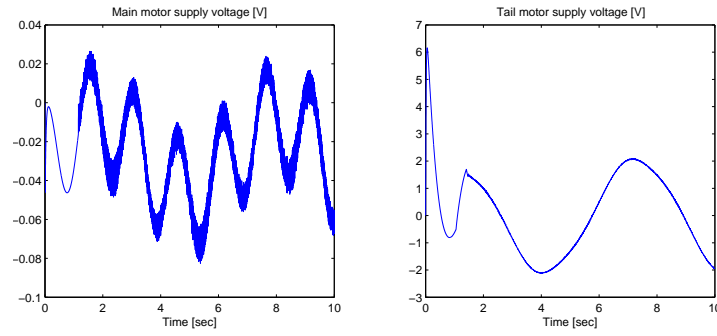


Figure 4.10. The control input  $u(t)$ .

## 4.5. Experiment Results

In this section, proposed robust optimal controller is validated on the twin rotor system. In the experiment, both pitch rate and yaw rate of the twin rotor system are controlled. Reference model and control gains were chosen as in Section 3.5. Weighting matrices were chosen as  $Q = 100I_2$  and  $R = 0.01I_2$  to penalize the output tracking error. The tracking errors and the control inputs are presented in Figures 4.11-4.12 and 4.13-4.14, respectively. From Figures 4.11 and 4.12, it is clear that the tracking objective was satisfied. In Table 4.5, the values of quadratic performance index  $J$  for different values of weight matrix  $R$  are given.

Table 4.5. Tabulated performance index  $J$  for different values of weighting matrix  $R$ .

Weighting matrix $Q$	Weighting matrix $R$	Performance Index $J$
$0.1I_2$	$10I_2$	$5.4854 \times 10^6$
$I_2$	$I_2$	$5.4772 \times 10^5$
$10I_2$	$0.1I_2$	$5.5979 \times 10^4$
$100I_2$	$0.01I_2$	$2.0860 \times 10^4$
$1000I_2$	$0.001I_2$	$4.1853 \times 10^4$



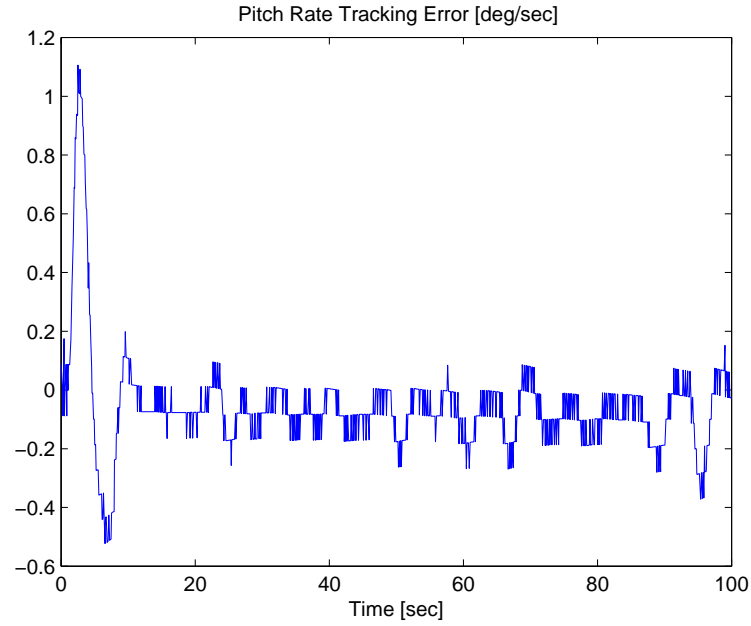


Figure 4.11. Pitch rate tracking error.

## 4.6. Conclusions

A robust optimal controller was designed for the general aircraft model given in the Chapter 2. Different from the controller input in Chapter 3, following quadratic performance index is minimized by using an optimal term in the controller input

$$J = \int_{t_0}^{\infty} \left[ \frac{1}{2} e^T(t) Q e(t) + \frac{1}{2} u^{*T}(t) R u^*(t) \right] dt. \quad (4.26)$$

Lyapunov type stability analysis techniques were utilized to ensure global asymptotic tracking of the output of a reference model. Numerical simulations were conducted that demonstrate the efficacy of the proposed robust optimal controller where robustness to external disturbances and variation of the initial states were also shown. The proposed controller was verified via experiments performed on a twin rotor system.

Following robust controller was designed in Chapter 3 to overcome the shortcomings of the robust controller of MacKunis (2009) which was previously given in (3.35)

$$u = -DK[e(t) - e(0) + \Lambda \int_0^t e(\tau) d\tau] - D \int_0^t \beta \text{Sgn}(e(\tau)) d\tau.$$

In this chapter, a robust optimal controller is designed as follows

$$u = -DK[e(t) - e(0) + \Lambda \int_0^t e(\tau) d\tau] - D\beta \int_0^t \text{Sgn}(e(\tau)) d\tau - DR^{-1}e$$

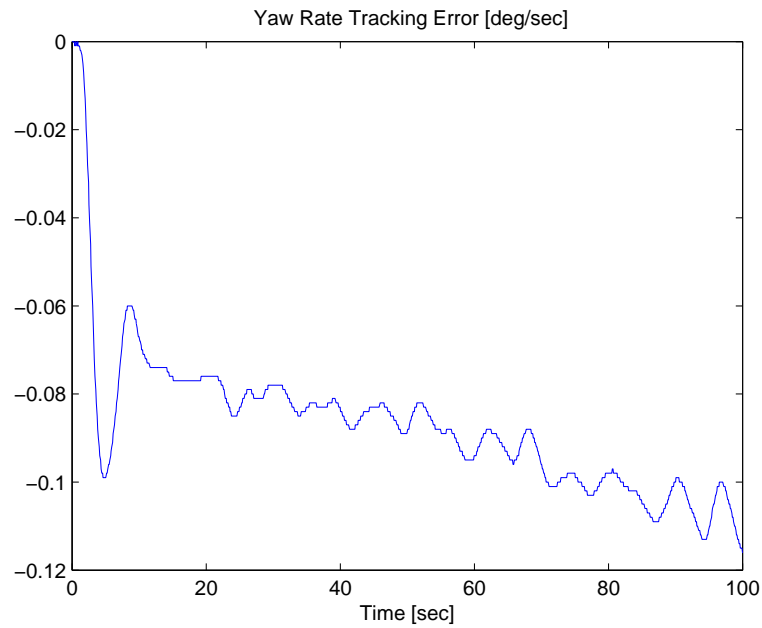


Figure 4.12. Yaw rate tracking error.

where the last term is the optimal term that minimizes the quadratic performance index  $J$ . Despite the similar structures, a novel optimality analysis was performed. From Table 4.4, it is clear that the error performance of the robust optimal controller gets better when the tracking error is penalized by a higher  $Q$  matrix. Better error or control input performances can be achieved by varying the weight matrices  $Q$  and  $R$ .

An additional robust optimal controller is also designed for the cases when acceleration measurements are available for the control design. The details of this design is available in Tanyer et al. (2014).

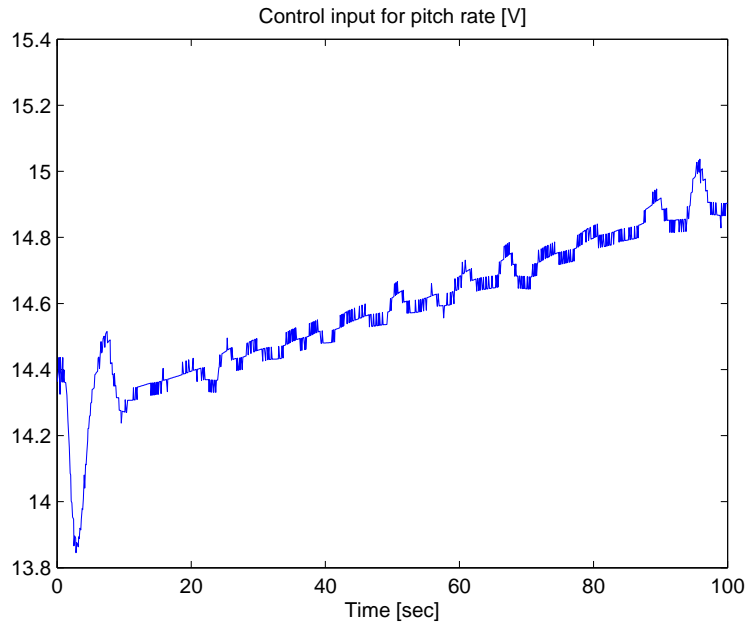


Figure 4.13. Control input for pitch rate.

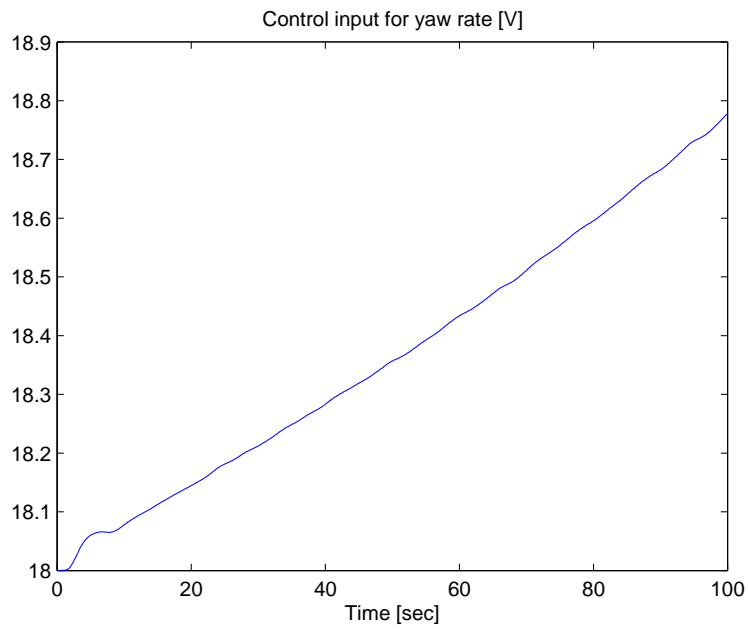


Figure 4.14. Control input for yaw rate.

# CHAPTER 5

## ROBUST ADAPTIVE CONTROL OF UAV

### 5.1. Abstract

In this section, an adaptive component is added to the robust controller to compensate for the linearly parameterizable uncertainties. This adaptive component compensates for the linearly parameterizable terms by dynamically updating an adaptive law while open-loop error dynamics is similar to that of the one in robust controller, as a result of the adaptive component in the controller, the associated stability analysis required a new term corresponding to the adaptive update rule. Similarly, global asymptotic tracking is ensured. Numerical simulation and experiment results are also presented.

### 5.2. Control Design

The derivations are same as the robust controller in Chapter 3 till (3.10) and thus continues afterwards. For the purposes of the adaptive control design, the auxiliary vector in (3.9) is now partitioned as

$$N = N_c + N_e + N_{ad} \quad (5.1)$$

where  $N_c(t) \in \mathbb{R}^m$  contains functions that can be bounded by constants in the sense that

$$|N_{c,i}| \leq \zeta_{N_{c,i}} \quad \forall i = 1, \dots, m \quad (5.2)$$

where  $\zeta_{N_{c,i}} \in \mathbb{R}$  are positive bounding constants and  $N_e(x, \dot{x}, e, \dot{e}) \in \mathbb{R}^m$  contains functions that can be bounded by function of error signals as

$$|N_{e,i}| \leq \rho_{e,i} \|z\| \quad \forall i = 1, \dots, m \quad (5.3)$$

where  $\rho_{e,i} \in \mathbb{R}$  are positive bounding constants and  $z(t)$  is the combined error defined in (3.14) and  $N_{ad}(t) \in \mathbb{R}^m$  denotes the terms that can be linearly parameterized. This auxiliary term will be used for the design of the adaptive term in the control input and it must be written as a multiplication of a known regression matrix and an uncertain constant parameter vector. As a result, the expression in (3.10) can be written as

$$M\dot{r} = N_c + N_e + N_{ad} - e + DU\dot{u}. \quad (5.4)$$

In this case, the control input  $u(t)$  is designed as

$$u = -DK[e(t) - e(0) + \Lambda \int_0^t e(\sigma)d\sigma] - D\beta \int_0^t \text{Sgn}(e(\tau))d\tau - D \int_0^t Y(\sigma)\hat{\psi}(\sigma)d\sigma \quad (5.5)$$

where  $D, K, \Lambda$  are same as in (3.16). In (5.5),  $Y(t) \in \mathbb{R}^{m \times p}$  denotes the regression matrix which is composed of reference signal, its time derivatives and other known quantities, and is defined from

$$Y\psi = N_{ad} - D(U - I_m)DY\hat{\psi} \quad (5.6)$$

where  $\psi \in \mathbb{R}^{p \times 1}$  denotes unknown constant parameters and  $\hat{\psi}(t) \in \mathbb{R}^{p \times 1}$  is the estimate of  $\psi$ . The update rule for  $\hat{\psi}(t)$  is designed as

$$\dot{\hat{\psi}} = \text{Proj} \left( \Gamma(Y^T e - \int_0^t \frac{dY^T(\sigma)}{d\sigma} e(\sigma)d\sigma + \int_0^t Y^T(\sigma)\Lambda e(\sigma)d\sigma) \right) \quad (5.7)$$

where  $\Gamma \in \mathbb{R}^{p \times p}$  is a positive definite constant matrix. The term  $\text{Proj}(\cdot)$  is the projection operator that ensures the boundedness of the parameter estimate vector and its time derivative. Furthermore, as explained in Ioannou and Sun (1995) in detail, the projection operator is considered to retain the properties of the adaptive law without the projection algorithm. According to this design, derivative of the  $\hat{\psi}$  can be obtained as

$$\dot{\hat{\psi}} = \text{Proj}(\Gamma Y^T r) \quad (5.8)$$

where (3.4) was utilized. The time derivative of the control input in (5.5) is obtained as

$$\dot{u} = -DKr - D\beta \text{Sgn}(e) - DY\hat{\psi}. \quad (5.9)$$

After substituting (5.9) into (5.4), following closed-loop error system is obtained

$$\begin{aligned} M\dot{r} = & N_c + N_e + N_{ad} - e - D(U - I_m)DKr - Kr - DUD\beta \text{Sgn}(e) \\ & - D(U - I_m)DY\hat{\psi} - Y\hat{\psi}. \end{aligned} \quad (5.10)$$

Substituting (5.6) into (5.10), closed-loop error system can be simplified as

$$M\dot{r} = N_c + N_e - e - D(U - I_m)DKr - Kr - DUD\beta \text{Sgn}(e) + Y\tilde{\psi} \quad (5.11)$$

where  $\tilde{\psi}(t) \in \mathbb{R}^p$  is the parameter estimation error defined as  $\tilde{\psi} \triangleq \psi - \hat{\psi}$ .

### 5.3. Stability Analysis

**Theorem 5.3.1** *The robust adaptive controller in (5.5) and the parameter update rule in (5.7) ensures global asymptotic tracking in the sense that*

$$\|e(t)\| \rightarrow 0 \text{ as } t \rightarrow \infty \quad (5.12)$$

provided that the control gain matrices  $K$  and  $\beta$  are selected by using the following procedure:

1. For  $i = m$ ,  $\beta_m$  is selected according to (3.25) and from  $i = m - 1$  to  $i = 1$ ,  $\beta_i$  are selected according to (3.26).
2. Control gain  $k_g$  is chosen big enough to decrease the constant  $\sum_{i=1}^m \frac{\rho_{\Delta,i}^2}{4k_g}$  where  $\rho_{\Delta,i}$  are positive bounding constants.
3. Control gains  $k_{d,i}$ ,  $i = 1, \dots, (m - 1)$  are chosen big enough to decrease the constant  $\sum_{i=1}^{m-1} \frac{\zeta_{\Phi_i}^2}{4k_{d,i}}$ .

**Proof** Similar to the proof of Theorem 3.3.1, the proof consists of four subproofs. Firstly, boundedness of all the signals under the closed-loop operation will be presented by utilizing  $\Theta_i = N_{c,i} - [Y\tilde{\psi}]_i$  and  $\Delta_i = N_{e,i}$  in (A.3) of Appendix A. Secondly, in Appendix B, a supporting lemma and its proof is presented. The non-negativeness of an auxiliary integral term will be demonstrated with  $\Theta_i = N_{c,i}$  in Appendix C. Finally, in Appendix E, the asymptotic convergence of the output tracking error is proven.

## 5.4. Simulation Results

Two numerical simulation studies were conducted to demonstrate the performance of the proposed adaptive controller.

### 5.4.1. Osprey Aircraft

The system matrices in (3.27) and the reference input in (3.28) were utilized for the reference model. Control gains  $\beta$ ,  $K$  and  $\Lambda$  were chosen same as in (3.30)-(3.31) and adaptive gain matrix  $\Gamma$  in (5.7) was chosen as  $2I_{300}$ .

In order to obtain  $Y(t)$ , we began from the last (4th) row of (5.6) as

$$(Y\psi)_4 = N_{ad,4} - [D(U - I_4)DY\hat{\psi}]_4 \quad (5.13)$$

and since the last row of the term  $(U - I_4)$  is zero from the structure of  $U$ , the following expression can be written

$$(Y\psi)_4 = N_{ad,4} \quad (5.14)$$

where  $N_{ad}$  is defined as

$$N_{ad} = MCA\dot{x}_m - MCA_m\dot{x}_m - MCB_m\dot{u}_m \quad (5.15)$$

which consists of the reference model terms and uncertain constant parameters. Uncertain constant parameters are collected into  $\psi \in \mathbb{R}^{300}$  as follows

$$\psi = \begin{bmatrix} \psi_1 \\ U_{1,2}\psi_2 \\ U_{1,2}U_{2,3}\psi_3 \\ U_{1,2}U_{2,3}U_{3,4}\psi_3 \\ U_{1,2}U_{2,4}\psi_4 \\ U_{1,3}\psi_3 \\ U_{1,3}U_{3,4}\psi_4 \\ U_{1,4}\psi_4 \\ \psi_2 \\ U_{2,3}\psi_3 \\ U_{2,3}U_{3,4}\psi_3 \\ U_{2,4}\psi_4 \\ \psi_3 \\ U_{3,4}\psi_4 \\ \psi_4 \end{bmatrix} \quad (5.16)$$

where  $\psi_i \in \mathbb{R}^{20}$   $i = 1, 2, 3, 4$  is obtained as

$$\psi_i = \begin{bmatrix} M_{i,1} \\ M_{i,2} \\ M_{i,3} \\ M_{i,4} \\ A_{1,1}M_{i,2} \\ A_{3,1}M_{i,1} \\ A_{1,2}M_{i,2} \\ A_{3,2}M_{i,1} \\ A_{1,3}M_{i,2} \\ A_{3,3}M_{i,1} \\ A_{1,4}M_{i,2} \\ A_{3,4}M_{i,1} \\ A_{6,5}M_{i,3} \\ A_{7,5}M_{i,4} \\ A_{6,6}M_{i,3} \\ A_{7,6}M_{i,4} \\ A_{6,7}M_{i,3} \\ A_{7,7}M_{i,4} \\ A_{6,8}M_{i,3} \\ A_{7,8}M_{i,4} \end{bmatrix}. \quad (5.17)$$



Reference model terms are collected into  $Y \in \mathbb{R}^{4 \times 300}$  as follows

$$Y = \begin{bmatrix} \Sigma & 0_{20 \times 1} & 0_{20 \times 1} & 0_{20 \times 1} \\ -\Sigma & 0_{20 \times 1} & 0_{20 \times 1} & 0_{20 \times 1} \\ -\Sigma & 0_{20 \times 1} & 0_{20 \times 1} & 0_{20 \times 1} \\ -\Sigma & 0_{20 \times 1} & 0_{20 \times 1} & 0_{20 \times 1} \\ -\Sigma & 0_{20 \times 1} & 0_{20 \times 1} & 0_{20 \times 1} \\ -\Sigma & 0_{20 \times 1} & 0_{20 \times 1} & 0_{20 \times 1} \\ -\Sigma & 0_{20 \times 1} & 0_{20 \times 1} & 0_{20 \times 1} \\ -\Sigma & 0_{20 \times 1} & 0_{20 \times 1} & 0_{20 \times 1} \\ -\Sigma & \Sigma & 0_{20 \times 1} & 0_{20 \times 1} \\ 0_{20 \times 1} & -\Sigma & 0_{20 \times 1} & 0_{20 \times 1} \\ 0_{20 \times 1} & -\Sigma & 0_{20 \times 1} & 0_{20 \times 1} \\ 0_{20 \times 1} & -\Sigma & \Sigma & 0_{20 \times 1} \\ 0_{20 \times 1} & 0_{20 \times 1} & -\Sigma & 0_{20 \times 1} \\ 0_{20 \times 1} & 0_{20 \times 1} & -\Sigma & 0_{20 \times 1} \\ 0_{20 \times 1} & 0_{20 \times 1} & 0_{20 \times 1} & \Sigma \end{bmatrix}^T \quad (5.18)$$

where  $\Sigma \in \mathbb{R}^{20}$  is defined as

$$\Sigma = \begin{bmatrix} -\dot{x}_{m,1}A_m^{(3,1)} - \dot{x}_{m,2}A_m^{(3,2)} - \dot{x}_{m,3}A_m^{(3,3)} - \dot{x}_{m,4}A_m^{(3,4)} - \dot{u}_{m,1}B_m^{(3,1)} - \dot{u}_{m,2}B_m^{(3,1)} \\ -\dot{x}_{m,1}A_m^{(1,1)} - \dot{x}_{m,2}A_m^{(1,2)} - \dot{x}_{m,3}A_m^{(1,3)} - \dot{x}_{m,4}A_m^{(1,4)} - \dot{u}_{m,1}B_m^{(1,1)} - \dot{u}_{m,2}B_m^{(1,2)} \\ -\dot{x}_{m,5}A_m^{(6,5)} - \dot{x}_{m,6}A_m^{(6,6)} - \dot{x}_{m,7}A_m^{(6,7)} - \dot{x}_{m,8}A_m^{(6,8)} - \dot{u}_{m,3}B_m^{(6,3)} - \dot{u}_{m,4}B_m^{(6,4)} \\ -\dot{x}_{m,5}A_m^{(7,8)} - \dot{x}_{m,6}A_m^{(7,6)} - \dot{x}_{m,7}A_m^{(7,7)} - \dot{x}_{m,8}A_m^{(7,8)} - \dot{u}_{m,4}B_m^{(7,4)} - \dot{u}_{m,3}B_m^{(7,3)} \\ \dot{x}_{m,1} \\ \dot{x}_{m,1} \\ \dot{x}_{m,2} \\ \dot{x}_{m,2} \\ \dot{x}_{m,3} \\ \dot{x}_{m,3} \\ \dot{x}_{m,4} \\ \dot{x}_{m,4} \\ \dot{x}_{m,5} \\ \dot{x}_{m,5} \\ \dot{x}_{m,6} \\ \dot{x}_{m,6} \\ \dot{x}_{m,7} \\ \dot{x}_{m,7} \\ \dot{x}_{m,8} \\ \dot{x}_{m,8} \end{bmatrix}^T$$

(5.19)

The tracking performance, tracking error and the control inputs are presented in Figures 5.1-5.4, 5.5 and 5.6, respectively. From Figures 5.1-5.4 and 5.5, it is clear that the tracking

objective was satisfied. From Figure 5.6 and Table 3.1, it is clear that the control inputs are in acceptable limits.

In Tables 5.1 and 5.2, average maximum steady state error and average root mean square error are presented. Five Monte Carlo simulations are performed for different initial state values. The error values in Tables 5.1 and 5.2 shows that the proposed controller ensures asymptotic tracking for different initial values of the states.

In Table 5.3, a comparison of robust adaptive controller in this chapter and robust controller in Chapter 3 is given for different values of control gain matrices.

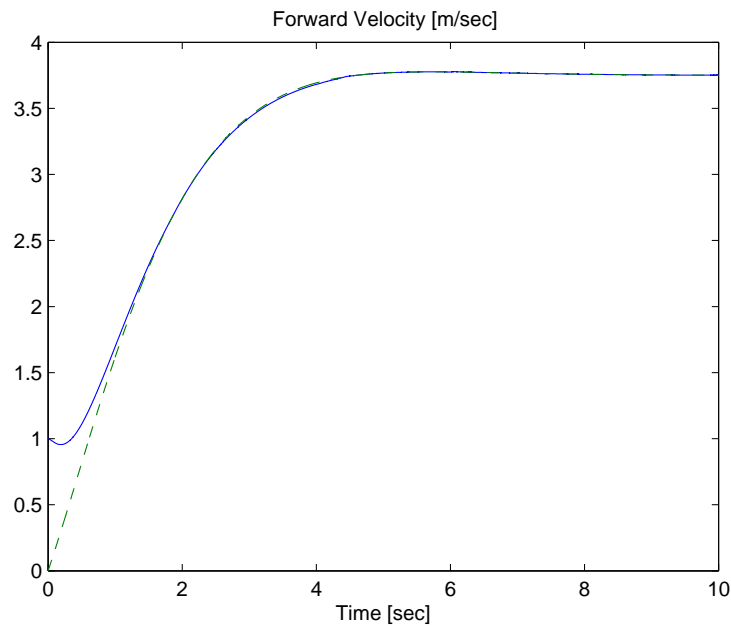


Figure 5.1. The reference velocity (dashed line) and the actual velocity (solid line).

Table 5.1. Tabulated steady state error values for 5 simulation runs.

State	Average Maximum Steady State Error
Forward Velocity	$3.2 \times 10^{-4}$
Pitch Rate	$1 \times 10^{-4}$
Roll Rate	$3.6 \times 10^{-3}$
Yaw Rate	$1.6 \times 10^{-3}$

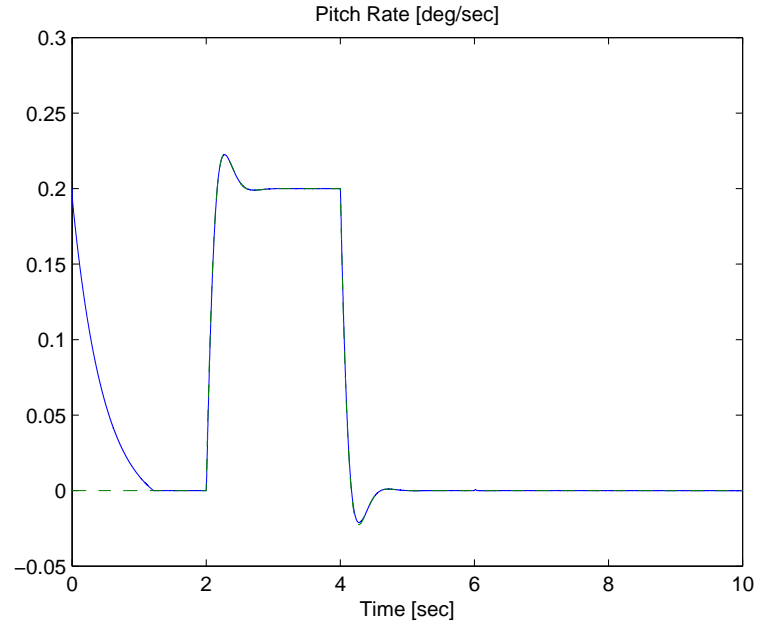


Figure 5.2. The reference pitch rate (dashed line) and the actual pitch rate (solid line).

Table 5.2. Tabulated root mean square error values for 5 simulation runs.

State	Average Root Mean Square Error
Forward Velocity	0.83
Pitch Rate	0.088
Roll Rate	0.086
Yaw Rate	0.082

Table 5.3. Comparison of robust controller and robust adaptive controller.

Type of controller	$K$	$\beta$	$\Lambda$	Mean Squared Error
Robust	$100 I_4$	$20 I_4$	$2 I_4$	$7.1 \times 10^{-2}$
Robust Adaptive	$100 I_4$	$20 I_4$	$2 I_4$	$5.6 \times 10^{-2}$
Robust Adaptive	$100 I_4$	$10 I_4$	$2 I_4$	$6.1 \times 10^{-2}$
Robust Adaptive	$100 I_4$	$5 I_4$	$2 I_4$	$6.4 \times 10^{-2}$
Robust Adaptive	$100 I_4$	$1 I_4$	$2 I_4$	$6.8 \times 10^{-2}$

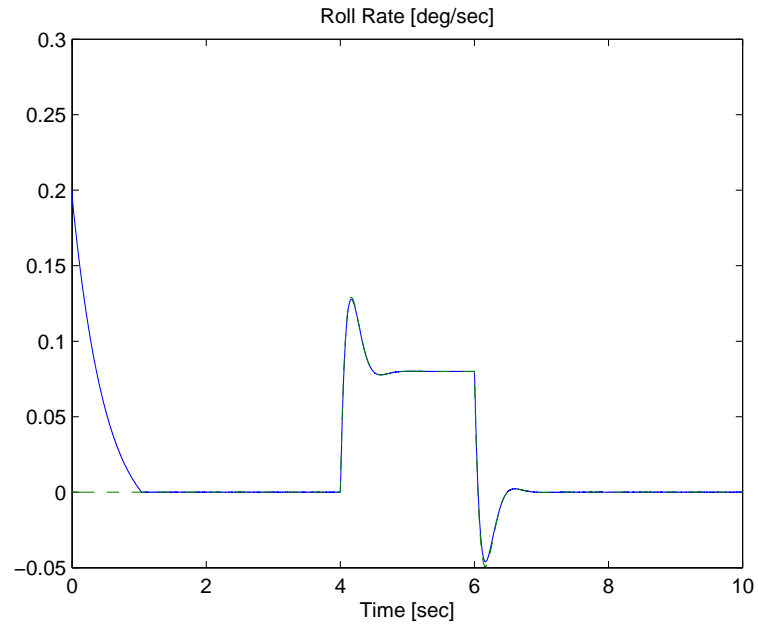


Figure 5.3. The reference roll rate (dashed line) and the actual roll rate (solid line).

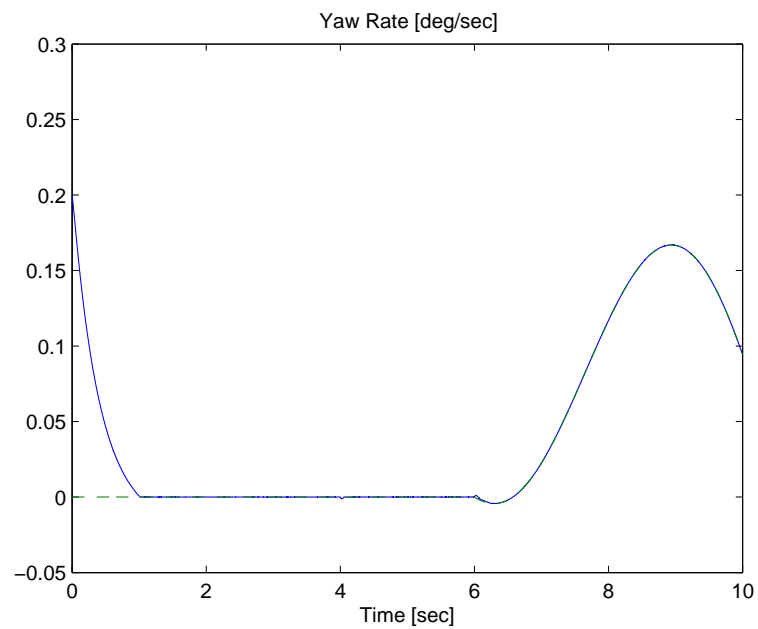


Figure 5.4. The reference yaw rate (dashed line) and the actual yaw rate (solid line).

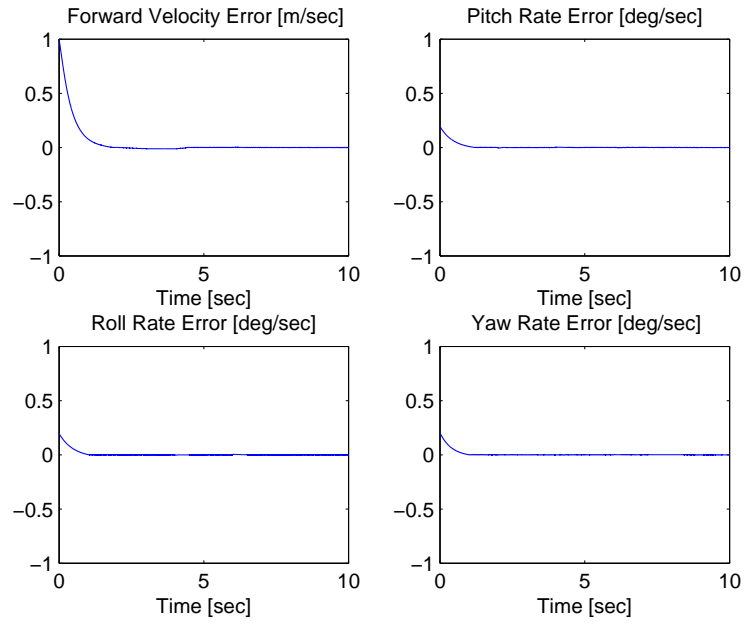


Figure 5.5. The output tracking error  $e(t)$ .

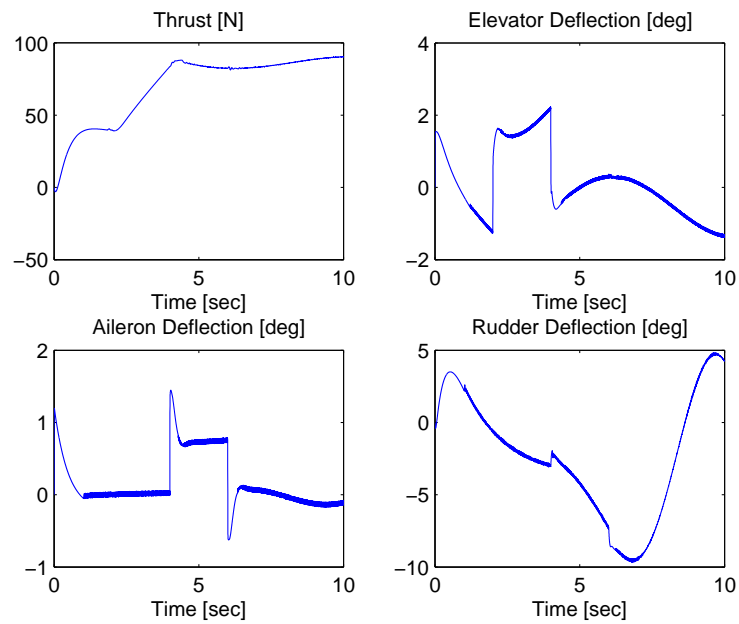


Figure 5.6. The control input  $u(t)$ .

## 5.4.2. Twin Rotor System

The system matrices in (3.32) were utilized for the reference model. Entries of the reference input  $u_m(t) \in \mathbb{R}^2$  were designed as  $\sin(t)$ . Control gains were chosen as  $\beta = 5I_2$ ,  $K = 15I_2$  and  $\Lambda = 2I_2$ , and adaptive gain matrix  $\Gamma$  in (5.7) was chosen as  $2I_{18}$ . Uncertain constant parameters are collected into  $\psi \in \mathbb{R}^{18}$  as follows

$$\psi = \begin{bmatrix} \psi_1 \\ U_{1,2}\psi_2 \\ \psi_2 \end{bmatrix}^T \quad (5.20)$$

where  $\psi_i \in \mathbb{R}^6$   $i = 1, 2, 3$  is obtained as

$$\psi_i = \begin{bmatrix} M_{i,1} \\ M_{i,2} \\ A_{2,1}M_{i,1} \\ A_{2,2}M_{i,2} \\ A_{4,3}M_{i,1} \\ A_{4,4}M_{i,2} \end{bmatrix}^T. \quad (5.21)$$

Reference model terms are collected into  $Y \in \mathbb{R}^{2 \times 18}$  as follows

$$Y = \begin{bmatrix} \Sigma & -\Sigma & 0_{1 \times 6} \\ 0_{1 \times 6} & 0_{1 \times 6} & \Sigma \end{bmatrix} \quad (5.22)$$

where  $\Sigma \in \mathbb{R}^6$  is defined as

$$\Sigma = \begin{bmatrix} -\dot{x}_{m,1}A_m^{(2,1)} - \dot{x}_{m,2}A_m^{(2,1)} - B_m^{(1,1)}A_m^{(2,1)}\dot{u}_{m,1} - B_m^{(2,1)}A_m^{(2,2)}\dot{u}_{m,1} \\ -\dot{x}_{m,3}A_m^{(4,3)} - \dot{x}_{m,4}A_m^{(4,4)} - B_m^{(3,2)}A_m^{(4,3)}\dot{u}_{m,2} - B_m^{(4,2)}A_m^{(4,4)}\dot{u}_{m,2} \\ \dot{x}_{m,1} \\ \dot{x}_{m,2} \\ \dot{x}_{m,3} \\ \dot{x}_{m,4} \end{bmatrix}^T. \quad (5.23)$$

In the simulations, the output vector consisted of pitch rate and yaw rate. Sampling time was chosen as 0.001 seconds.

The tracking performance, tracking error and the control inputs are presented in Figures 5.7, 5.8, 5.9 and 5.10, respectively. From Figures 5.7, 5.8 and 5.9, it is clear that

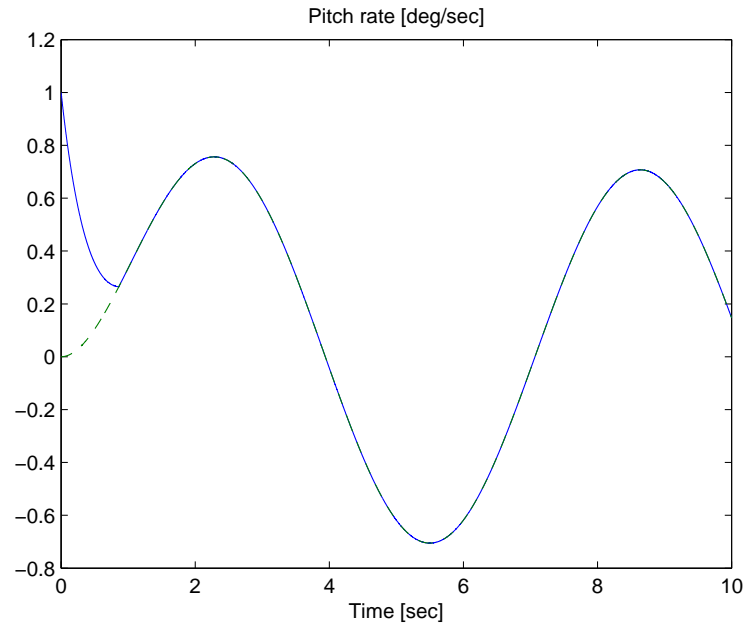


Figure 5.7. The reference pitch rate (dashed line) and the actual pitch rate (solid line).

the tracking objective was satisfied. From Figure 5.10, it is clear that the control inputs are bounded.

## 5.5. Experiment Results

In this section, proposed robust adaptive controller is validated on the twin rotor system. In the experiment, both pitch rate and yaw rate of the twin rotor system are controlled. Reference model and control gains were chosen as in Section 3.5 and adaptive gain matrix  $\Gamma$  in (5.7) was chosen as  $100I_{18}$ . The tracking errors and the control inputs are presented in Figures 5.11-5.12 and 5.13-5.14, respectively. From Figures 5.11 and 5.12, it is clear that the tracking objective was satisfied.

## 5.6. Conclusions

A robust adaptive controller was designed for the general aircraft model given in the Chapter 2. Different from the controller input in Chapter 3, robust integral of the

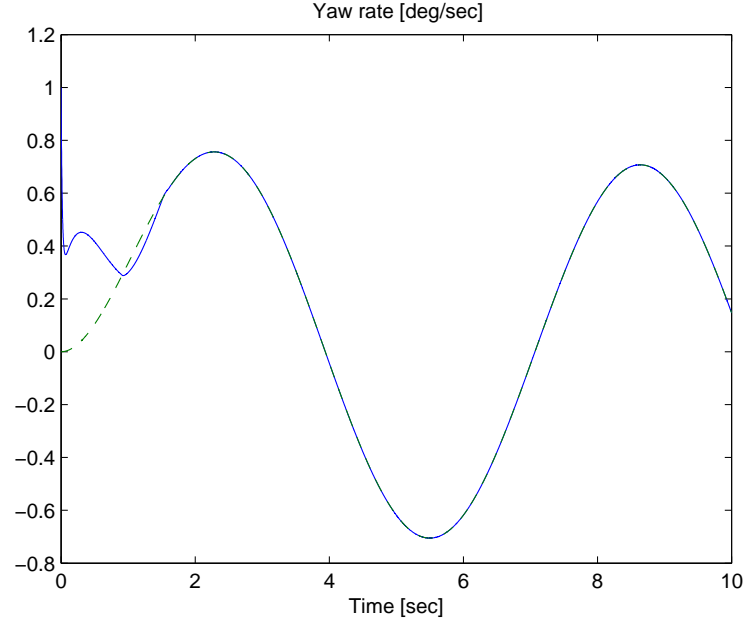


Figure 5.8. The reference yaw rate (dashed line) and the actual yaw rate (solid line).

signum of the error feedback was fused with an adaptive term to compensate for linearly parameterized uncertainties. Lyapunov type stability analysis techniques were utilized to ensure global asymptotic tracking of the output of a reference model. Numerical simulations were conducted that demonstrate the efficacy of the proposed robust adaptive controller where robustness to external disturbances and variation of the initial states were also shown. The performance of the proposed adaptive controller was evaluated on an experimental twin rotor system.

Following robust controller was designed in Chapter 3 to overcome the shortcomings of the controller in (3.35)

$$u = -DK[e(t) - e(0) + \Lambda \int_0^t e(\tau)d\tau] - D \int_0^t \beta \text{Sgn}(e(\tau))d\tau.$$

In this chapter, a robust adaptive controller is designed as follows

$$u = -DK[e(t) - e(0) + \Lambda \int_0^t e(\sigma)d\sigma] - D\beta \int_0^t \text{Sgn}(e(\tau))d\tau - D \int_0^t Y(\sigma)\hat{\psi}(\sigma)d\sigma.$$

The last term in the control input above,  $-D \int_0^t Y(\sigma)\hat{\psi}(\sigma)d\sigma$  is the adaptive term that compensates for the parametric uncertainties in the closed-loop system. The main advantage of this controller is, it shows a similar performance as the robust controller in Chapter



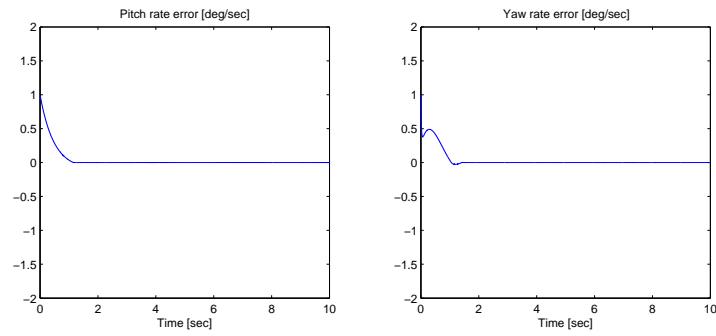


Figure 5.9. The output tracking error  $e(t)$ .

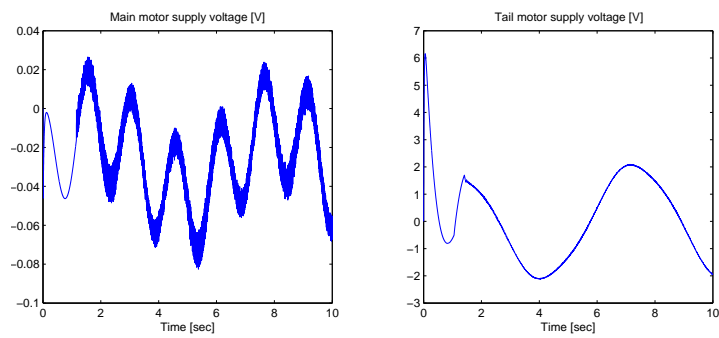


Figure 5.10. The control input  $u(t)$ .

3 for smaller  $\beta$  values. From Table 5.3, it is clear that the error performance of the robust controller with  $\beta = 20$  is same as the error performance of the robust adaptive controller with  $\beta = 1$ . It is critically important because the same performance is obtained with the robust adaptive controller by using a smaller control input. Better performances can be achieved by varying the adaptive gain matrix  $\Gamma$ .

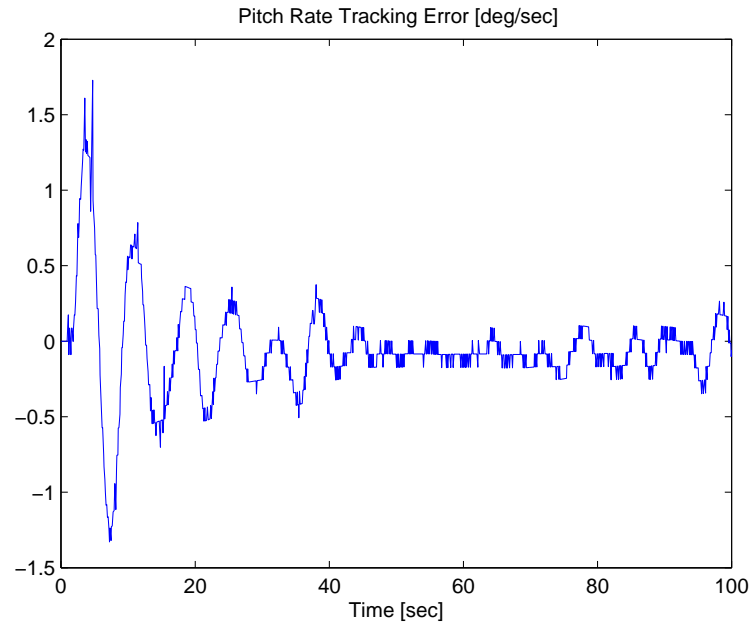


Figure 5.11. Pitch rate tracking error.

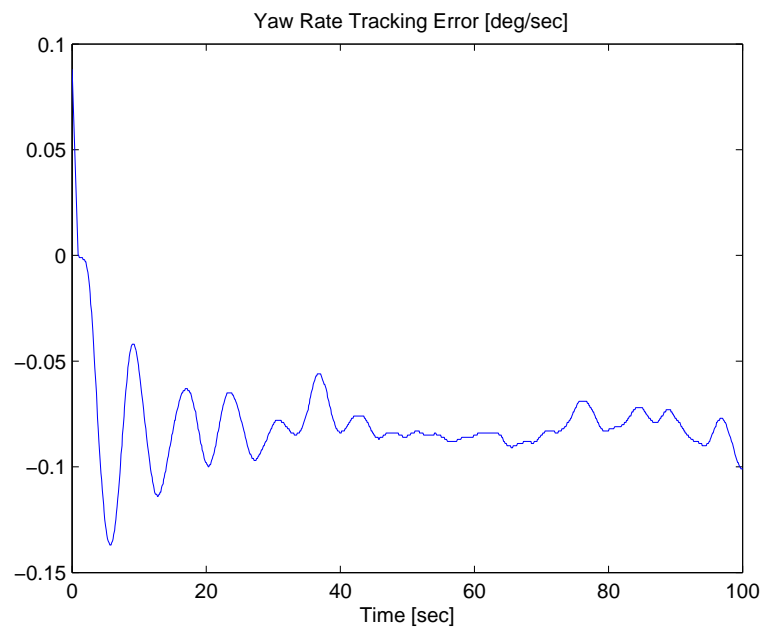


Figure 5.12. Yaw rate tracking error.

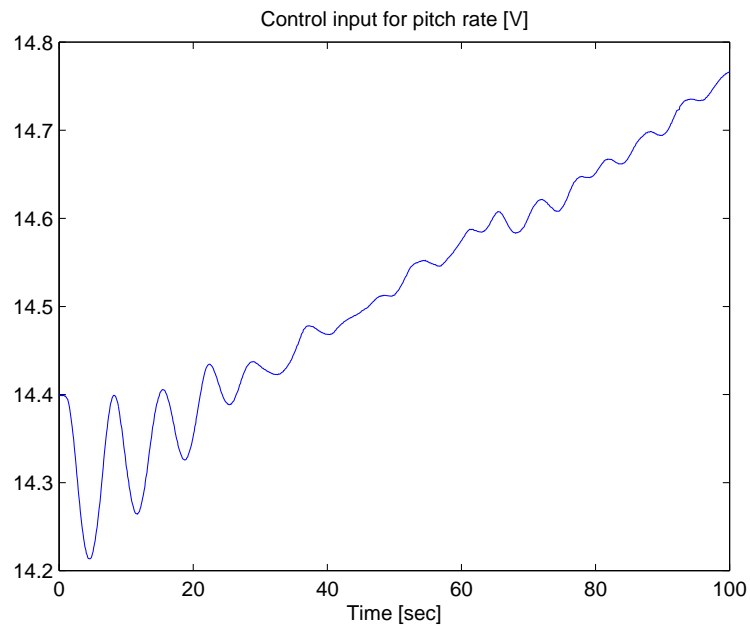


Figure 5.13. Control input for pitch rate.

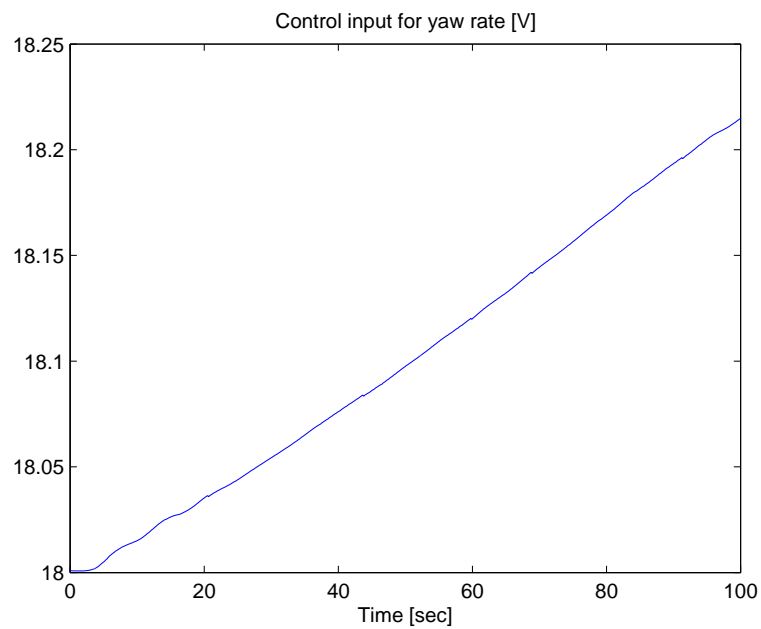


Figure 5.14. Control input for yaw rate.

## CHAPTER 6

### ROBUST NEURAL NETWORK BASED CONTROL OF UAV

#### 6.1. Abstract

In this chapter, a neural network based approach is fused with the robust controller to reduce the heavy control effort. Specifically, some part of the model uncertainties is separated to be compensated by a dynamic neural network term. While the design of the neural network term resembles the design of the adaptive component in Chapter 5, it is fundamentally different as there is no linear parametrization restriction. As a result of the neural network compensation term in the control input and thus in the closed-loop error dynamics, a new term is introduced in the Lyapunov function. Global asymptotic tracking is ensured. Simulation as well as experiment results are also presented.

#### 6.2. Control Design

The derivations are same as the robust controller in Chapter 3 till (3.10) and thus continues afterwards. For the purposes of the robust neural network based control design, the auxiliary vector in (3.9) is partitioned as

$$N = N_b + N_z + N_{nn} \quad (6.1)$$

where  $N_b(t) \in \mathbb{R}^m$  contains functions that can be bounded by constants in the sense that

$$|N_{b,i}| \leq \zeta_{N_{b,i}} \quad \forall i = 1, \dots, m \quad (6.2)$$

where  $\zeta_{N_{b,i}} \in \mathbb{R}$  are positive bounding constants and  $N_z(x, \dot{x}, e, \dot{e}) \in \mathbb{R}^m$  contains functions that can be bounded by function of error signals as

$$|N_{z,i}| \leq \rho_{z,i} \|z\| \quad \forall i = 1, \dots, m \quad (6.3)$$

where  $\rho_{z,i} \in \mathbb{R}$  are positive bounding constants and  $z(t)$  is the combined error defined in (3.14) and the term  $N_{nn}(t) \in \mathbb{R}^m$  includes the terms that depend on  $x_m, \dot{x}_m, \ddot{x}_m$ .

The expression in (3.10) can be written as

$$M\dot{r} = N_b + N_z + N_{nn} - e + DU\dot{u}. \quad (6.4)$$

In this case, the control input  $u(t)$  is designed as

$$u = -DK[e(t) - e(0) + \Lambda \int_0^t e(\sigma)d\sigma] - D\beta \int_0^t \text{Sgn}(e(\sigma))d\sigma - D \int_0^t \hat{N}_{nn}(\sigma)d\sigma \quad (6.5)$$

where  $D, K, \Lambda$  are same as in (3.16), and  $\hat{N}_{nn}(t) \in \mathbb{R}^m$  is the neural network approximation of  $N_{nn}$  that is yet to be designed. In the control in (6.5), the neural network approximation term  $\hat{N}_{nn}(t)$  is introduced to compensate for  $N_{nn}$  in (6.1). The time derivative of the control input in (6.5) is obtained as

$$\dot{u} = -DKr - D\beta \text{Sgn}(e) - D\hat{N}_{nn}. \quad (6.6)$$

After substituting (6.6) into (6.4), following closed-loop error system is obtained

$$M\dot{r} = N_b + N_z + N_{nn} - e - D(U - I_m)DKr - Kr - DUD\beta \text{Sgn}(e) - DUD\hat{N}_{nn} \quad (6.7)$$

An auxiliary term  $\bar{N}_{nn}(t) \in \mathbb{R}^m$  is defined as follows

$$\bar{N}_{nn} \triangleq N_{nn} - D(U - I_m)D\hat{N}_{nn}. \quad (6.8)$$

In (6.8),  $U$  and  $N_{nn}$  are uncertain terms that must be compensated. From the universal approximation property of neural networks,  $\bar{N}_{nn}$  can be represented by a one-layer, functional link basis neural network as Hornik et al. (1989), Lewis (1999)

$$\bar{N}_{nn} = \varphi^T \sigma + \epsilon \quad (6.9)$$

where  $\varphi \in \mathbb{R}^{3n \times m}$  is a bounded constant ideal weight matrix,  $\sigma(x_d) \in \mathbb{R}^{3n}$  is the activation function where hyperbolic tangent function is used as,  $\epsilon(x_d) \in \mathbb{R}^{3n}$  is the functional reconstruction error and  $x_d(t) \in \mathbb{R}^{3n}$  is the input of neural network structure and it is a function of reference model states and its time derivatives which is defined as

$$x_d \triangleq \begin{bmatrix} x_m \\ \dot{x}_m \\ \ddot{x}_m \end{bmatrix}. \quad (6.10)$$

The neural network approximation term  $\hat{N}_{nn}$  is designed as

$$\hat{N}_{nn} = \hat{\varphi}^T \sigma(x_d) \quad (6.11)$$

where  $\hat{\varphi}(t) \in \mathbb{R}^{3n \times m}$  is the estimate of the ideal weight matrix  $\varphi$  and is designed as

$$\hat{\varphi} = k_n \text{Proj} \left( \sigma(x_d) e^T - \int_0^t \dot{\sigma}(x_d) e^T(\tau) d\tau + \int_0^t \sigma(x_d) \Lambda e^T(\tau) d\tau \right) \quad (6.12)$$

where  $k_n \in \mathbb{R}$  is a positive constant. The time derivative of  $\hat{\varphi}$  is obtained as

$$\dot{\hat{\varphi}} = k_n \text{Proj} (\sigma r^T). \quad (6.13)$$

After substituting (6.8), (6.9) and (6.11) into (6.7), closed-loop error system can be obtained as

$$M\dot{r} = N_b + \tilde{\varphi}^T \sigma(x_d) + \epsilon(x_d) + N_z - e - \begin{bmatrix} \Phi \\ 0 \end{bmatrix} - Kr - DUD\beta \text{Sgn}(e) \quad (6.14)$$

where  $\tilde{\varphi}(t) \in \mathbb{R}^{3n \times m}$  is defined as follows

$$\tilde{\varphi} = \varphi - \hat{\varphi}. \quad (6.15)$$

### 6.3. Stability Analysis

**Theorem 6.3.1** *The neural network based robust controller in (6.5), (6.11), (6.12) ensures global asymptotic tracking in the sense that*

$$\|e(t)\| \rightarrow 0 \text{ as } t \rightarrow \infty \quad (6.16)$$

*provided that the control gain matrices  $K$  and  $\beta$  are selected by using the following procedure:*

1. For  $i = m$ ,  $\beta_m$  is selected according to (3.25) and from  $i = m - 1$  to  $i = 1$ ,  $\beta_i$  are selected according to (3.26).
2. Control gain  $k_g$  is chosen big enough to decrease the constant  $\sum_{i=1}^m \frac{\rho_{\Delta,i}^2}{4k_g}$  where  $\rho_{\Delta,i}$  are positive bounding constants.
3. Control gains  $k_{d,i}$ ,  $i = 1, \dots, (m - 1)$  are chosen big enough to decrease the constant  $\sum_{i=1}^{m-1} \frac{\zeta_{\Phi_i}^2}{4k_{d,i}}$ .

**Proof** Similar to the proof of Theorem 3.3.1, the proof consists of four subproofs. Firstly, boundedness of all the signals under the closed-loop operation will be presented by utilizing  $\Theta_i = N_{b,i} + [\tilde{\varphi}^T \sigma(x_d) + \epsilon]_i$  and  $\Delta_i = N_{z,i}$  in (A.3) of Appendix A. Secondly, in Appendix B, a supporting lemma and its proof is presented. The non-negativeness of an auxiliary integral term will be demonstrated with  $\Theta_i = N_{b,i} + \epsilon_i$  in Appendix C. Finally, in Appendix F, the asymptotic convergence of the output tracking error is proven.

## 6.4. Simulation Results

### 6.4.1. Osprey Aircraft

The system matrices in (3.27) and the reference input in (3.28) were utilized for the reference model. Control gains  $\beta$ ,  $K$  and  $\Lambda$  were chosen same as in (3.30) and (3.31) and  $k_n$  in (6.12) was chosen as 10.

The tracking performance, tracking error and the control inputs are presented in Figures 6.1-6.4, 6.5 and 6.6, respectively. From Figures 6.1-6.4 and 6.5, it is clear that the tracking objective was satisfied. From Figure 6.6 and Table 3.1, it is clear that the control inputs are in acceptable limits.

In Tables 6.1 and 6.2, average maximum steady state error and average root mean square error are presented. Five Monte Carlo simulations are performed for different initial state values. The error values in Tables 6.1 and 6.2 shows that the proposed controller ensures asymptotic tracking for different initial values of the states.

In Table 6.3, a comparison of neural network based robust controller in this chapter and robust controller in Chapter 3 is given for different values of control gain matrices.

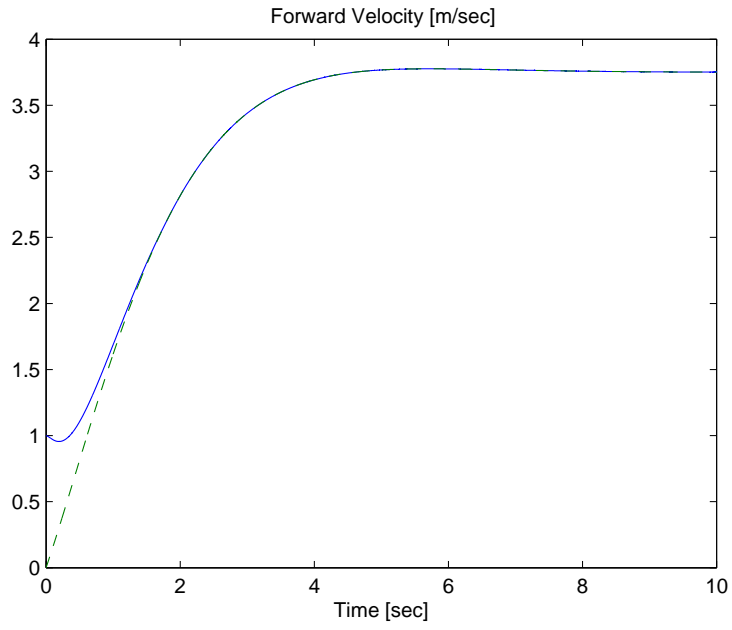


Figure 6.1. The reference velocity (dashed line) and the actual velocity (solid line).

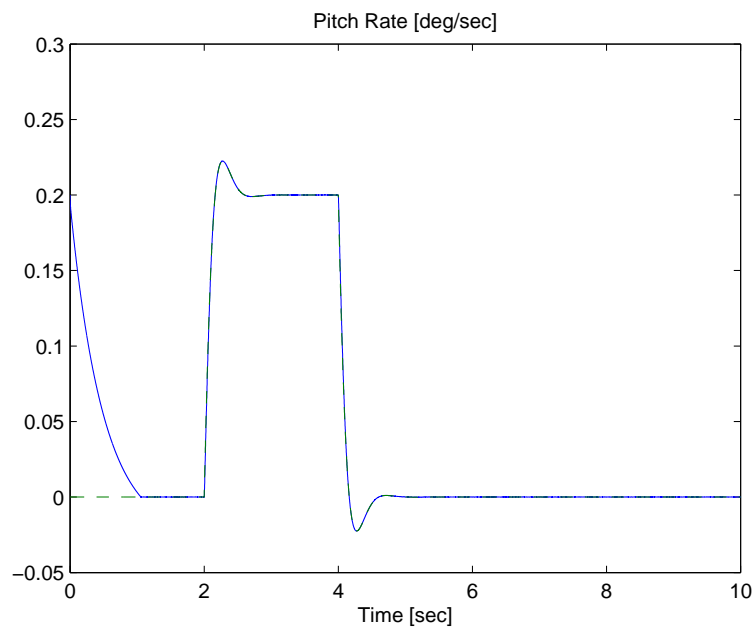


Figure 6.2. The reference pitch rate (dashed line) and the actual pitch rate (solid line).



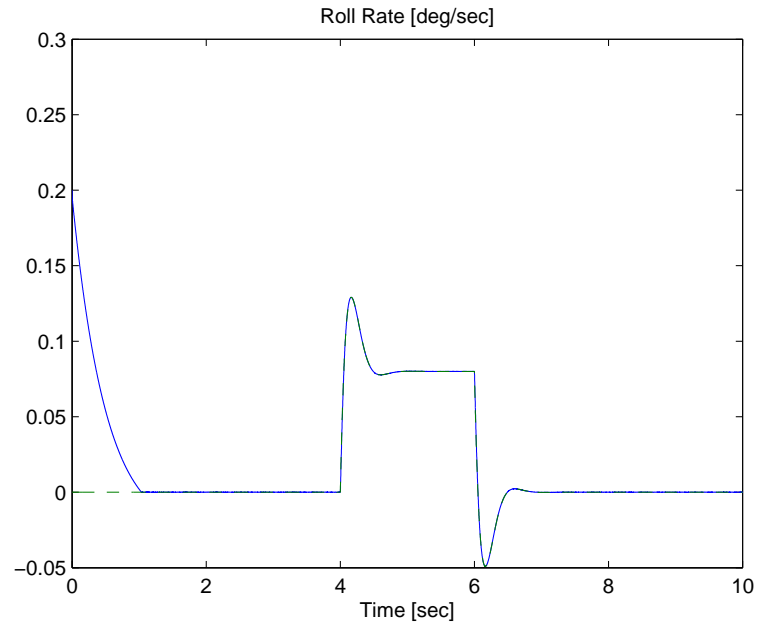


Figure 6.3. The reference roll rate (dashed line) and the actual roll rate (solid line).

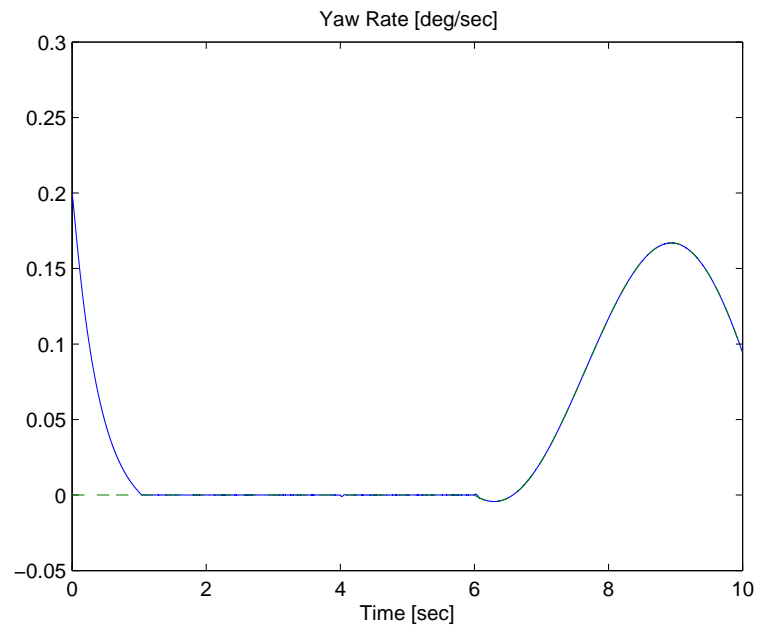


Figure 6.4. The reference yaw rate (dashed line) and the actual yaw rate (solid line).

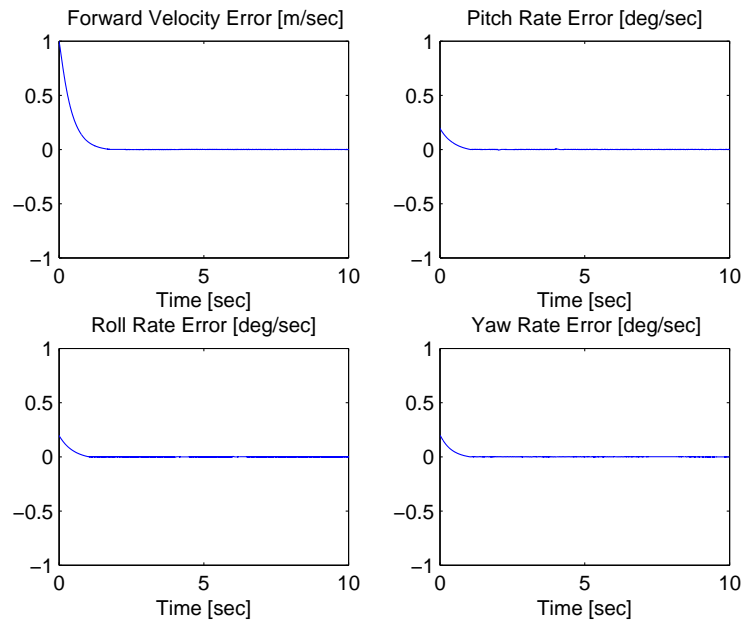


Figure 6.5. The output tracking error  $e(t)$ .

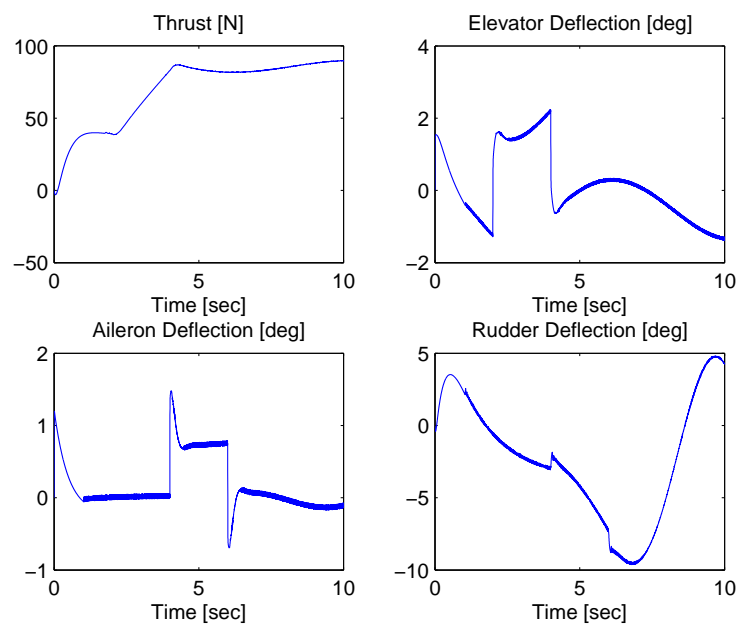


Figure 6.6. The control input  $u(t)$ .

Table 6.1. Tabulated steady state error values for 5 simulation runs.

State	Average Maximum Steady State Error
Forward Velocity	$3.1 \times 10^{-4}$
Pitch Rate	$1 \times 10^{-4}$
Roll Rate	$3.5 \times 10^{-3}$
Yaw Rate	$1.5 \times 10^{-3}$

Table 6.2. Tabulated root mean square error values for 5 simulation runs.

State	Average Root Mean Square Error
Forward Velocity	0.84
Pitch Rate	0.089
Roll Rate	0.087
Yaw Rate	0.083

Table 6.3. Comparison of robust controller and neural network based robust controller.

Type of controller	$K$	$\beta$	$\Lambda$	Mean Squared Error
Robust	$100 I_4$	$20 I_4$	$2 I_4$	$7.1 \times 10^{-2}$
NN Based Robust	$100 I_4$	$20 I_4$	$2 I_4$	$5.5 \times 10^{-2}$
NN Based Robust	$100 I_4$	$10 I_4$	$2 I_4$	$6.1 \times 10^{-2}$
NN Based Robust	$100 I_4$	$5 I_4$	$2 I_4$	$6.5 \times 10^{-2}$
NN Based Robust	$100 I_4$	$1 I_4$	$2 I_4$	$7 \times 10^{-2}$

## 6.4.2. Twin Rotor System

The system matrices in (3.32) and the reference input in (3.33) were utilized for the reference model. Control gains and initial conditions were chosen same as in Section 3.4.2 while  $k_n$  in (6.12) was chosen as 10.

In the simulations, the output vector consisted of pitch rate and yaw rate. Sampling time was chosen as 0.001 seconds.

The tracking performance, tracking error and the control inputs are presented in Figures 6.7, 6.8, 6.9 and 6.10, respectively. From Figures 6.7, 6.8 and 6.9, it is clear that the tracking objective was satisfied. From Figure 6.10, it is clear that the control inputs are bounded.

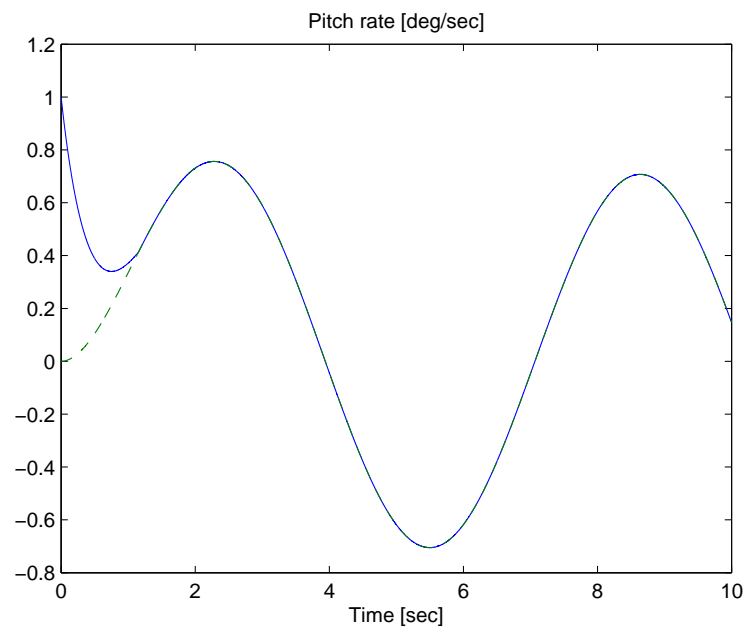


Figure 6.7. The reference pitch rate (dashed line) and the actual pitch rate (solid line).

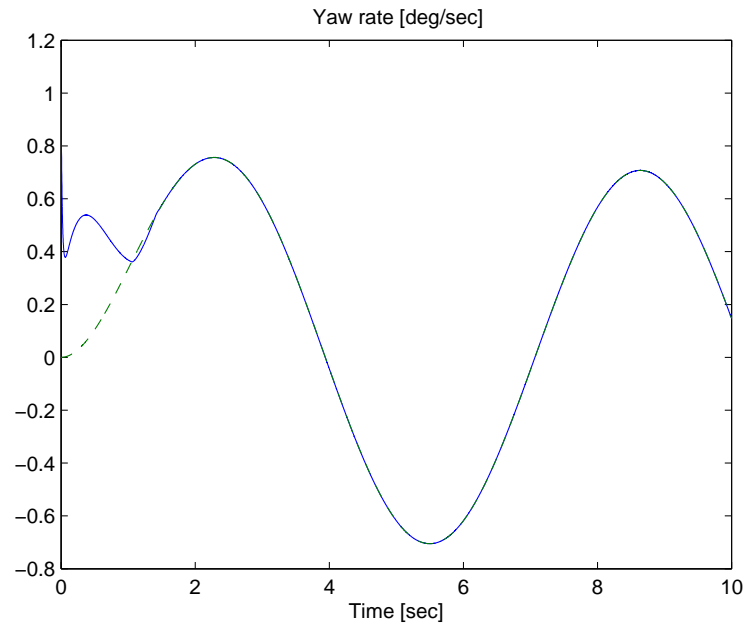


Figure 6.8. The reference yaw rate (dashed line) and the actual yaw rate (solid line).

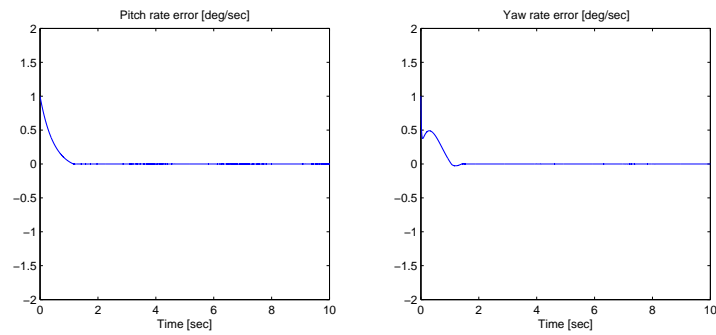


Figure 6.9. The output tracking error  $e(t)$ .

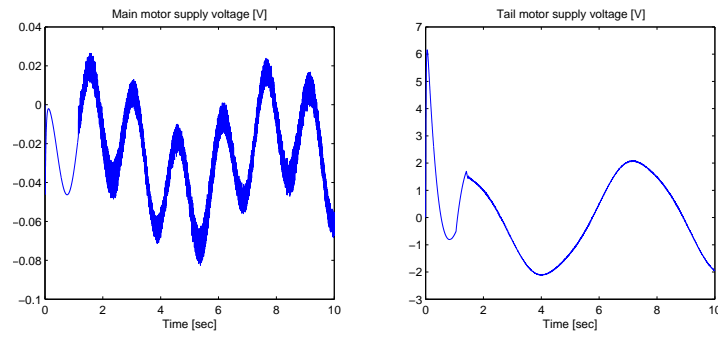


Figure 6.10. The control input  $u(t)$ .

## 6.5. Experiment Results

In this section, proposed neural network based robust controller is validated on the twin rotor system. In the experiment, both pitch rate and yaw rate of the twin rotor system are controlled. Reference model and control gains were chosen as in Section 3.5 and  $k_n$  in (6.12) was chosen as 10. The tracking errors and the control inputs are presented in Figures 6.11-6.12 and 6.13-6.14, respectively. From Figures 6.11 and 6.12, it is clear that the tracking objective was satisfied.

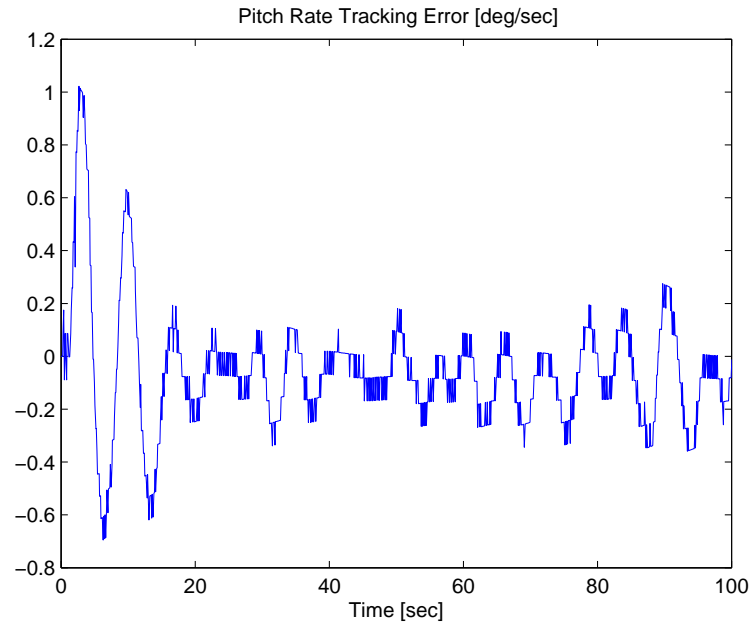


Figure 6.11. Pitch rate tracking error.

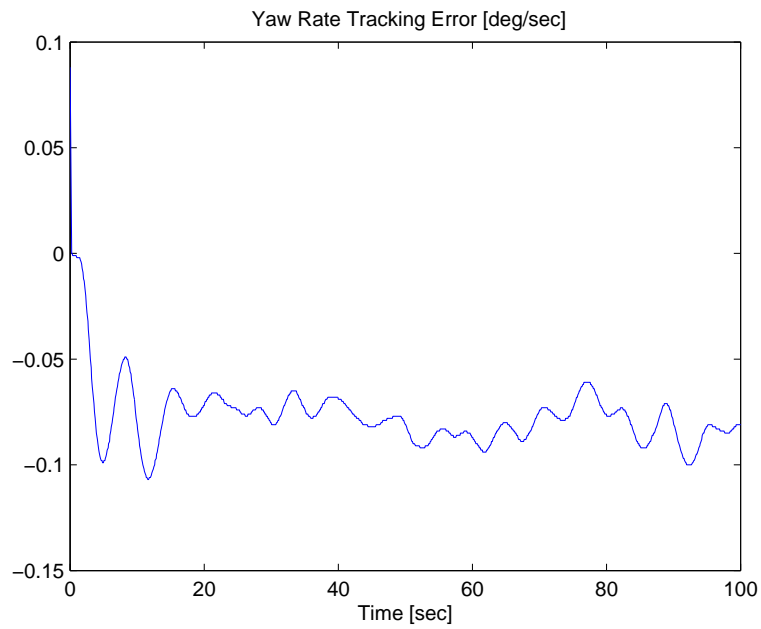


Figure 6.12. Yaw rate tracking error.

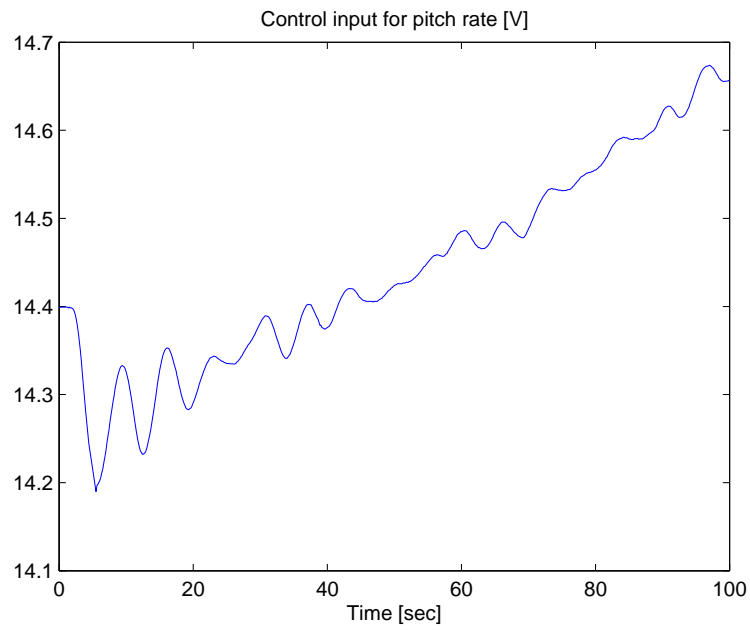


Figure 6.13. Control input for pitch rate.

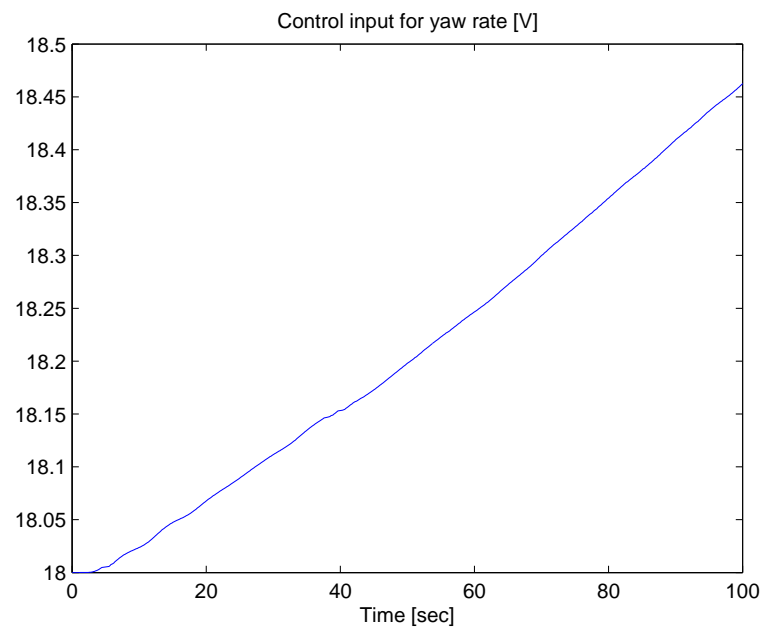


Figure 6.14. Control input for yaw rate.



## 6.6. Conclusions

A neural network based robust controller was designed for the general aircraft model given in the Chapter 2. Different from the controller input in Chapter 3, robust integral of the signum of the error feedback is utilized with a neural network term to compensate the uncertainties. Lyapunov type stability analysis techniques were utilized to ensure global asymptotic tracking of the output of a reference model. Numerical simulations were conducted that demonstrate the efficacy of the proposed controller where robustness to external disturbances and variation of the initial states were also shown. The performance of the proposed controller was evaluated on a twin rotor system via experiments.

Following robust controller was designed in Chapter 3 to overcome the shortcomings of the controller in (3.35)

$$u = -DK[e(t) - e(0) + \Lambda \int_0^t e(\tau)d\tau] - D \int_0^t \beta \text{Sgn}(e(\tau))d\tau.$$

In this chapter, a neural network based robust controller is designed as follows

$$u = -DK[e(t) - e(0) + \Lambda \int_0^t e(\sigma)d\sigma] - D\beta \int_0^t \text{Sgn}(e(\sigma))d\sigma - D \int_0^t \hat{N}_{nn}(\sigma)d\sigma.$$

The last term in the control input above,  $D \int_0^t \hat{N}_{nn}(\sigma)d\sigma$  is the neural network term that compensates for some part of the uncertainties in the closed-loop system. Controller looks like the adaptive design, neural network term is updated in every time step, however the dimension of the matrices are lower than the adaptive case, so the processing cost is reduced. The main advantage of this controller is, it shows a similar performance as the robust controller in Chapter 3 for smaller  $\beta$  values. From Table 6.3, it is clear that the error performance of the robust controller with  $\beta = 20$  is same as the error performance of the neural network based robust controller with  $\beta = 1$ . It is critically important because the same performance is obtained with the neural network based robust controller by using a smaller control input. Better performances can be achieved by varying the neural network gain constant  $k_n$ .

# CHAPTER 7

## COMPARISON OF NUMERICAL RESULTS

In this chapter comparison of the simulation results and the experiment results are given.

### 7.1. Comparison of Simulation Results

In this section, the simulation performances of the proposed robust controllers are compared for the Osprey aircraft model. In Table 7.1, the tracking error performances are compared when the control gains are chosen same for all of the proposed controllers.

Table 7.1. Comparison of proposed robust controllers.

Type of controller	$K$	$\beta$	$\Lambda$	Mean Squared Error
Robust	$100 I_4$	$20 I_4$	$2 I_4$	$7.1 \times 10^{-2}$
Robust Optimal	$100 I_4$	$20 I_4$	$2 I_4$	$4.6 \times 10^{-2}$
Robust Adaptive	$100 I_4$	$20 I_4$	$2 I_4$	$5.6 \times 10^{-2}$
NN Based Robust	$100 I_4$	$20 I_4$	$2 I_4$	$5.5 \times 10^{-2}$

Secondly, the performances of the proposed robust controllers are compared while the initial conditions of the system are varied. The initial value of each element of the state vector was varied from 0 to 4, while initial value of each element of reference state vector was set to 0. Each simulation for the robust controllers in Chapter 3 to Chapter 6 was

performed five times. So the initial conditions are selected as

$$x^i(0) = \begin{bmatrix} i - 1 \\ i - 1 \\ i - 1 \\ i - 1 \\ i - 1 \\ i - 1 \\ i - 1 \\ i - 1 \end{bmatrix} \quad (7.1)$$

where  $i = 1, 2, 3, 4, 5$  is the sequence number of the simulation.

The results are given in Table 7.2. In Table 7.2, average maximum steady state error, average root mean square (RMS) error, average RMS control input, error standard deviation, control input standard deviation and runtime of simulation are presented for all of the controllers. Maximum steady state error is defined as the mean of the last 5 second of the error values. RMS error is defined as

$$e_{rms} = \sqrt{\frac{\sum_{i=1}^n e_i^2}{n}}. \quad (7.2)$$

RMS torque is defined as

$$u_{rms} = \sqrt{\frac{\sum_{i=1}^n u_i^2}{n}}. \quad (7.3)$$

Standard deviation of error is defined as

$$\sigma_e = \sqrt{\frac{1}{n} \sum_{i=1}^n (e_i - \bar{e})^2} \quad (7.4)$$

where  $\bar{e}$  is the mean value of the tracking error. Standard deviation of control input is defined as

$$\sigma_u = \sqrt{\frac{1}{n} \sum_{i=1}^n (u_i - \bar{u})^2} \quad (7.5)$$

where  $\bar{u}$  is the mean of the control input.

The tracking errors of robust controllers are presented in Figures 7.1-7.4. It is clear that the tracking objective was satisfied for different initial conditions of the system.

Error Metric	State	Robust	Optimal	Adaptive	NN Based	MacKunis (2009)
Avg. Max SS Error	Forward Velocity	0.269	0.269	0.266	0.269	0.268
	Pitch Rate	0.032	0.032	0.034	0.032	0.032
	Roll Rate	0.014	0.013	0.016	0.014	0.015
	Yaw Rate	0.028	0.028	0.037	0.030	0.030
Avg. RMS Error	Forward Velocity	0.388	0.391	0.422	0.386	0.337
	Pitch Rate	0.289	0.294	0.287	0.290	0.185
	Roll Rate	0.299	0.304	0.304	0.300	0.241
	Yaw Rate	0.365	0.368	0.379	0.363	0.365
Avg. RMS Control input	Forward Velocity	107.95	107.11	106.7	107.8	118.6
	Pitch Rate	9.697	9.7630	9.688	9.716	8.137
	Roll Rate	2.363	2.411	2.408	2.376	1.787
	Yaw Rate	46.804	46.460	45.530	46.850	48.065
Error Std. Dev.	Forward Velocity	0.378	0.379	0.404	0.373	0.325
	Pitch Rate	0.277	0.281	0.274	0.277	0.178
	Roll Rate	0.287	0.291	0.291	0.287	0.234
	Yaw Rate	0.353	0.356	0.365	0.350	0.352
Control input Std. Dev.	Forward Velocity	43.37	43.53	42.07	43.59	41.37
	Pitch Rate	9.434	9.491	9.420	9.450	7.955
	Roll Rate	2.240	2.284	2.279	2.251	1.699
	Yaw Rate	35.60	35.38	34.80	35.76	35.43
Avg. Execution Time of Simulation (sec)		193	190	313	204	199

Table 7.2. Tabulated values for the 5 runs for the developed controllers on the Osprey aircraft model while the initial conditions are varied as in (7.1).

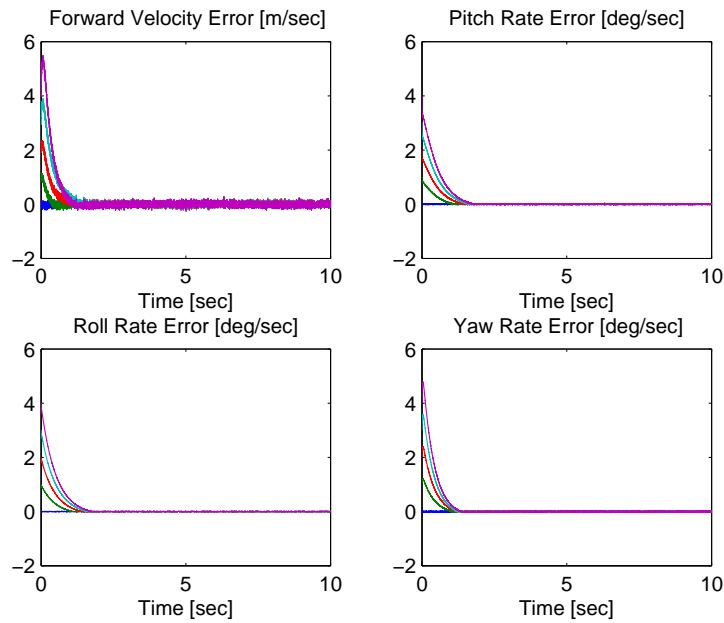


Figure 7.1. Tracking errors for the 5 runs of the robust controller simulation.

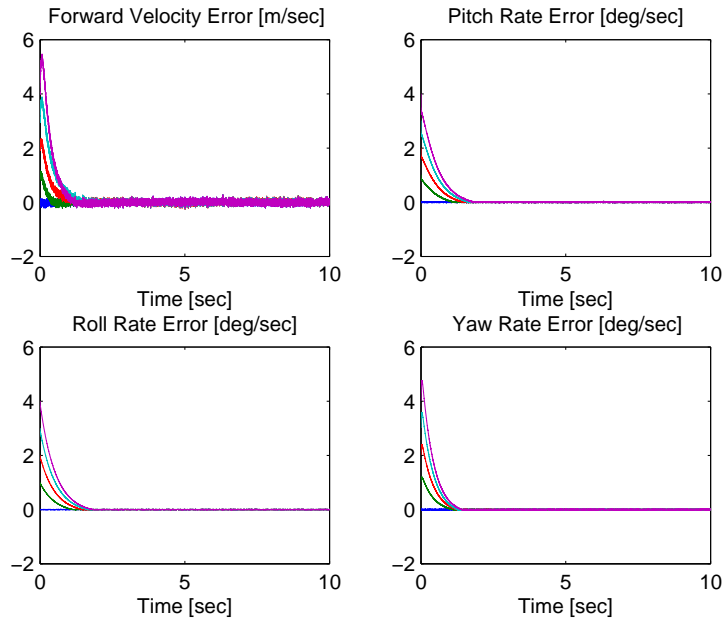


Figure 7.2. Tracking errors for the 5 runs of the robust optimal controller simulation.

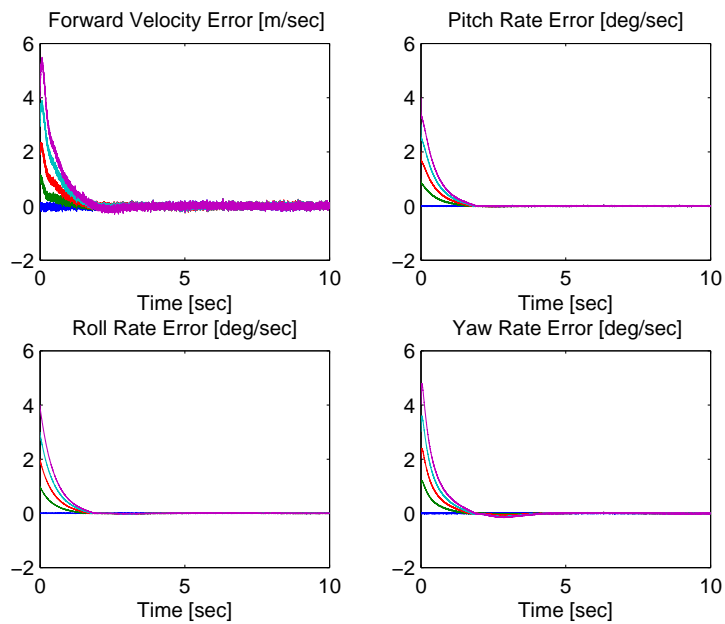


Figure 7.3. Tracking errors for the 5 runs of the robust adaptive controller simulation.

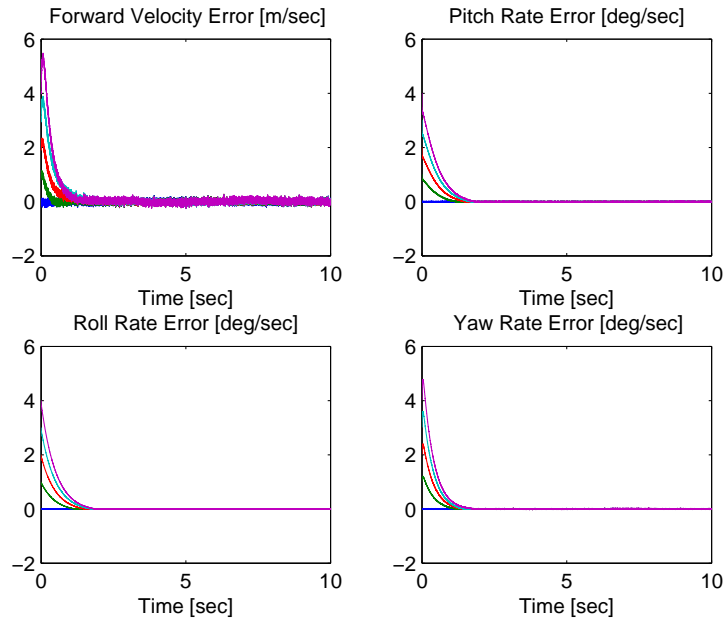


Figure 7.4. Tracking errors for the 5 runs of the neural network based robust controller simulation.

## 7.2. Comparison of Experiment Results

In this section, the experiment results which were presented in Chapters 3-6 are compared. The tracking error of the robust controllers are presented in Figures 7.5 and 7.6. It is clear that the tracking objective was satisfied.

In Table 7.3, the tracking error performances are compared for the robust controllers.

Table 7.3. Comparison of the proposed robust controllers.

Type of controller	Mean Squared Error
Robust	$78 \times 10^{-3}$
Robust Optimal	$41 \times 10^{-3}$
Robust Adaptive	$154 \times 10^{-3}$
NN Based Robust	$80 \times 10^{-3}$

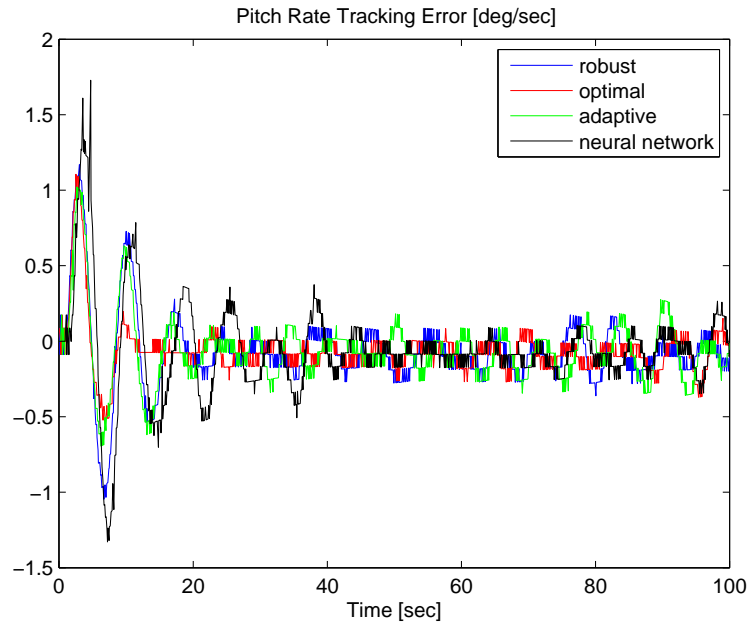


Figure 7.5. Pitch rate tracking error results of twin rotor system.

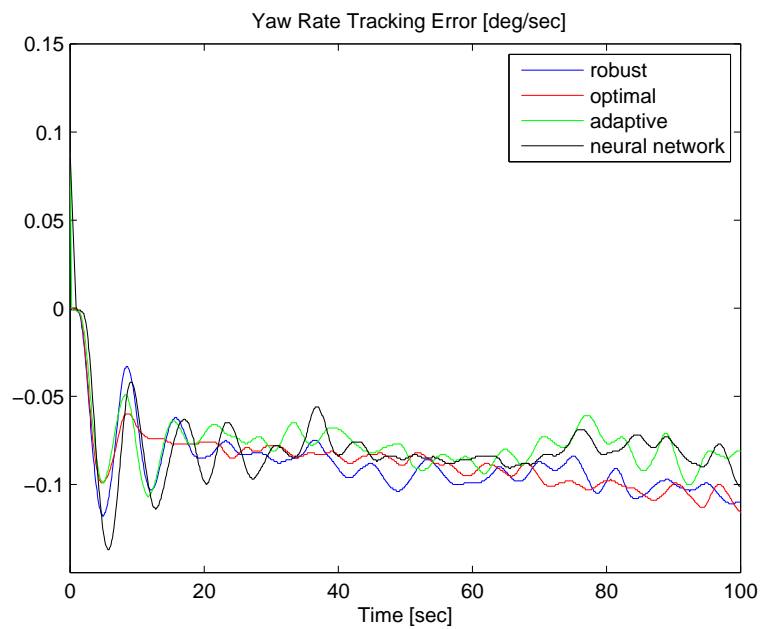


Figure 7.6. Yaw rate tracking error results of twin rotor system.

## CHAPTER 8

### CONCLUSIONS

In this thesis, control of unmanned aerial vehicles subject to uncertainties and additive state-dependent disturbances in their dynamic models was discussed. Specifically, a linear time invariant state space model of an aircraft was considered where the unmodeled effects were considered as an additive state-dependent disturbance-like term. Furthermore, in the linear time-invariant state space model,  $A$  and  $B$  matrices were considered to be uncertain. Tracking of output of a reference model was aimed under the restriction that only the output of the aircraft was available for control design purposes.

Given the uncertainties and disturbances, a robust approach was decided as a solution to the control problem at hand. To initiate the control design, an auxiliary error-like term was designed to ensure only first order time derivatives appear in the stability analysis for simplicity reasons. The open-loop error system was then obtained where the input gain matrix was uncertain. The design problem was further complicated by the lack of positive definiteness or symmetry of this input gain matrix. A matrix decomposition was suggested as a possible solution to this. While the matrix decomposition was previously utilized for some control problems, its utilization for the problem considered in this thesis is **novel**. Works in MacKunis et al. (2010), MacKunis (2009) aimed a similar control problem and considered utilizing constant best guess estimates of uncertain system matrices to deal with the uncertain input gain matrix issue. While in these works satisfactory performance was demonstrated in numerical simulations, it was not clear how the constant estimates were chosen and no procedure was suggested. While the uncertain input gain matrix issue was solved via the matrix decomposition, this introduced a new problem that should be dealt with. After the matrix decomposition, the control input was first pre-multiplied with an uncertain matrix in unity upper triangular structure and this resulting term was then multiplied from left with a diagonal matrix with entries equal to either  $+1$  or  $-1$ . While several past works considered the diagonal matrix to be available, applying the matrix decomposition to several aircraft models found in the literature resulted in the entries of the diagonal matrix to be equal to  $+1$ .



To deal with the uncertain unity upper triangular matrix multiplying the control input, its diagonal entries being equal to 1 was made use of. Specifically, this uncertain unity upper-triangular matrix was written as sum of identity matrix and a strictly upper triangular matrix. This forced the control design to be started from its bottom entry and the continue upwards, while the upper entries of the control input treats the entries below it as disturbances. This partially solved the above mentioned uncertain unity upper triangular matrix multiplying the control input problem in the sense that there were some consequences which will then be faced in the stability analysis.

Next, a robust controller was designed. In the design, integral of signum of the output tracking error was fused with a standard proportional integral controller. The integral of signum of the output tracking error was utilized as part of the controller primarily to reject uncertainties in the dynamic model. The signum of error terms are commonly preferred as part of control designs to deal with model uncertainties. But it introduces a discontinuity as a result of the sign function. While for some applications this does not constitute a problem, when designing controllers for UAVs, discontinuity in the control input may yield in unwanted consequences. In view of this, integration of the signum of the output tracking error was fused to proportional integral controller. While the integral of signum of error control structure was previously used in the literature to reject uncertainties, it being used in conjunction with the matrix decomposition of the uncertain input gain matrix precluded the previously available stability analysis.

As a result, in this thesis, a **novel** four-step Lyapunov based stability analysis was developed. Specifically, first boundedness of all the time-varying terms under the closed-loop operation was aimed. There are two aspects of achieving boundedness, where one is for practical reasons while the other is a technical requirement. The main practical reason is the limits of the control inputs. The control inputs of a UAV are almost all the time restricted to remain within certain bounds and are saturated outside these bounds. So any design should take this boundedness criteria into account. On the other hand, the technical requirement is that boundedness of the output tracking error and its time derivative are essential for Lemma B.0.1. In the first step, ultimate boundedness of all the time-varying terms were ensured via Lyapunov-type techniques. Secondly, a bound on the integration of the absolute values of the entries of the time derivative of the output tracking error depending on the absolute values of the entries of the output tracking error and their integrals are obtained. This bound is essential for Lemma C.0.2 where the non-

negativeness analysis of an auxiliary integral term is investigated. The main difference of the auxiliary integral term from the existing literature is that, as a direct consequence of the matrix decomposition, the signum of the tracking term was pre-multiplied with a matrix including the uncertain unity upper triangular matrix. To address this, the results of Lemma B.0.1 was utilized to construct a **novel** proof. After ensuring the non-negativeness of an auxiliary integral term, it was added to the Lyapunov function which was used to ensure boundedness to form a new Lyapunov function to investigate the convergence of the tracking error. Negative semi-definiteness of the time derivative of the Lyapunov function was proven. After utilizing Barbalat's Lemma, global asymptotic convergence of the output tracking error was guaranteed.

Secondly, considering the limitations on the resources of a UAV, an optimal control design is aimed. However, almost all of the optimal controllers in the literature required accurate knowledge of aircraft dynamics, which was obviously not the case for the control problem discussed in this thesis. As a result, initially, a temporary assumption was made on the availability of system uncertainties. Then, a quadratic performance index, which is a function of the output tracking error and the control input, is chosen. The optimal part of the control input that minimizes the quadratic performance index was then designed. Since the aircraft dynamics were uncertain, a time-varying observer-like term was designed and fused with the optimal part of the control input. The boundedness and convergence analysis were very similar to the robust controller's where global asymptotic tracking was ensured. Then the convergence of the time-varying observer-like term to the term that included uncertain aircraft dynamics was proven thus concluding the optimality analysis.

Afterwards, in an attempt to reduce the heavy control effort required by robust controllers, controllers with learning components were aimed. Specifically, in Chapter 5, after linearly parameterizing some part of the model uncertainties, by writing it as a multiplication of an available known regressor matrix and an uncertain constant parameter vector, an adaptive update rule was designed. An adaptive component was fused to the robust controller to obtain an adaptive controller. While the boundedness analysis was similar, a new term was added to the Lyapunov function used for convergence analysis, due to the adaptation, and global asymptotic stability was proven.

In Chapter 6, another extension was aimed without requiring the linear parameterizability condition. Specifically, the terms that depend on reference model state vector and

its time derivatives were regrouped and were rewritten by using the universal approximation property of neural networks. Next, neural network approximation term was designed via the design of the time-varying estimate of the ideal weight matrix. This neural network approximation term was fused with the robust controller. The boundedness analysis was similar to the previous controller's, while a new term due to the neural network approximation was introduced to the Lyapunov function utilized for convergence analysis. Similar to the previous cases, global asymptotic results was proven.

To validate the proposed robust controllers, numerical simulations and experimental studies are performed. First, Osprey UAV model and twin rotor model are used for the MATLAB simulations, robustness to external disturbances and variation of the initial states were also considered. Simulation results showed that the proposed controllers effectively reached the control objectives for both of the models. Secondly, the proposed controllers are validated on a twin rotor experimental system. The controllers are implemented on LabVIEW and control signals are sent to DC motors on the twin rotor system. Disturbance rejection performance of the controllers is also considered, a ventilator which is shown in Figure 2.8 is used as a disturbance.

In Chapter 7, the comparison of the proposed controllers is given. In Section 7.1, the simulation results are compared. From Table 7.1, it is obvious that the tracking error and the control input performances are improved with the optimal, adaptive and neural network modifications of the robust controller. Also in Table 7.2, the proposed controllers are compared with the controller in MacKunis et al. (2010) for different initial conditions. It was clear that the error and control input statistics of the proposed controllers were close with the study in MacKunis et al. (2010). Also in Table 7.2, average execution time of the controllers are presented. As expected, the execution time of the adaptive and neural network based controllers are longer due to the update laws in the control designs. Then the experiment results are compared in Section 7.2. As shown in Figures 7.5-7.6 and Table 7.3, the optimal controller showed the best performance for our experimental system. Pitch rate tracking error results of the twin rotor system was better than yaw rate tracking error results, because cross coupling effect and high nonlinearities in the experimental system complicated the yaw rate control. Figure 7.6 indicated that the robust adaptive and neural network based robust controller showed the best performance on yaw rate tracking objective.

## 8.1. Future Work

In this thesis, robust controllers were developed for an aircraft model subject to additive, state-dependent, nonlinear, uncertain disturbance-like terms. As possible future works, following open problems can be attacked.

As described in detail in Chapter 2, the number of system output is considered to be equal to the number of the inputs for the aircraft model presented in this thesis. However, in different aircraft models (*i.e.*, the model of an F-16 in Stevens and Lewis (2003)), the number of the inputs may be greater than the number of outputs. So, it can be said that these kinds of systems have actuator redundancy. The matrix decomposition in (3.6) cannot be applied since the input gain matrix becomes a non-square matrix. According to our best knowledge, this is an open problem.

Another important issue in almost every mechatronic control system is the delay in actuation. If the delay in the control input exceeds a certain value then some type of compensation should be designed. Modifying the robust controllers designed in this thesis to address input delay may be considered as a possible future work.

In Chapter 2, it was considered that the output matrix  $C$  was known. A possible extension can be considering the output matrix as uncertain (fully or partially) and try to deal with this as well.

After the matrix decomposition the diagonal matrix  $D$  was investigated for several aircraft models in the literature and it was observed to be equal to identity matrix. Additionally, it was considered to be available for control design purposes. A possible extension may be considering situations where  $D$  is not an identity matrix and that it is also unavailable. While Nussbaum gain can be considered as a possible method for this problem, the solution is not straightforward due to the uncertain unity upper triangular matrix multiplying the control input before the diagonal matrix  $D$ .

## REFERENCES

- Adams, R. J. and S. S. Banda (1993). Robust flight control design using dynamic inversion and structured singular value synthesis. *Control Systems Technology, IEEE Transactions on* 1(2), 80–92.
- Al-Hiddabi, S. (2009). Quadrotor control using feedback linearization with dynamic extension. In *Mechatronics and its Applications, 2009. ISMA'09. 6th International Symposium on*, pp. 1–3. IEEE.
- Arapostathis, A., R. K. George, and M. K. Ghosh (2001). On the controllability of a class of nonlinear stochastic systems. *Systems & Control Letters* 44(1), 25–34.
- Austin, R. (2010). Unmanned aircraft systems. *UAVS Design, Development and Deployment*. Wiley.
- Bayrak, A., F. Dogan, E. Tatlicioglu, and B. Ozdemirel (2015). Design of an experimental twin-rotor multi-input multi-output system. *Computer Applications in Engineering Education*.
- Bidikli, B., E. Tatlicioglu, A. Bayrak, and E. Zergeroglu (2013). A new robust integral of sign of error feedback controller with adaptive compensation gain. In *Decision and Control (CDC), 2013 IEEE 52nd Annual Conference on*, pp. 3782–3787. IEEE.
- Bidikli, B., E. Tatlicioglu, and E. Zergeroglu (2014). A self tuning rise controller formulation. In *American Control Conference (ACC), 2014*, pp. 5608–5613. IEEE.
- Blanchini, F. (2009). Lyapunov methods in robustness an introduction. *Lecture notes in Automatic Control, Bertinoro (Italy)*.
- Cai, G., A. K. Cai, B. M. Chen, and T. H. Lee (2008). Construction, modeling and control of a mini autonomous uav helicopter. In *Automation and Logistics, 2008. ICAL 2008. IEEE International Conference on*, pp. 449–454. IEEE.

- Calise, A. J. and R. T. Rysdyk (1998). Nonlinear adaptive flight control using neural networks. *Control Systems, IEEE* 18(6), 14–25.
- Chen, J., D. Li, X. Jiang, and X. Sun (2006). Adaptive feedback linearization control of a flexible spacecraft. In *Intelligent Systems Design and Applications, 2006. ISDA'06. Sixth International Conference on*, Volume 2, pp. 225–230. IEEE.
- Das, A., K. Subbarao, and F. Lewis (2009). Dynamic inversion with zero-dynamics stabilisation for quadrotor control. *IET control theory & applications* 3(3), 303–314.
- Department of Defense, U. (2010). Dictionary of military and associated terms. *Online* 14, 1–02.
- Dogan, F. (2014). Design, development and control of a twin rotor system. Master's thesis, Izmir Institute of Technology.
- Doman, D. B. and A. D. Ngo (2002). Dynamic inversion-based adaptive/reconfigurable control of the x-33 on ascent. *Journal of Guidance, Control, and Dynamics* 25(2), 275–284.
- Dupree, K. (2009). *Optimal control of uncertain Euler-Lagrange systems*. Ph. D. thesis, University of Florida.
- Dupree, K., P. M. Patre, Z. D. Wilcox, and W. E. Dixon (2011). Asymptotic optimal control of uncertain nonlinear euler-lagrange systems. *Automatica* 47(1), 99–107.
- Enns, D., D. Bugajski, R. Hendrick, and G. Stein (1994). Dynamic inversion: an evolving methodology for flight control design. *International Journal of control* 59(1), 71–91.
- Enns, D. and T. Keviczky (2006). Dynamic inversion based flight control for autonomous rmax helicopter. In *American Control Conference, 2006*, pp. 8–pp. IEEE.
- Gertler, J. (2012). Us unmanned aerial systems. DTIC Document.

- Hornik, K., M. Stinchcombe, and H. White (1989). Multilayer feedforward networks are universal approximators. *Neural networks* 2(5), 359–366.
- How, J. P., E. Frazzoli, and G. Chowdhary (2012). Handbook of unmanned aerial vehicles, chapter nonlinear flight control techniques for unmanned aerial vehicles.
- Ioannou, P. and J. Sun (1995). Stable and robust adaptive control. *Englewood Cliffs, NJ: Printice Hall* 2.
- John, L. and S. Mija (2014). Robust h infinity control algorithm for twin rotor mimo system. In *Advanced Communication Control and Computing Technologies (ICACCCT), 2014 International Conference on*, pp. 168–173. IEEE.
- Johnson, E. N. and A. J. Calise (2000). Pseudo-control hedging: a new method for adaptive control. In *Advances in navigation guidance and control technology workshop*, pp. 1–2.
- Kahvecioglu, S. and H. Oktal (2014). Turkish uav capabilities as a new competitor in the market. *International Journal of Intelligent Unmanned Systems* 2(3), 183–191.
- Khalil, H. K. and J. Grizzle (2002). *Nonlinear systems*, Volume 3. Prentice hall Upper Saddle River.
- Kim, Y. H., F. L. Lewis, and D. M. Dawson (2000). Intelligent optimal control of robotic manipulators using neural networks. *Automatica* 36(9), 1355–1364.
- Kokotović, R. R., L. Hsu, and P. Imai, Alvaro K (2003). Lyapunov-based adaptive control of mimo systems. *Automatica* 39(7), 1251–1257.
- Krstic, M. (2009). *Delay compensation for nonlinear, adaptive, and PDE systems*. Springer.
- Lavretsky, E. and N. Hovakimyan (2005). Adaptive compensation of control dependent modeling uncertainties using time-scale separation. In *Decision and Control, 2005 and 2005 European Control Conference. CDC-ECC'05. 44th IEEE Conference on*,

pp. 2230–2235. IEEE.

Leitner, J., A. Calise, and J. R. Prasad (1997). Analysis of adaptive neural networks for helicopter flight control. *Journal of Guidance, Control, and Dynamics* 20(5), 972–979.

Levine, W. S. (1996). *The control handbook*. CRC press.

Lewis, F. (1999). Nonlinear network structures for feedback control. *Asian Journal of Control* 1(4), 205–228.

Lewis, F. L., D. Vrabie, and V. L. Syrmos (2012). *Optimal control*. John Wiley & Sons.

Liu, X.-J., F. Lara-Rosano, and C. Chan (2004). Model-reference adaptive control based on neurofuzzy networks. *Systems, Man, and Cybernetics, Part C: Applications and Reviews, IEEE Transactions on* 34(3), 302–309.

Liu, Z., F. Zhou, and J. Zhou (2006). Flight control of unpowered flying vehicle based on robust dynamic inversion. In *Control Conference, 2006. CCC 2006. Chinese*, pp. 693–698. IEEE.

MacKunis, W. (2009). *Nonlinear control for systems containing input uncertainty via a Lyapunov-based approach*. Ph. D. thesis, University of Florida.

MacKunis, W., P. M. Patre, M. K. Kaiser, and W. E. Dixon (2010). Asymptotic tracking for aircraft via robust and adaptive dynamic inversion methods. *Control Systems Technology, IEEE Transactions on* 18(6), 1448–1456.

Mondal, S. and C. Mahanta (2012). Adaptive second-order sliding mode controller for a twin rotor multi-input–multi-output system. *IET Control Theory & Applications* 6(14), 2157–2167.

Nodland, D., H. Zargarzadeh, and S. Jagannathan (2013). Neural network-based optimal adaptive output feedback control of a helicopter uav. *Neural Networks and Learning Systems, IEEE Transactions on* 24(7), 1061–1073.



- Oppenheimer, M. W. and D. Doman (2005). Control of an unstable, nonminimum phase hypersonic vehicle model. In *Aerospace Conference, 2006 IEEE*, pp. 7–pp. IEEE.
- Part, F. A. R. (2002). 25: Airworthiness standards: Transport category airplanes. *Federal Aviation Administration, Washington, DC 7*.
- Patre, P. M., W. MacKunis, C. Makkar, and W. E. Dixon (2008). Asymptotic tracking for systems with structured and unstructured uncertainties. *Control Systems Technology, IEEE Transactions on 16(2)*, 373–379.
- Phillips, A. and F. Sahin (2014). Optimal control of a twin rotor mimo system using lqr with integral action. In *World Automation Congress (WAC), 2014*, pp. 114–119. IEEE.
- Rysdyk, R., F. Nardi, and A. Calise (1999). Robust adaptive nonlinear flight control applications using neural networks. In *American Control Conference, 1999. Proceedings of the 1999*, Volume 4, pp. 2595–2599 vol.4.
- Satici, A. C., H. Poonawala, and M. W. Spong (2013). Robust optimal control of quadrotor uavs. *Access, IEEE 1*, 79–93.
- Savran, A., R. Tasaltin, and Y. Becerikli (2006). Intelligent adaptive nonlinear flight control for a high performance aircraft with neural networks. *ISA transactions 45(2)*, 225–247.
- Schumacher, C. and J. Johnson (1999). Pi control of a tailless fighter aircraft with dynamic inversion and neural networks. In *American Control Conference, 1999. Proceedings of the 1999*, Volume 6, pp. 4173–4177. IEEE.
- Shin, J., H. J. Kim, Y. Kim, and W. E. Dixon (2010). Asymptotic attitude tracking of the rotorcraft-based uav via rise feedback and nn feedforward. In *Decision and Control (CDC), 2010 49th IEEE Conference on*, pp. 3694–3699. IEEE.

- Shin, J., H. J. Kim, Y. Kim, and W. E. Dixon (2012). Autonomous flight of the rotorcraft-based uav using rise feedback and nn feedforward terms. *Control Systems Technology, IEEE Transactions on* 20(5), 1392–1399.
- Shin, Y. (2005). Neural network based adaptive control for nonlinear dynamic regimes.
- Slotine, J.-J. E., W. Li, et al. (1991). *Applied nonlinear control*, Volume 60. Prentice-Hall Englewood Cliffs, NJ.
- Stevens, B. L. and F. L. Lewis (2003). *Aircraft control and simulation*. John Wiley & Sons.
- Tandale, M. D. and J. Valasek (2005). Adaptive dynamic inversion control of a linear scalar plant with constrained control inputs. In *American Control Conference, 2005. Proceedings of the 2005*, pp. 2064–2069. IEEE.
- Tanyer, I., E. Tatlicioglu, and E. Zergeroglu (2013). İha'lar için gürbüz takip denetçisi. In *Signal Processing and Communications Applications Conference (SIU), 2013*, pp. 1–4. IEEE.
- Tanyer, I., E. Tatlicioglu, and E. Zergeroglu (2014). İha'lar için optimal gürbüz takip denetçisi. In *National Conference of Turkish National Comitee of Automatic Control, 2014*.
- Tao, G. (2003). *Adaptive control design and analysis*, Volume 37. John Wiley & Sons.
- Wang, Q. and R. F. Stengel (2005). Robust nonlinear flight control of a high-performance aircraft. *Control Systems Technology, IEEE Transactions on* 13(1), 15–26.
- Wang, S., J. Li, and S. Wang (2011). A dynamic inversion controller design for miniature unmanned aerial vehicles. In *Consumer Electronics, Communications and Networks (CECNet), 2011 International Conference on*, pp. 1916–1921. IEEE.
- Xian, B., D. M. Dawson, M. S. de Queiroz, and J. Chen (2004). A continuous asymp-

otic tracking control strategy for uncertain nonlinear systems. *IEEE Transactions on Automatic Control* 49(7), 1206–1211.

Xie, Z., Y. Xia, and M. Fu (2011). Robust trajectory-tracking method for uav using nonlinear dynamic inversion. In *Cybernetics and Intelligent Systems (CIS), 2011 IEEE 5th International Conference on*, pp. 93–98. IEEE.

Yamasaki, T., H. Sakaida, K. Enomoto, H. Takano, and Y. Baba (2007). Robust trajectory-tracking method for uav guidance using proportional navigation. In *Control, Automation and Systems, 2007. ICCAS'07. International Conference on*, pp. 1404–1409. IEEE.

Zhang, Z., F. Hu, and J. Li (2011). Autonomous flight control system designed for small-scale helicopter based on approximate dynamic inversion. In *Advanced Computer Control (ICACC), 2011 3rd International Conference on*, pp. 185–191. IEEE.

# APPENDIX A

## BOUNDEDNESS PROOF

In this appendix, the boundedness of all the signals under the closed-loop operation will be demonstrated. While the boundedness proof is similar for all the different control designs, the main sketch of the proof are same. As a result, the closed-loop error systems are put in a form where  $\Theta(t)$  and  $\Delta(t) \in \mathbb{R}^m$  in (A.3) are different for each control design as given in Table A.1, and rest are same. Let  $V_b(z) \in \mathbb{R}$  be a Lyapunov

Table A.1.  $\Theta(t)$  and  $\Delta(t)$  for different control designs.

Type of controller	$\Theta(t)$	$\Delta(t)$
Robust Controller	$N_d$	$\tilde{N}$
Robust Optimal Controller	$N_d$	$\tilde{N} - DUDR^{-1}(r - \Lambda e)$
Robust Adaptive Controller	$N_{c,i} - Y\tilde{\psi}$	$N_e$
Neural Network Based Robust Controller	$N_b + \tilde{\varphi}^T \sigma(x_d) + \epsilon$	$N_z$

function defined as

$$V_b \triangleq \frac{1}{2}e^T e + \frac{1}{2}r^T M r \quad (\text{A.1})$$

which can be upper and lower bounded as

$$\frac{1}{2} \min\{1, M_{\min}\} \|z\|^2 \leq V_b(z) \leq \frac{1}{2} \max\{1, M_{\max}\} \|z\|^2 \quad (\text{A.2})$$

where  $M_{\min}$  and  $M_{\max}$  denote minimum and maximum eigenvalues of  $M$ , respectively.

Time derivative of the Lyapunov function can be written as

$$\begin{aligned} \dot{V}_b = & - e^T \Lambda e + r^T (\Theta + \Delta) - r^T DUD\beta \text{Sgn}(e) \\ & - r^T \begin{bmatrix} \Phi \\ 0 \end{bmatrix} - r^T r - k_g r^T r - \sum_{i=1}^{m-1} k_{d,i} r_i^2 \end{aligned} \quad (\text{A.3})$$

where (3.20) and (3.21) were utilized. The auxiliary signal  $\Theta(t) \in \mathbb{R}^m$  contains functions that can be bounded by constants in the sense that

$$|\Theta_i| \leq \zeta_{\Theta_i} \quad \forall i = 1, \dots, m \quad (\text{A.4})$$

where  $\zeta_{\Theta_i} \in \mathbb{R}$  are positive bounding constants and  $\Delta(x, \dot{x}, e, \dot{e}) \in \mathbb{R}^m$  contains functions that can be bounded by error signals as

$$|\Delta_i| \leq \rho_{\Delta,i} \|z\| \quad \forall i = 1, \dots, m \quad (\text{A.5})$$

where  $\rho_{\Delta,i} \in \mathbb{R}$  are positive bounding constants. After utilizing (3.23), following upper bound can be obtained

$$r^T \begin{bmatrix} \Phi \\ 0 \end{bmatrix} \leq \sum_{i=1}^{m-1} \zeta_{\Phi_i} |r_i| \|z\|. \quad (\text{A.6})$$

After substituting the upper bounds in (A.4), (A.5) and utilizing (A.6) along with (A.3), following expression can be obtained

$$\begin{aligned} \dot{V}_b \leq & -e^T \Lambda e - \|r\|^2 + \sum_{i=1}^m \zeta_{\Theta_i} |r_i| + \zeta_1 \|r\| + \sum_{i=1}^m \rho_{\Delta,i} |r_i| \|z\| \\ & - k_g \|r\|^2 + \sum_{i=1}^{m-1} \zeta_{\Phi_i} |r_i| \|z\| - \sum_{i=1}^{m-1} k_{d,i} r_i^2 \end{aligned} \quad (\text{A.7})$$

where  $|r^T D U D \beta \text{Sgn}(e)| \leq \zeta_1 \|r\|$  was utilized with  $\zeta_1 \in \mathbb{R}$  being a positive bounding constant. After utilizing following manipulations

$$\zeta_1 \|r\| + \sum_{i=1}^m \zeta_{\Theta_i} |r_i| \leq \frac{1}{2\delta} \|r\|^2 + \delta \left( \zeta_1^2 + \sum_{i=1}^m \zeta_{\Theta_i}^2 \right) \quad (\text{A.8})$$

$$\rho_{\Delta,i} |r_i| \|z\| - k_g r_i^2 \leq \frac{\rho_{\Delta,i}^2}{4k_g} \|z\|^2 \quad (\text{A.9})$$

$$\zeta_{\Phi_i} |r_i| \|z\| - k_{d,i} r_i^2 \leq \frac{\zeta_{\Phi_i}^2}{4k_{d,i}} \|z\|^2 \quad (\text{A.10})$$

$\forall i = 1, \dots, (m-1)$ , where  $\delta \in \mathbb{R}$  is a positive damping constant, the right-hand side of (A.7) can be upper bounded as

$$\dot{V}_b \leq -[\min\{\Lambda_{\min}, (1 - \frac{1}{2\delta})\}] - \sum_{i=1}^m \frac{\rho_{\Delta,i}^2}{4k_g} - \sum_{i=1}^{m-1} \frac{\zeta_{\Phi_i}^2}{4k_{d,i}} \|z\|^2 + \delta \left( \zeta_1^2 + \sum_{i=1}^m \zeta_{\Theta_i}^2 \right) \quad (\text{A.11})$$

where  $\Lambda_{\min}$  denotes the minimum eigenvalue of  $\Lambda$ . Provided that the control gains  $\Lambda$ ,  $k_g$ ,  $k_{d,1}$ , ...,  $k_{d,m-1}$  are selected sufficiently high, following expression can be obtained for the time derivative of the Lyapunov function

$$\dot{V}_b \leq -c_1 V_b + c_2 \quad (\text{A.12})$$

where  $c_1$  and  $c_2$  are some positive bounding constants. From (A.12), it can be concluded that  $V_b(t) \in L_\infty$ , and thus,  $e(t)$ ,  $r(t) \in L_\infty$ . The definition of  $r(t)$  in (3.4) can be utilized

to prove that  $\dot{e}(t) \in L_\infty$ . By using (3.2) and its time derivative, along with the assumption that the reference model signals being bounded, it can be proven that  $y(t), \dot{y}(t), x(t), \dot{x}(t) \in \mathcal{L}_\infty$ . The above boundedness statements can be utilized along with (2.1) to prove that  $u(t) \in \mathcal{L}_\infty$ . From (3.19), it is easy to see that  $\dot{u}(t) \in \mathcal{L}_\infty$ . After utilizing the above boundedness statements, it is clear that  $\dot{r}(t) \in \mathcal{L}_\infty$ . Standard signal chasing algorithms can be used to prove that all remaining signals are bounded.

## APPENDIX B

### LEMMA 1 AND ITS PROOF

**Lemma B.0.1** *Provided that  $e(t)$  and  $\dot{e}(t)$  are bounded, the following expression for the upper bound of the integral of the absolute value of the  $i$ -th entry of  $\dot{e}(t)$  can be obtained*

$$\int_{t_0}^t |\dot{e}_i(\tau)| d\tau \leq \gamma_1 + \gamma_2 \int_{t_0}^t |e_i(\tau)| d\tau + |e_i| \quad (\text{B.1})$$

where  $\gamma_1, \gamma_2 \in \mathbb{R}$  are some positive bounding constants.

**Proof** First, it is noted that if  $e_i(t) \equiv 0$  on some interval, then  $\dot{e}_i(t) \equiv 0$  on the same interval, and the inequality (B.1) yields this qualification. Therefore, without loss of generality, the case that  $e_i(t)$  is absolutely greater than zero on the interval of  $[t_0, t]$  is considered. Let  $T \in [t_0, t)$  be the last instant of time when  $\dot{e}_i(t)$  changes sign. Then, on the interval  $[T, t]$ ,  $\dot{e}_i(t)$  has a constant sign, hence

$$\begin{aligned} \int_T^t |\dot{e}_i(\tau)| d\tau &= \left| \int_T^t \dot{e}_i(\tau) d\tau \right| \\ &= |e_i(t) - e_i(T)|. \end{aligned} \quad (\text{B.2})$$

From the boundedness of  $\dot{e}_i(t)$ , it follows that there exist a constant  $\gamma > 0$  such that  $|\dot{e}_i(t)| \leq \gamma$ , therefore

$$\int_{t_0}^T |\dot{e}_i(\tau)| d\tau \leq \gamma(T - t_0). \quad (\text{B.3})$$

On the other hand, by applying the Mean Value Theorem Khalil and Grizzle (2002), following expression can be obtained

$$\int_{t_0}^T |e_i(\tau)| d\tau = (T - t_0)e_{i*}. \quad (\text{B.4})$$

where  $e_{i*} > 0$  is some intermediate value of  $|e_i(t)|$  on the interval  $[t_0, T]$ . By assumption,  $e_{i*}$  is bounded away from zero. Therefore, from (B.3) and (B.4), following expression can be stated

$$\int_{t_0}^T |\dot{e}_i(\tau)| d\tau \leq \gamma_2 \int_{t_0}^T |e_i(\tau)| d\tau \quad (\text{B.5})$$

where  $\gamma_2 \triangleq \frac{\gamma}{e_{i^*}}$ . Combining the relationships in (B.2) and (B.5), following expression can be obtained

$$\int_{t_0}^t |\dot{e}_i(\tau)| d\tau \leq |e_i(t)| + \gamma_2 \int_{t_0}^t |e_i(\tau)| d\tau + |e_i(T)| \quad (\text{B.6})$$

which yields in (B.1) with  $\gamma_1 \triangleq \sup |e_i(T)|$ .



## APPENDIX C

### LEMMA 2 AND ITS PROOF

In an attempt to present similar results under the same section, a general version of the lemma and its accompanying proof are presented in this appendix. Specifically, the auxiliary term  $\Theta(t) \in \mathbb{R}^m$  in (C.1) is considered to vary for each control design as given in Table C.1.

Table C.1.  $\Theta(t)$  and  $\Delta(t)$  for different control designs.

Type of controller	$\Theta(t)$
Robust Controller	$N_d$
Robust Optimal Controller	$N_d$
Robust Adaptive Controller	$N_c$
Neural Network Based Robust Controller	$N_b + \epsilon$

**Lemma C.0.2** *Let the auxiliary function  $L(t) \in \mathbb{R}$  be defined as*

$$L \triangleq r^T(\Theta - DUD\beta\text{Sgn}(e)). \quad (\text{C.1})$$

*If the entries of  $\beta$  are selected to satisfy the conditions in (3.25) and (3.26), then it can be concluded that the auxiliary function  $P(t) \in \mathbb{R}$  defined as*

$$P \triangleq \zeta_b - \int_0^t L(\tau) d\tau \quad (\text{C.2})$$

*is non-negative where  $\zeta_b \in \mathbb{R}$  is a positive bounding constant.*

**Proof** Before proving the non-negativeness of  $P(t)$ , the term  $DUD\beta\text{Sgn}(e)$  is rewritten as

$$DUD\beta\text{Sgn}(e) = \begin{bmatrix} \Psi \\ 0 \end{bmatrix} + \beta\text{Sgn}(e) \quad (\text{C.3})$$

where the entries of  $\Psi(t) \in \mathbb{R}^{(m-1) \times 1}$  are defined as

$$\Psi_i \triangleq d_i \sum_{j=i+1}^m d_j \beta_j U_{i,j} \text{sgn}(e_j). \quad (\text{C.4})$$

The upper bounds for the entries of  $\Psi$  can be obtained as

$$|\Psi_i| \leq \zeta_{\Psi_i} \quad (\text{C.5})$$

where  $\zeta_{\Psi_i} \in \mathbb{R}$  are positive bounding constants. Note that,  $\zeta_{\Psi_i}$  depends on the control gains  $\beta_{i+1}, \dots, \beta_m$ .

Integrating  $L(t)$  results in

$$\begin{aligned} \int_0^t L(\tau) d\tau = & \int_0^t e^T(\tau) \Lambda^T [\Theta(\tau) - \beta \mathbf{Sgn}(e(\tau))] d\tau \\ & - \int_0^t e^T(\tau) \Lambda^T D(U - I_m) D \beta \mathbf{Sgn}(e(\tau)) d\tau \\ & + \int_0^t \dot{e}^T(\tau) \Theta(\tau) d\tau \\ & - \int_0^t \dot{e}^T(\tau) D(U - I_m) D \beta \mathbf{Sgn}(e(\tau)) d\tau \\ & - \int_0^t \dot{e}^T(\tau) \beta \mathbf{Sgn}(e(\tau)) d\tau. \end{aligned} \quad (\text{C.6})$$

Each term on the right-hand side of (C.6) is considered separately. The first term can be bounded as

$$\begin{aligned} \int_0^t e^T(\tau) \Lambda^T [\Theta(\tau) - \beta \mathbf{Sgn}(e(\tau))] d\tau &= \int_0^t \sum_{i=1}^m \Lambda_i e_i(\tau) (\Theta_i(\tau) - \beta_i \mathbf{sgn}(e_i(\tau))) \\ &\leq \sum_{i=1}^m \Lambda_i (\zeta_{\Theta_i} - \beta_i) \int_0^t |e_i(\tau)| d\tau. \end{aligned} \quad (\text{C.7})$$

The second term can be bounded as

$$\begin{aligned} - \int_0^t e^T(\tau) \Lambda^T D(U - I_m) D \beta \mathbf{Sgn}(e(\tau)) d\tau &= - \int_0^t \sum_{i=1}^{m-1} \Lambda_i e_i(\tau) \sum_{j=i+1}^m \beta_j \Psi_{i,j} \mathbf{sgn}(e_j(\tau)) d\tau \\ &\leq \sum_{i=1}^{m-1} \sum_{j=i+1}^m \Lambda_i \beta_j \zeta_{\Psi_{i,j}} \int_0^t |e_i(\tau)| d\tau. \end{aligned} \quad (\text{C.8})$$

The third term can be bounded as

$$\begin{aligned} \int_0^t \dot{e}^T(\tau) \Theta(\tau) d\tau &= \int_0^t \sum_{i=1}^m \dot{e}_i^T(\tau) \Theta_i(\tau) d\tau \\ &\leq \sum_{i=1}^m \zeta_{\Theta_i} \int_0^t |\dot{e}_i(\tau)| d\tau \\ &\leq \sum_{i=1}^m \zeta_{\Theta_i} (\gamma_1 + \gamma_2 \int_0^t |e_i(\tau)| d\tau + |e_i|) \end{aligned} \quad (\text{C.9})$$

where (B.1) was utilized to obtain the last line. The fourth term can be bounded as

$$\begin{aligned}
-\int_0^t \dot{e}^T(\tau)D(U - I_m)D\beta \text{Sgn}(e(\tau))d\tau &= -\int_0^t \sum_{i=1}^{m-1} \dot{e}_i(\tau) \sum_{j=i+1}^m \beta_j \Psi_{i,j} \text{sgn}(e_j(\tau))d\tau \\
&\leq \sum_{i=1}^{m-1} \sum_{j=i+1}^m \beta_j \zeta_{\Psi_{i,j}} \int_0^t |\dot{e}_i(\tau)|d\tau \quad (\text{C.10}) \\
&\leq \sum_{i=1}^{m-1} \sum_{j=i+1}^m \beta_j \zeta_{\Psi_{i,j}} (\gamma_1 + \gamma_2 \int_0^t |e_i(\tau)|d\tau + |e_i|)
\end{aligned}$$

where (B.1) was utilized to obtain the last line. The fifth term can be evaluated as Krstic (2009)

$$\begin{aligned}
-\int_0^t \dot{e}^T(\tau)\beta \text{Sgn}(e(\tau))d\tau &= -\int_0^t \sum_{i=1}^m \beta_i \dot{e}_i(\tau) \text{sgn}(e_i(\tau))d\tau \\
&= -\sum_{i=1}^m \beta_i \int_0^t \text{sgn}(e_i(\tau))d(e_i) \\
&= -\sum_{i=1}^m \beta_i \int_0^t d(|e_i|) \\
&= -\sum_{i=1}^m \beta_i |e_i(t)| + \sum_{i=1}^m \beta_i |e_i(0)|. \quad (\text{C.11})
\end{aligned}$$

Combining the upper bounds in (C.7)-(C.11) yields

$$\begin{aligned}
\int_0^t L(\tau)d\tau &\leq \zeta_b + \sum_{i=1}^{m-1} \Lambda_i \left[ \left(1 + \frac{\gamma_2}{\Lambda_i}\right) (\zeta_{\Theta_i} + \sum_{j=i+1}^m \zeta_{\Psi_{i,j}} \beta_j) - \beta_i \right] \int_0^t |e_i(\tau)|d\tau \\
&+ \Lambda_m \left[ \left(1 + \frac{\gamma_2}{\Lambda_m}\right) \zeta_{\Theta_m} - \beta_m \right] \int_0^t |e_m(\tau)|d\tau \\
&+ (\zeta_{\Theta_m} - \beta_m) |e_m| + \sum_{i=1}^{m-1} (\zeta_{\Theta_i} + \sum_{j=i+1}^m \zeta_{\Psi_{i,j}} \beta_j - \beta_i) |e_i| \quad (\text{C.12})
\end{aligned}$$

where  $\zeta_b$  is defined as

$$\zeta_b \triangleq \gamma_1 \sum_{i=1}^{m-1} \sum_{j=i+1}^m \zeta_{\Omega_{i,j}} \beta_j + \gamma_1 \sum_{i=1}^m \zeta_{\Theta_i} + \sum_{i=1}^m \beta_i |e_i(0)|. \quad (\text{C.13})$$

After choosing  $\beta$  as in (3.25) and (3.26), it can easily be shown that  $P(t)$  in (C.2) is non-negative.

## APPENDIX D

### ASYMPTOTIC STABILITY PROOF FOR CHAPTERS 3 AND 4

In this appendix, the asymptotic stability of the output tracking error for robust and robust optimal controller designs are presented. Since the closed-loop error systems are similar, the results are analyzed in this appendix by varying the term  $\Delta(t) \in \mathbb{R}^m$  in (D.3) as given in Table A.1. Let  $V_{Re}(w) \in \mathbb{R}$  be a Lyapunov function defined as

$$V_{Re} \triangleq V_b + P \quad (\text{D.1})$$

where  $w(t) \triangleq \begin{bmatrix} e^T & r^T & \sqrt{P} \end{bmatrix}^T \in \mathbb{R}^{(2m+1) \times 1}$ . It should be noted that, the non-negativeness of  $P(t)$ , which is essential to prove that  $V_{Re}(w)$  is a valid Lyapunov function, was proven in Appendix C.

The Lyapunov function in (D.1) can be upper and lower bounded as follows

$$\frac{1}{2} \min\{1, M_{\min}\} \|w\|^2 \leq V_{Re}(w) \leq \max\{1, \frac{1}{2} M_{\max}\} \|w\|^2. \quad (\text{D.2})$$

Taking the time derivative of the Lyapunov function in (D.1), substituting (A.3) and time derivative of (C.2), and after some straightforward manipulations, following expression can be obtained

$$\dot{V}_{Re} = -e^T \Lambda e + r^T \Delta - r^T \begin{bmatrix} \Phi \\ 0 \end{bmatrix} - r^T r - k_g r^T r - \sum_{i=1}^{m-1} k_{d,i} r_i^2. \quad (\text{D.3})$$

After utilizing (A.9) and (A.10), the right-hand side of (D.3) can be upper bounded as

$$\dot{V}_{Re} \leq - \left[ \min\{\lambda_{\min}(\Lambda), 1\} - \sum_{i=1}^m \frac{\rho_{\Delta,i}^2}{4k_g} - \sum_{i=1}^{m-1} \frac{\zeta_{\Phi_i}^2}{4k_{d,i}} \right] \|z\|^2. \quad (\text{D.4})$$

Provided that the control gains  $\Lambda$ ,  $k_g$ ,  $k_{d,1}$ , ...,  $k_{d,m-1}$  are selected sufficiently high, the below expression can be obtained for the derivative of the Lyapunov function

$$\dot{V}_{Re} \leq -c_3 \|z\|^2 \quad (\text{D.5})$$

where  $c_3$  is some positive bounding constant. From (D.1) and (D.5), it is clear that  $V_{Re}(w)$  is non-increasing and bounded. After integrating (D.5), it can be concluded that  $z(t) \in$

$\mathcal{L}_2$ . Since  $z(t) \in \mathcal{L}_\infty \cap \mathcal{L}_2$  and  $\dot{z}(t) \in \mathcal{L}_\infty$ , from Barbalat's Lemma Khalil and Grizzle (2002),  $\|z(t)\| \rightarrow 0$  as  $t \rightarrow \infty$ , thus meeting the control objective. Since no restrictions with respect to the initial conditions of the error signals were imposed on the control gains, the result is **global**.

## APPENDIX E

### ASYMPTOTIC STABILITY PROOF FOR CHAPTER 5

Let  $V_A(w) \in \mathbb{R}$  be a Lyapunov function defined as

$$V_A = V_b + P + \frac{1}{2} \tilde{\psi}^T \Gamma^{-1} \tilde{\psi} \quad (\text{E.1})$$

where  $w(t) \triangleq \begin{bmatrix} e^T & r^T & \sqrt{P} & \tilde{\psi}^T \end{bmatrix}^T \in \mathbb{R}^{(2m+p+1) \times 1}$  with  $\Theta = N_c$  in  $P(t)$  in Appendix C. The Lyapunov function in (E.1) can be upper and lower bounded as follows

$$\frac{1}{2} \min\{1, \bar{M}_{\min} \Gamma_{\max}\} \|w\|^2 \leq V_A(w) \leq \max\{\frac{1}{2} \bar{M}_{\max}, \frac{1}{2} \Gamma_{\min}\} \|w\|^2. \quad (\text{E.2})$$

Taking the time derivative of (E.1), substituting (A.3), (3.21), and time derivative of (C.2), results in

$$\begin{aligned} \dot{V}_A = & e^T(r - \Lambda e) + r^T[N_c + N_e - e - \begin{bmatrix} \Phi \\ 0 \end{bmatrix} - r - k_g r \\ & - \text{diag}\{k_{d,1}, \dots, k_{d,m-1}, 0\}r - DUD\beta \text{Sgn}(e) - Y\tilde{\psi}] - \tilde{\psi}^T \Gamma^{-1} \dot{\tilde{\psi}} \\ & - r^T(N_c - DUD\beta \text{Sgn}(e)) \end{aligned} \quad (\text{E.3})$$

where  $\dot{\tilde{\psi}} = -\hat{\tilde{\psi}}$  was utilized. After cancelling same terms, utilizing (5.8), (A.5) and (A.6) in (E.3), time derivative of the Lyapunov function can be upper bounded as

$$\begin{aligned} \dot{V}_A \leq & -e^T \Lambda e + \rho_e \|r\| \|z\| + \sum_{i=1}^{m-1} \zeta_{\Phi_i} |r_i| \|z\| - r^T r - k_g r^T r - \sum_{i=1}^{m-1} k_{d,i} |r_i|^2 \\ & - r^T Y \tilde{\psi} + \tilde{\psi}^T \Gamma^{-1} \Gamma Y^T r. \end{aligned} \quad (\text{E.4})$$

After utilizing (A.9) and (A.10), the right-hand side of (E.4) can be upper bounded as

$$\dot{V}_A \leq -[\min\{\lambda_{\min}(\Lambda), 1\} - \frac{\rho_e^2}{4k_g} - \sum_{i=1}^{m-1} \frac{\zeta_{\Phi_i}^2}{4k_{d,i}}] \|z\|^2. \quad (\text{E.5})$$

Provided that the control gains  $\Lambda, k_g, k_{d,1}, \dots, k_{d,m-1}$  are selected sufficiently high, the below expression can be obtained for the derivative of the Lyapunov function

$$\dot{V}_A \leq -c_4 \|z\|^2 \quad (\text{E.6})$$

where  $c_4$  is some positive bounding constant. From (E.1) and (E.6), it is clear that  $V_A(w)$  is non-increasing and bounded. After integrating (E.6), it can be concluded that  $z(t) \in \mathcal{L}_2$ .

Since  $z(t) \in \mathcal{L}_\infty \cap \mathcal{L}_2$  and  $\dot{z}(t) \in \mathcal{L}_\infty$ , from Barbalat's Lemma Khalil and Grizzle (2002),  $\|z(t)\| \rightarrow 0$  as  $t \rightarrow \infty$ , thus meeting the control objective. Since no restrictions with respect to the initial conditions of the error signals were imposed on the control gains, the result is **global**.

## APPENDIX F

### ASYMPTOTIC STABILITY PROOF FOR CHAPTER 6

Let  $V_N(e, r, \varphi, t) \in \mathbb{R}$  be a Lyapunov function defined as

$$V_N = V_b + P + \frac{1}{2k_n} \text{tr}(\tilde{\varphi} \tilde{\varphi}^T) \quad (\text{F.1})$$

where  $V_b(t)$  was defined in (A.1) and auxiliary function  $P(t)$  was given in (C.2) with  $\Theta = N_b + \epsilon$ . Time derivative of the Lyapunov function in (F.1) is obtained as

$$\dot{V}_N = e^T \dot{e} + r^T M \dot{r} + \dot{P} + \frac{1}{k_n} \text{tr}(\tilde{\varphi}^T \dot{\tilde{\varphi}}). \quad (\text{F.2})$$

Substituting (6.14) and time derivative of (C.2) into (F.2) results in

$$\begin{aligned} \dot{V}_N = & e^T(r - \Lambda e) + r^T [N_b + N_z - e - \begin{bmatrix} \Phi \\ 0 \end{bmatrix} - r - k_g r \\ & - \text{diag}\{k_{d,1}, \dots, k_{d,m-1}, 0\}r - DUD\beta \text{Sgn}(e) + \tilde{W}^T \sigma(x_d) + \epsilon] \\ & - \frac{1}{k_n} \text{tr}(\tilde{\varphi}^T \dot{\tilde{\varphi}}) - r^T (N_b + \epsilon - DUD\beta \text{Sgn}(e)). \end{aligned} \quad (\text{F.3})$$

After utilizing simplifications on (F.3), time derivative of the Lyapunov function is rewritten as

$$\dot{V}_N = -e^T \Lambda e + r^T \tilde{\varphi}^T \sigma + r^T N_z - r^T K r - r^T \begin{bmatrix} \Phi \\ 0 \end{bmatrix} + \frac{1}{k_n} \text{tr}(\tilde{\varphi}^T \dot{\tilde{\varphi}}). \quad (\text{F.4})$$

From (6.13), following expression can be obtained

$$\begin{aligned} \frac{1}{k_n} \text{tr}(\tilde{\varphi}^T \dot{\tilde{\varphi}}) &= -\text{tr}(\tilde{\varphi}^T \sigma r^T) \\ &= -\text{tr}(r^T \tilde{\varphi}^T \sigma) \\ &= -r^T \tilde{\varphi}^T \sigma \end{aligned} \quad (\text{F.5})$$

where properties of trace were utilized. Substituting (F.5) into (F.4) yields

$$\dot{V}_N = -e^T \Lambda e + r^T N_z - r^T K r - r^T \begin{bmatrix} \Phi \\ 0 \end{bmatrix}. \quad (\text{F.6})$$

Utilizing (3.23) and (6.3) in (F.6), time derivative of the Lyapunov function can be upper bounded as

$$\dot{V}_N \leq -e^T \Lambda e + \rho_z \|r\| \|z\| + \sum_{i=1}^{m-1} \zeta_{\Phi_i} |r_i| \|z\| - r^T r - k_g r^T r - \sum_{i=1}^{m-1} k_{d,i} |r_i|^2. \quad (\text{F.7})$$



After utilizing (A.9) and (A.10), the right-hand side of (F.7) can be upper bounded as

$$\dot{V}_N \leq -[\min\{\lambda_{\min}(\Lambda), 1\} - \sum_{i=1}^m \frac{\rho_{z,i}^2}{4k_g} - \sum_{i=1}^{m-1} \frac{\zeta_{\Phi_i}^2}{4k_{d,i}}] \|z\|^2. \quad (\text{F.8})$$

Provided that the control gains  $\Lambda$ ,  $k_g$ ,  $k_{d,1}$ , ...,  $k_{d,m-1}$  are selected sufficiently high, the below expression can be obtained for the derivative of the Lyapunov function

$$\dot{V}_N \leq -c_5 \|z\|^2 \quad (\text{F.9})$$

where  $c_5$  is some positive bounding constant. From (F.1) and (F.9), it is clear that  $V_N(\cdot)$  is non-increasing and bounded. After integrating (F.9), it can be concluded that  $z(t) \in \mathcal{L}_2$ . Since  $z(t) \in \mathcal{L}_\infty \cap \mathcal{L}_2$  and  $\dot{z}(t) \in \mathcal{L}_\infty$ , from Barbalat's Lemma Khalil and Grizzle (2002),  $\|z(t)\| \rightarrow 0$  as  $t \rightarrow \infty$ , thus meeting the control objective. Since no restrictions with respect to the initial conditions of the error signals were imposed on the control gains, the result is **global**.

## VITA

İlker Tanyer was born in İzmir, Turkey, in June 24th, 1982. After his graduation from 60. Year Anatolian High School he attended Electrical and Electronics Engineering Department at Anadolu University. Soon after acquiring his BSc degree from Anadolu University in 2005, he started the MSc program in Electrical and Electronics Department at İzmir Institute of Technology (IZTECH). In 2008, he started his PhD studies at the same department in IZTECH.

He worked as a research assistant at Electrical and Electronics Engineering department in IZTECH from 2007 to 2011. Meanwhile in 2007, he founded a Google Certified Partner Company named AdresGezgini with two of his colleagues at İzmir Technology Development Region. His current research is focused on flight control systems of unmanned aerial vehicles.

Permanent Address: İZMİR